Gas-Liquid-Liquid Microreactor for Biodiesel Synthesis

Aloisiyus Yuli Widianto

THÈSE

En vue de l'obtention du

DOCTORAT DE L'UNIVERSITÉ DE TOULOUSE

Délivré par :

Institut National Polytechnique de Toulouse (INP Toulouse)

Discipline ou spécialité :

Energétique, Génie de Procédés

Présentée et soutenue par :

ALOISIYUS YULI WIDIANTO

le Mercredi 9 Décembre 2020

Titre :

GAS-LIQUID-LIQUID MICROREACTOR
FOR BIODIESEL SYNTHESIS

Ecole doctorale :

Mécanique, Energétique, Génie civil, Procédés (MEGeP)

Unité de recherche :

LGC – INP TOULOUSE

Directeur(s) de Thèse :

Mme CATHERINE XUEREB
Mme JOELLE AUBIN

Rapporteurs :

M. LIONEL ESTEL, INSA ROUEN
Mme. SHALIZA IBRAHIM, UNIVERSITÉ DE MALAYA

Membre(s) du jury :

Mme. SOPHIE THIEBAUD-ROUX, INP TOULOUSE, Président
Mme. CATHERINE XUEREB, INP TOULOUSE, Membre
Mme. JOELLE AUBIN, INP TOULOUSE, Membre
Mme. LIEKE RIADI, UNIVERSITÉ DE SURABAYA, Membre
Mme. MARTINE POUX, INP TOULOUSE, Invite

Abstract

The current work aims to develop synthesis biodiesel through simultaneous transesterification and ozonation reactions in a microtube reactor of 1 mm diameter, which has low energy consumption, provides process safety, as well as enables high reaction yield and conversion. The synthesis were carried out by contacting two immiscible liquids oil-methanol and ozone gas in a microtube of 5 m long at 30 °C, 1 atm pressure, the oil-methanol molar ratio 1:3, 1:5, with 1 wt% catalyst NaOH. For the purposes of comparison and assessment the influence of ozone gas, biodiesel was also synthesized by performing the reactions in series, i.e., transesterification then ozonolysis, and vice versa, by utilizing the same experimental conditions.

After a preliminary study on gas-liquid-liquid flows, the result shows that the microtube reactor used is capable of producing a promising yield and conversion through the simultaneous processes in a much shorter reaction time around 15 minutes by applying the lower ozone flow rates and the smaller methanol-oil molar ratio 1:3 than the previous works in stirred tank reactors. Ozone in this synthesis has broken the double bounds carbon chains of methyl oleate, methyl linoleate, and methyl linolenate and converting them to the saturated methyl esters, therefore, the biodiesel product has a better stability.

Résumé

Les travaux menés visent à développer la synthèse de biodiesel par des réactions simultanées de transestérification et d'ozonation dans un microréacteur de 1 mm de diamètre en recherchant une meilleure qualité de biodiesel ainsi qu'un rendement et une conversion élevés. La synthèse a été réalisée en mettant en contact l'huile de tournesol (choisi comme huile modèle), le méthanol et l'ozone gazeux, dans un microréacteur de 5 m de long à 30 °C, 1 atm, avec un rapport molaire huile-méthanol 1:3, 1:5, et avec comme catalyseur NaOH à 1%. Afin de comparer et d'évaluer l'apport de l'ozone, le biodiesel a également été synthétisé en effectuant les réactions en série, c'est-à-dire la transestérification puis l'ozonolysis, et inversement, en utilisant les mêmes conditions expérimentales.

Après une étude sur les écoulements gaz-liquide-liquide, il a été montré que l'utilisation d'un microréacteur permet d'obtenir un rendement prometteur et une conversion du biodiesel par le procédé simultané avec un temps de réaction réduit (15 minutes), un débit d'ozone plus faible et un rapport molaire méthanol-huile plus faible (1:3) qu'avec un réacteur agité. L'ozone détruit les doubles liaisons des chaînes de carbone de l'oléate de méthyle, du linoléate de méthyle et du linolénate de méthyle et qui sont convertis en esters méthyliques saturés d'une meilleure stabilité.

Acknowledgments

Within this section, I would like to express my appreciation to the people who contributed to this thesis, either directly or indirectly. But before going to the specific enumeration of people who inspired this work, I like to thank the Government of Indonesia for financial support through the Indonesia Endowment Fund for Education (LPDP), Ministry of Finance; and the Directorate General of Higher Education (DIKTI), Ministry of Research, Technology and Higher Education, Republic of Indonesia.

First of all, I would like to thank my director Catherine Xuereb, my co-supervisor, Joëlle Aubin, and Martine Poux, for giving me the opportunity to work on this subject. I also thank for the scientific and organizational support in carrying out this work. I would also like to thank Martine Poux for the inputs and directions in carrying out the synthesis experiment, mainly in the last minutes of submitting the manuscript and the corrections to the manuscript.

I thank the rapporteurs, Lionel Estel and Shaliza Ibrahim, for the detailed evaluation of the manuscript. I am also very grateful to all the jury members, Sophie Thibaux-Roux and Ibu Lieke Riadi for the critical remarks and the abundant and enriching discussions on this subject.

I would like to thank the personal technique: Alain Pontier, Jean Louis Nadalin, Jean Louis Labat, Luc Etchevery, Mico, Thomas for the availability and advice on how to put the project into practice. I would like to thank Phillipe Destract for the fast response to any technical problem in the laboratory. I would especially like to thank Sofiane and Laure Latapie for the inputs and directions in carrying out the Gas Chromatography and carrying out quantitative and qualitative analysis.

I would like to warmly thank the doctoral students: Marco Avila, Timothy Oluwadero, Thibaud, Robby Rajagobalou, Masoud, Leticia Vitola Pasetto, and all doctoral student members of STPI for their advice, information, an interesting overview of their research project, and for the pleasant atmosphere in our office.

I would like to thank Dore Russel for measuring the bubble/slug length during his final project; Noemie Berne, Jeanne Gauchot, Theo Lerique, and Fleur Salmon for measuring the surface tension, interfacial tension, and contact angles, as well as in determining the continuous/dispersed phase of gas-liquid and gas-liquid-liquid systems during the project 3A-21 bis.

I would like to warmly thank my colleagues in the Chemical Engineering Department, University of Surabaya, who always support and encourage me.

Finally, I would like to special thank my family members: my beloved wife Natalia Widianto, my kids: Emanuella Widianto and Fransiskus Widianto, and my extended family in Indonesia for their support, pray, and enthusiasm during my studies.

Contents

General Introduction

Petroleum-based fuels are limited energy resources in the world, so alternative energy, especially green energy, needs to be developed. As fossil fuel resources are shortening day by day, the scarcity of petroleum reserves allows renewable energy sources to be a more attractive alternative. Biodiesel is considered to provide the best opportunity as renewable energy as diesel fuels. Biodiesel can reduce air pollutant emission and greenhouse gases, as well as reducing long term engine wear in diesel engines. More than 95% of biodiesel production today derived from palm oil, soybean oil, rapeseed oil, and sunflower oil, which are renewable sources [1][2]. Since traditional petroleum and diesel are non-renewable and thus will last for a limited period. These non-renewable fuels also produce pollutants in the form of oxides compounds such as oxides of nitrogen, oxides of sulfur, oxides of carbon, and lead [3]. Hence biodiesel is vital alternative energy as it can address the increased environmental pollution and depletion of non-renewable fuels [3][4].

Biodiesel is a very promising alternative biofuel due to the following attractive attributes: (1) it can be mixed at any proportion with diesel oil; (2) hence it can be applied immediately in diesel engines without much modification; (3) easy biodegradability and; (4) less poisonous compared to the ordinary diesel oil. The waste product contained less particles; hence, it is not black, less sulfur, and other aromatic contents [3].

Therefore the emissions are environmentally friendly and greener house gas-friendly as it emits less carbon dioxide in the atmosphere and thus contributes towards lessening further global warming [5].

Used cooking oil has high potential as a biofuel source. The local disposal of used frying oil becomes a huge problem due to the large volumes involved. In the fast-food business alone, a single branch that serves fried foods such as fried chicken, french frie and burgers can produce as much as 15 liters of used frying oil per day [1][4][5][6].

The disposal of waste cooking oil should be carried out carefully and the disposal method is regulated in some countries, such as Animal By-Product Regulation in May 2002, which does not allow catering premises to sell their used cooking oil to animal feed manufacturers [7]. Consequently, the caterers tend to dispose of their used cooking oil into the drain resulting in the deterioration of water stream quality and choking the drainage system, and aggregation of grease, which cause smelly odor and diseases.

Generally, biodiesel synthesis is conducted using a transesterification reaction; however, the transesterification product still has low stability due to the appearance of many double bonds carbon chains in the solution [6]. Since the double bonds are unsaturated, it readily reacts with other chemicals to form a new chemical compound. Therefore, the improvement of product stability could be made by reducing double bonds carbon chains in the solution by oxidation using ozone gas. In this synthesis, ozone cuts the double bond carbon chain to produce a shorter alkyl ester with high stability [8].

An investigation of the catalytic ozone chemistry application for improving biodiesel quality was performed by several previous works [9][10][11]. They studied the conversion of double bonds in the methyl soyate through ozonolysis and concluded that the conversion of double bonds up to 90% was achieved within 2 hours of reaction time using the batch stirrer tank reactor. In this study, Baber et al. (2005) have proven that ozone gas can effectively eliminate the double bonds

and form volatile methyl and dimethyl ester products. Ambient temperature and a solvent-free system can be engineered to develop an economically viable process[11]. However, ozonolysis carrying out in a batch reactor has a potential issue related to safety, especially remembering ozone is a strong oxidation agent, highly reactive, and hazardous chemical. Further, the synthesis of biodiesel in a batch reactor takes a very long reaction time (3 – 5 hours) [4][12], as well as the process needs a large amount of methanol feedstock. Molar ratio oil to methanol used is 1:5 up to 1:28 [13][2][11].

In the last three-decade, a new type of reacor (microreactor) has been developed for many application processes, particularly for a high exothermic or endothermic reaction. The studies show that the new system performs multiphase reactions with high yield, selectivity, and conversion in shorter reaction times than those in the conventional reactor. Indeed, the development of a new reactor system is an excellent opportunity for carrying out biodiesel synthesis through ozonolysis, and confident that this reactor can improve the yield and conversion of the biodiesel product.

In this work, the biodiesel is synthesized by using sunflower oil as a model through transesterification-ozonolysis reactions. For having an optimum result, there are several steps before doing the main experiment: first, study the contacting mechanism and mass transfer on the gas-liquid-liquid reaction applications (chapter 1), and review the developed reactor technologies for gas-liquid-liquid systems (chapter 2). Second, the study of the characteristics of two-phase flow (gas-liquid) and three-phase flow (gas-liquid-liquid) in a microtube (chapter 3 and 4). Finally, the biodiesel synthesis experiments are conducted based on the best experimental conditions from the previous results (chapter 5). In a future work, the model could be implemented for biodiesel synthesis by using waste/virgin palm oil, which is abundant in Indonesia, as a feedstock.

This work is funded by the government of Indonesia within the framework of Indonesia Endowment Fund for Education (LPDP), and it was carried out at Laboratoire de Génie Chimique (LGC) Toulouse, France.

Literature

[1] P. By, “World ’ s largest Science , Technology & Medicine Open Access book publisher Biodiesel Production from Waste Cooking Oil.”

[2] S. B. Mohapatra, P. Das, D. Swain, S. Satapathy, and S. R. Sahu, “A Review on Rejuvenated Techniques in Biodiesel Production from Vegetable Oils,” vol. 6, no. 1, pp. 100–111, 2016.

[3] H. Yang, S. Chien, M. Lo, J. C. Lan, W. Lu, and Y. Ku, “Effects of biodiesel on emissions of regulated air pollutants and polycyclic aromatic hydrocarbons under engine durability testing,” vol. 41, pp. 7232–7240, 2007.

[4] M. G. Kulkarni and A. K. Dalai, “Waste Cooking Oil s An Economical Source for Biodiesel : A Review,” pp. 2901–2913, 2006.

[5] S. César, D. E. Werderits, G. Leal, D. O. Saraiva, and S. Guabiroba, “The potential of waste cooking oil as supply for the Brazilian biodiesel chain,” *Renew. Sustain. Energy Rev.*, vol. 72, no. November 2016, pp. 246–253, 2017.

[6] J. Fu, S. Q. Turn, B. M. Takushi, and C. L. Kawamata, “Storage and oxidation stabilities of

biodiesel derived from waste cooking oil," *FUEL*, vol. 167, pp. 89–97, 2016.

[7] EPC, "REGULATION (EC) No 1774/2002," *Off. J. Eur. Communities*, vol. OJ L 273, no. October 2002, p. 163, 2002.

[8] Z. Yaakob, B. N. Narayanan, S. Padikkaparambil, S. Unni K., and M. Akbar P., "A review on the oxidation stability of biodiesel," *Renew. Sustain. Energy Rev.*, vol. 35, pp. 136–153, 2014.

[9] D. Milan and D. Peal, "(12) Patent Application Publication (10) Pub . No .: US 2002/0187020 A1," 2013.

[10] M. F. Díaz, F. Hernández, O. Ledea, J. A. Gavín Sazatornil, and J. Moleiro, "1H NMR study of methyl linoleate ozonation," *Ozone Sci. Eng.*, vol. 25, no. 2, pp. 121–126, 2003.

[11] T. M. Baber, D. Graiver, C. T. Lira, and R. Narayan, "Application of catalytic ozone chemistry for improving biodiesel product performance," *Biomacromolecules*, vol. 6, no. 3, pp. 1334–1344, 2005.

[12] A. MAZUBERT, "Selection, Development and Design of a Continuous and Intensified Reactor Technology To Transform Waste Cooking Oil in Biodiesel and Biosourced Formulations," pp. 1–192, 2014.

[13] L. Riadi, A. Y. Widianto, E. Purwanto, A. Pono, and R. Theresia, "Synthesis of biodiesel from waste cooking oil by two steps process transesterification and ozonation," *J. Chem. Pharm. Res.*, vol. 7, no. 9, pp. 17–21, 2015.

Chapter 1

Gas-Liquid-Liquid Reactions: Contacting Mechanisms and Effective Process Technologies

Contents

The content of this chapter has been published in "Gas-liquid-liquid reactions: Contacting mechanisms and effective process technologies," Cataysis Today, no 346 (2020).

1.1. Introduction

Most industrially important chemical reactions are not carried out in a single phase. The vast majority of industrial reactions involve two or more phases, including liquids, gases and/or solids, which need to be put into contact. The different phases can play various roles in the reactor, not only as a source or storage of reactants to be converted, but also as catalysts or simply as a means to improve mixing or transport processes in the reactor [1].

This paper focuses on GLL multiphase reacting systems. There are two options to perform such three phase processes. The first consists in separating the mass transport and reaction steps in series in different devices, for example by initially transferring the gas to the liquid phase by absorption, then by carrying out the reaction between the two immiscible liquids in a reactor. The second option is to perform the three phase GLL reaction in a single step and a single device. The latter is an approach of processes intensification where several operations can be carried out in a multi-functional device.

The main challenge in performing combined mass transfer and reaction in multiphase GLL system is in contacting the chemical reactants present in the dispersed gas and dispersed liquid phases, which are totally separated by the continuous bulk phase and by two different interfaces (gas-liquid and liquid-liquid). The continuous phase may play different roles in the reaction depending on the application; it may contain a reagent or catalyst, or it could simply be used as a vector that enables the transport of a reactive species by absorption or diffusion from one phase to another.

Reactions involving a three-phase system are frequently encountered in the practice of chemical processes [2]. More specifically the applications of GLL reactions include hydroformylation of olefin and styrene [2][3][4][5], hydrogenation of α,β–unsaturated aldehyde [6], synthesis of hydrogen peroxide via the anthraquinone method [7][8], synthesis of hydrogen through H_2S splitting cycle [9], carboxylation of olefins [2][10], ozonolysis of biodiesel [11], ozonolysis of polycyclic aromatic hydrocarbons [12], ozonation of methyl linoleate [13], synthesis of biodiesel from waste cooking oil by transesterification and ozonolysis [14][15][16].Most of these reactions have been applied at industrial scale.

Identification of the contacting mechanisms between the gas and liquid phases is a real challenge for development of GLL reactions. In multiphase reactors, not only the reacting components must be efficiently mixed, but the conditions in the reactor must also allow the different components in the different phases to be able to come into contact and react. Depending on the physical and chemical properties of the system, the reaction then will take place either at the surface of a gas bubble (G/L interface), at the surface of a liquid drop (L/L interface) or within the continuous liquid bulk. If the selected reactor type or the steps used to put the gas and liquid into contact are not well adapted to the reaction mechanism, there will be a low yield of product caused by ineffective interphase contact within the reaction process. Furthermore, it may also result in the failure to obtain the desired product of the chemical reaction. In GLL reactions, the means in which the gas and liquid phases are contacted is strongly determined by the technological characteristic of the reactor, and therefore a good

understanding of the contacting mechanisms and mass transfer between phases is needed before designing or choosing a chemical reactor. Whilst there are a number of studies in the literature dealing with the demonstration and performance of GLL reactions, none of these identify in which phase the chemical reaction takes place, nor the limiting steps that control it. In addition, the available studies do not evaluate if the reactor type and phase contacting method are well adapted to the reaction being performed, or not. Indeed, identification of the limiting steps of a chemical process and designing the reactor and operating conditions such that the limitations can be minimized or even suppressed is the basis of process intensification.

Considering the wide application of GLL systems and the great opportunity for developing this field, the objective of this article is to understand multiphase contacting and mass transfer mechanisms that can occur between gas and liquid-liquid phases for a range of GLL reactions. It also aims at describing several simple models that allow various application of GLL reactions to be identified clearly. The objective of these models is provide useful information to aide the choice and implementation of the contacting method. Phase contacting is represented with different dispersed systems of varying solubility and diffusion limits of the species. Understanding the phase contacting model is necessary for the prediction of mass transfer mechanisms, as well as for the identification of the most appropriate contacting technology for the chemical reaction that allows the limiting steps to be minimized, thereby intensifying the process.

In the first part of this article, the contacting and mass transfer mechanisms between phases in GLL reactions are described by different models of dispersed systems. The second part of the manuscript present some applications of GLL reactions and discusses the obstacles and challenges for performing the reactions. Finally, different possible solutions that could improve GLL reaction performance are put forth, based on how the different phases should be contacted.

1.2. Phase contacting models for gas-liquid-liquid reactions

Three-phase chemical reaction systems always involve the partial dissolution or diffusion of a species from one phase to another. If not, the different species are not brought into contact and chemical reaction is not possible. Often, diffusion and reaction occur in the same region (i.e. either in the continuous bulk fluid or at the interface between two phases), and the rates of mass transfer and chemical reaction are so closely dependant that they have to be taken into account simultaneously. Studying the kinetics of GLL reactions requires a comprehensive knowledge of mass transfer, rate of reaction, solubility, and the fluid contacting mechanism [17][18]. In this section, the possible contacting mechanisms between different phases that are necessary to carry out a given chemical reaction will be analyzed. These mechanisms are explained through three models as described below.

For each model, the gas phase (G) is considered to be dispersed as bubbles in a continuous liquid phase. The two liquid phases are denoted as an oil phase (O) and an aqueous phase (W). Depending on both the physical and chemical properties of the liquid phases, as well as the choice of the contacting process and associated operating conditions, one of two types of dispersion can occur: either the oil phase phase is dispersed as droplets in the aqueous phase, resulting in a G-O/W system, or the aqueous phase is dispersed as droplets in

the oil phase, leading to a G-W/O system. Following this, three schematic models are proposed depending on where the reaction takes place:

- Model 1: the reaction mainly occurs at the L/L interface;
- Model2: the reaction mainly occurs at the G/L interface;
- Model3: the reaction mainly occurs within the continuous liquid bulk.

Three steps of the dispersion and consequent mass transfer and reaction processes are then systematically considered:

- Step 1 is the initial physical state of the three-phase system where the gas is dispersed into bubbles and the second liquid phase is dispersed into droplets in the liquid bulk;
- Step 2 describes the three-phase system considering the partial absorption or dissolution of the different species into different phases;
- Step 3 shows how and where the reaction takes place.

1.2.1. Model 1: reaction at the L/L interface

Fig. 1 shows the different processes that occur following model 1 where the reaction between components A, B and C takes place at the L/L interface. Initially either a G-O/W or G-W/O dispersion is formed. In this case, the gas is partially soluble in the continuous liquid phase, while the reactant in the droplets is not. As a result, component C, which is initially in the gas phase only, migrates into the continuous phase and bubble size decreases simultaneously. Henry's law is used to describe the equilibrium concentrations of species, which are distributed between phases. The concentration of C in the liquid phase increases until a certain limit depending on the gas solubility at the operating pressure and temperature. This leads to a possible reaction occurring between components A, B and C at the interface of the droplet.

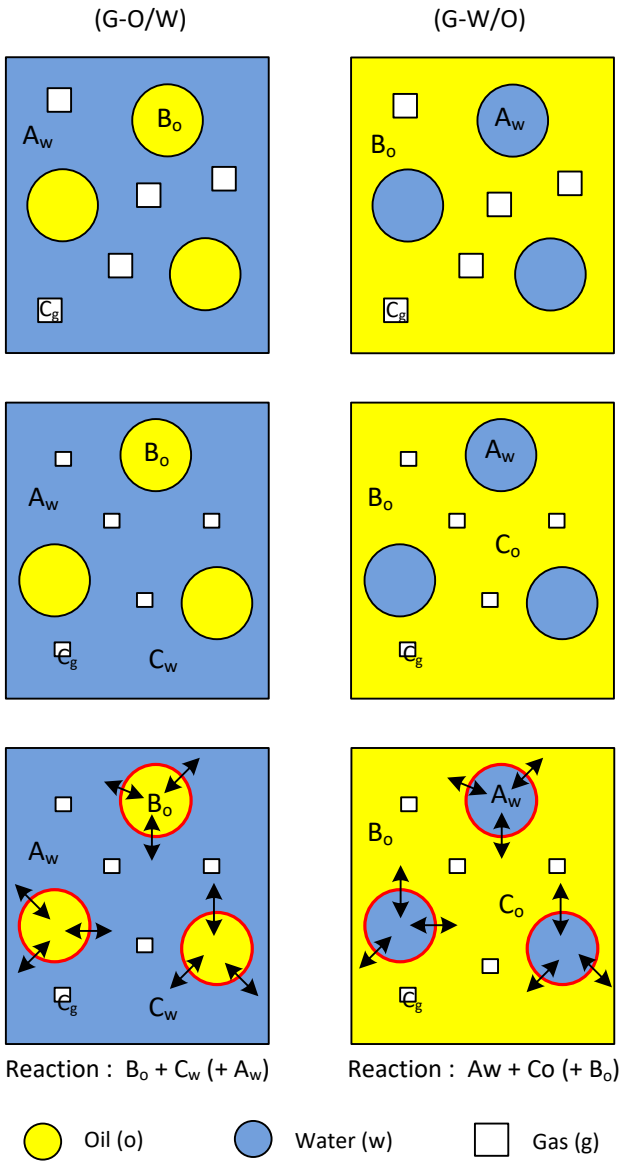

Fig. 1.Model 1: reaction occurring at liquid-liquid interface. (i) Initial state. A_w = component A in water; B_o = component B in oil; C_g = component C in gas. (ii) Partial dissolution of gas in the continuous phase. (iii) The reaction takes place in the liquid-liquid interface.

Figure 2 presents the gas mass transfer process in the case of a G-O/W system where the continuous phase is aqueous, where C_{go} tends to zero in the case of a chemical reaction consuming C at the L/L interface (in red).

An analogous mass transfer process occurs in G-W/O systems (the water and oil phases are just inverted); component C moves from the bubbles to the oil phase and then from the oil phase to the O/W interface where the reaction takes place.

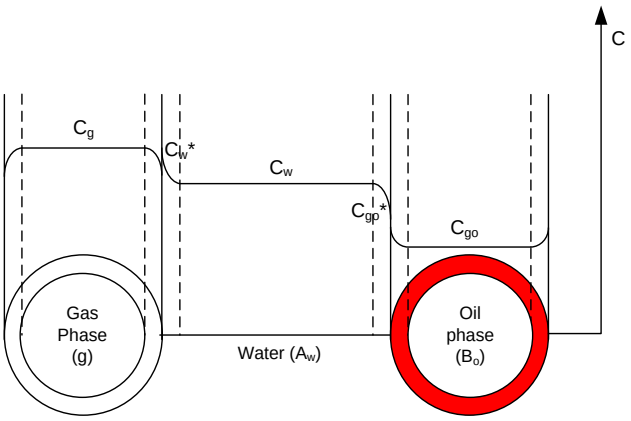

Fig.2. Schematic diagram of the mass transfer of component C from the gas bubble via the continuous water phase to an oil droplet and possible concentration profiles (model 1)

1.2.2. Model 2: reaction at the G/L interface

Fig. 3 shows the schematic diagram of the processes occurring in the case of a reaction occurring at the G/L interface in a three-phase system. In this configuration, the gas is not soluble in the continuous liquid phase. However, a partial miscibility of the liquid phases enables component B, which is initially present in the dispersed liquid phase, to migrate into the continuous liquid phase, resulting in a decrease of drop size until equilibrium is reached. Component B can then diffuse to the G/L interface, leading to a possible reaction between components A, B and C present in the continuous and gas phases.

In the case of a G-O/W dispersion, the concentration of oil in the continuous phase will depend on its solubility in the aqueous phase. Only the dissolved oil will react with the gas phase at the bubble interface, and possibly with other species or catalyst in the continuous liquid phase (Fig.4).

Similar phenomena occur in G-W/O systems where oil is the continuous phase. In contrast to the G-O/W system, in a G-W/O dispersion the component in the aqueous phase must be transferred from the water droplet to the gas phase via the continuous oil phase.

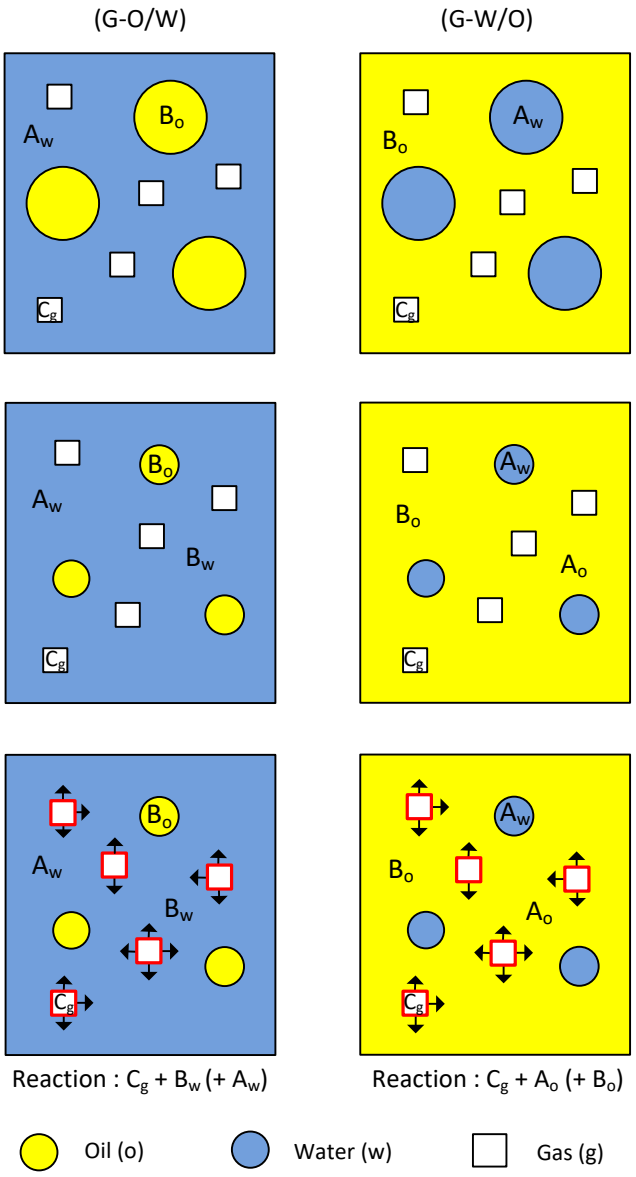

Fig 3. Model 2: reaction occurring at the gas-liquid interface. (i) Initial state. A_w = component A in water; B_o = component B in oil; C_g = component C in gas. (ii) Partial dissolution of dispersed phase in the continuous phase. (iii) The reaction takes place in the gas-liquid interface.

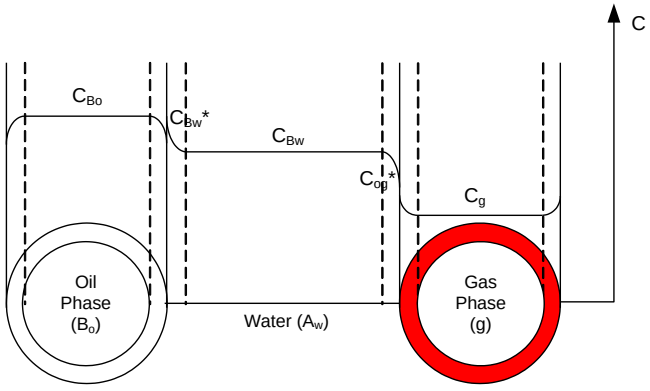

Fig. 4. Schematic diagram of the mass transfer from an oil droplet via water to a water/gas interface and possible concentration profiles (model 2)

1.2.3. Model 3: reaction in the continuous liquid phase

Fig. 5 describes three-phase systems where the reaction occurs in the continuous liquid phase. In this situation, both the gas phase and dispersed phase are partially miscible in the continuous liquid phase. The model is the combination of phenomena occurring in models 1 and 2, however the reactions principally take place in the continuous phase where all three components A, B and C, are present.

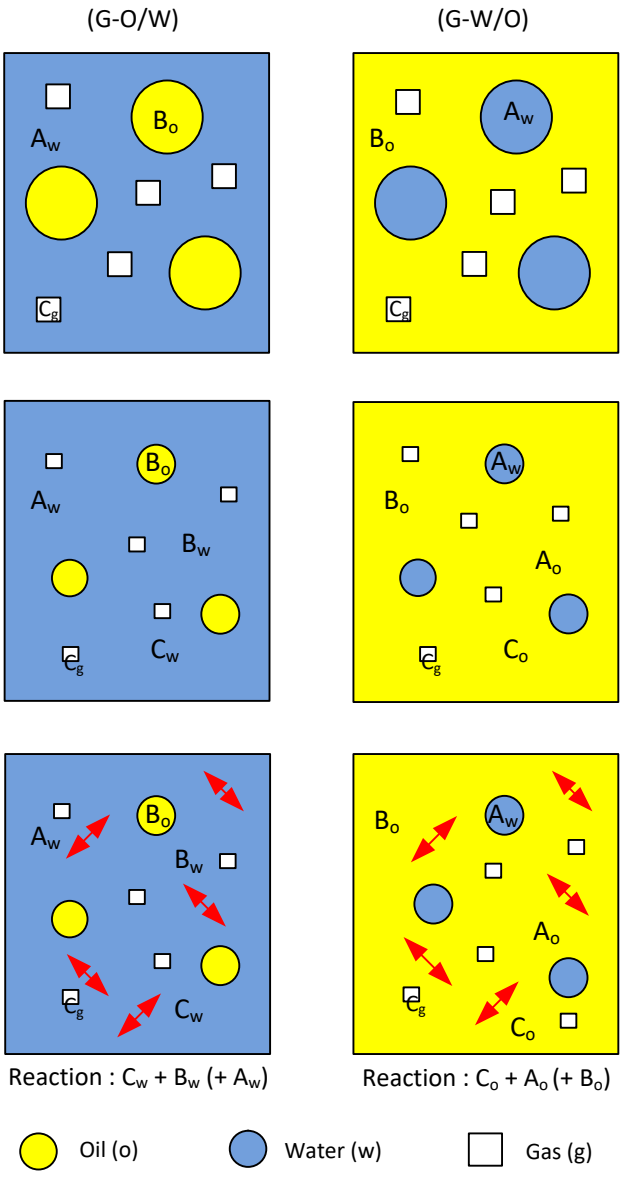

Fig 5. Model 3: reaction occurring at the continuous phase. (i) Initial state. A_w = component A in water; B_o = component B in oil; C_g = component C in gas. (ii) Partial dissolution of dispersion phase in the continuous phase. (iii) The reaction takes place in the bulk of continuous phase.

In G-O/W systems, both the gas bubbles and oil droplets decrease in size because of the partial dissolution of both oil and gas into the continuous aqueous phase. The dissolved oil and gas enhance both concentrations in this phase and subsequently, the reaction, essentially take

place in the bulk. The limiting step in this system is the mass transfer resistance in both the gas/water and oil/water interfaces. Identical phenomena occur in G-W/O systems. Gas and water droplets partially dissolve in the continuous oil phase, where the reaction takes place as indicated by the red arrows in Fig. 5.

1.3. Application to gas-liquid-liquid reactions

Some examples of GLL reacting systems are presented in Table 1. The physico-chemical properties of the system (e.g. solubility, volatility, density, viscosity, miscibility, interfacial tension, wettability with apparatus materials), the operating conditions (e.g. temperature, pressure, relative quantities) and the type of apparatus all play an important role in the type of multiphase system that will be generated, and therefore determine the limiting phenomena that occur [19][20].

1.3.1. Contacting scheme: model 1.

Table 1: Examples of gas-liquid-liquid reactions following model 1.

Gas-Liquid-Liquid Reactions	Apparatus	Operating Parameters	Result	Ref
Ozonation of Methyl Linoleate	Bubble column reactor	t_r= 5 h; Solvent: water, ethanol;Q_{O3}= 64 L/h	Yield reaction depends on the type of reaction medium. (model1 (G-O/W))	[13]
Synthesis of biodiesel from WCO (transesterification & ozonolysis)	Stirred Tank Reactor	Step 1. T_r=60 °C; WCO-methanol ratio= 1:5;V_r= 2 L; C_{cat}= 1.5 wt% NaOH; t_r= 1 h;N= 450 rpm Step 2. T_r= 20 °C; transesterification product-methanol ratio= 1:7;C_{cat}= 1,5wt%, 2 wt% H_2SO_4.	t_{opt}= 40 min, T_{opt}= 60 °C for transesterification, and 20 °C for ozonolysis (model1 (G-O/W))	[14]
Synthesis biodiesel using bio-based catalyst	Stirred Tank Reactor	Step 1. WCO:methanol ratio = 1:5;C_{cat}= 1.5 wt % KOH; V_r= 2 L; C_{O3}= 5.8 wt %;T_r=30 °C;N= 450 rpm; t_r= 3 h. Step 2. T_r= 60 °C, t_r= 2 h.	The optimum yield was reached using 1.5 wt% KOH & 17.3 wt % ash. (model1(G-O/W))	[15]
Ozonolysis of Used Cooking Oil using Ash Base-Catalyzed	Stirred Tank Reactor	Methanol:oil ratio = 1:5;C_{cat}= 0.5 wt% KOH; V_r= 1.5 L; C_{O3}= 5.8 wt%; T_r= 20, 30 °C;N= 300 rpm; t_r= 3 h.	Yield increase 8% (model 1(G-O/W))	[16]
Application of catalytic ozone for improving biodiesel product performance	Stirred Tank Reactor	Methyl soyate:methanol ratio = 1:28; C_{O3}= 6-10 wt%; T_r= -75 °C.	>90 % of double bonds was reduced after 2hr of ozonolysis. (model 1(G-O/W))	[11]
Ozonolysis of polycyclic aromatic hydrocarbons in participating solvent	Vessel	T_r= 20 °C; Solvent: water, methanol;t_r=5 min.	Conversion= up to 94% (model 1(G-O/W))	[12]
Ozonation of polycyclic aromatic hydrocarbons in oil/water emulsion	Stirred Tank Reactor	V_r= 3 L;N= 300-600 rpm; $C_{O3\ inlet}$ = 15.8-46 mg.L^{-1}	Ozonation is 1storder reaction, C_{PAH} controlled chemical reaction. (model 1 (G-O/W))	[21]

Hydroformylation of Allyl alcohol	Stirred tank Reactor (autoclave)	$T_{r,max}$= 80 °C; P_{max}= 5MPa; molar ratio $CO:H_2$ = 1:1; tr= 5 h; catalyst= HRh(CO)(PPh,) organic phase catalyst	Yield = 91% at T_r= 70 °C. (model 1 (G-O/W))	[22] [23] [24]

Reactions corresponding to model1, where reaction essentially takes place at the drop interface, include ozonolysis for synthesis biodiesel/alkyl ester compounds, ozonation of polycyclic aromatic hydrocarbons, as well as hydroformylation of allyl alcohol.

1. Ozonolysisfor biodiesel synthesis

Ozonolysis is an oxidation reaction between ozone, which is a strong an oxidizing agent, and an ethylenic compound to form ozonolysis products. Recently, ozone has been used for improving biofuel products produced from free fatty acids (FFA) in edible oils by the splitting double bonds in the carbon chain in unsaturated FAME (fatty acid methyl ester) to a saturated FAME [11][13][16]. The reaction scheme is as follows:

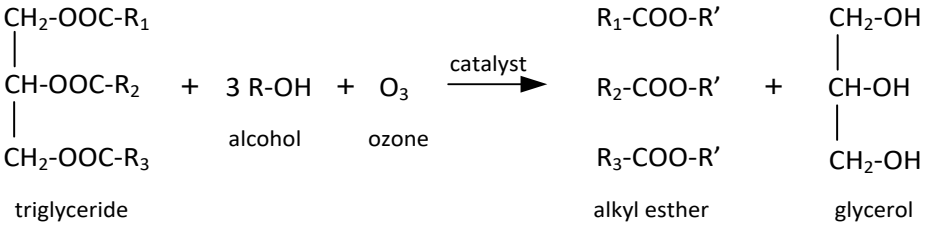

Fig.6. Ozonolysis scheme for biodiesel production

Baber et al. [11] studied the ozonolysis of methyl soyate, consisting of methyl palmitate, methyl stearate, methyl oleate, methyl linoleate, and methyl linolenate. The reaction took place at –75 °C using methanol and methyl soyate as reactants, dichloromethane (solvent) and triethylamine (catalyst). The ozone split the double bond of the carbon chain in the unsaturated methyl ester compound, which then reacts with methanol to give methyl and dimethyl esters products. In just two hours of reaction time, the total number of double bonds in the carbon chain was reduced by more than 90%. The role of the solvent dichloromethane in this reaction was also investigated. Without dichloromethane in the reaction mixture, the ozonolysis of methyl soyate do not take place. The poor solubility of methyl soyate in methanol at low temperature, which created a two-phase liquid mixture, may be the reason for this observation. At low temperature (–1.6 °C), metyl soyate/methanol solution separated in two liquid layers. Thus, when the ozonolysis reaction was performed at the low temperature (–75 °C), a separate liquid phase of methyl soyate most likely remained at the bottom of the reaction flask and was unaffected by ozone.

Indeed, there are several challenges associated with this reaction, including a very low reaction temperature (–75 °C), long reaction time and the large amount of methanol required for the reaction. High yield and conversion can be reached at a molar ratio methyl soyate to methanol of 1:28, whereas ideally 1 mol unsaturated fatty acid requires 3 mol of methanol to produce the alkyl ester compound, as shown in Fig. 6.

A similar study was carried out by Diaz et al. [13] who performed ozonolysis of methyl linoleate (99 %) in a bubble column reactor at room temperaure over 5 h. The effect of solvent

addition (water and ethanol) on the ozonolysis process was also investigated. In their work, the presence of water as a solvent promoted the reaction in different ways: carbonyl oxide reacted with water to form hydroxyl-hydro-peroxide, hydrogen peroxide and aldehyde compounds, and carbonyl oxide reacted with aldehyde compounds to give Criegee ozonide in minor amounts than with the organic solvent. In a more polar medium, greater amounts of ozonide and hydroperoxide are obtained. The yield of the ozonolysis product from unsaturated fatty acids therefore depends on the type of medium where the reaction takes place. The ozonolysis reaction followed the Criegee mechanism comprising of an electrophilic attack by ozone of the double bonds of the carbon chain. It produced 1, 2, 3 trioxolane/primary ozonide, which rapidly decomposed to form carbonyl oxide /zwitterions and carbonyl compounds (aldehyde/ketone). The greatest challenge encountered to achieve high yields of product is mainly related to the solubility of ozone in the liquid solution [25][26]. Riadi et al. [14] also faced similar difficulties to achieve high yields of the ozonolysis reaction. In their study, biodiesel was produced from waste cooking oil (WCO) through simultaneous transesterification–ozonolysis reactions in a stirred tank reactor. The effect of operating parameters (e.g. temperature, type and percentage of catalyst, molar ratio of methanol and oil, stirring speed) were also investigated. The transesterification reaction produced long-chain methyl esters and the ozonolysis reaction gave a short chain methyl ester, resulting from breaking the double bond of the unsaturated fatty acid. However, the reaction yield was low. The challenges associated with performing these reactions are numerous: different temperatures and catalyst types are required to achieve optimum yields of both reactions, the time needed to achieve high yields is very long and most importantly, the low solubility ozone in the solution limits the reactions. Following the schematic contacting mechanism and mass transfer models presented previously, the ozonolysis reaction follows Model 1 (G-O/W). This can be explained by several facts. Firstly, ozone has greater solubility in an organic solvent than in edible oil [27][28]. Secondly, ozone is much more reactive with carbon compounds [29][30] that have double bonds than those with a single bond [11][31]. For example, the ozonolysis reaction of waste cooking oil (WCO) in Table 1 consists of three-phases: methanol, FFA and ozone [14]. Ozone partially dissolves in methanol and has poorer solubility in WCO. The contact between methanol, which contains dissolved ozone, with WCO, which contains triglycerides, promotes ozonolysis. This mechanism is in agreement with the Criegee mechanism [11][13] where the ozone reaction with methanol progresses more slowly than that with the reactant with double bonds [32]. The mass transfer steps consist in the dissolution of ozone into methanol followed by the transfer of methanol Table 1 Examples of gas-liquid-liquid reactions following Model 1. to the oil phase. It is expected that the ozonolysis reaction takes place at the methanol/oil interface.

2. Ozonation of polycyclic aromatic hydrocarbons

Kornmuller and Wiesmann [21] studied the reaction kinetics of the ozonation of polycyclic aromatic hydrocarbons in an oil/water system in a stirred tank reactor and aimed at improving the gas/water and water/oil mass transfer in order to reduce ozone consumption. With increasing ozone inlet concentration, the ozone mass transfer flux over the interface gas/liquid increased. By increasing stirrer rotational speed, smaller ozone bubbles were

formed and were better dispersed in the reaction mixtures, thereby increasing the volumetric mass transfer coefficient. According to Henry's law, the partial pressure of ozone is directly proportional to the dissolved ozone concentration. At a fixed partial pressure, higher inlet ozone concentrations lead to larger concentration gradients at the methanol/oil interface and consequently mass transfer into the oil phase is improved.

3. Hydroformylation of allyl alcohol

Several authors [22][23][24] studied hydroformylation of allyl alcohol by using a n-heptanol-water mixture as a solvent. The catalyst is soluble in the organic phase and the product separates into the aqueous phase, such that there is an effective use of catalyst. HRh(CO)(PPh3)3 was used as a catalyst to synthesize 4-hydroxybutiraldehyde (4-HBA) and 2-metil-3-hydroxypropionaldehyda (2-MHP) from allyl alcohol compound. The reaction is as follows (Fig. 7):

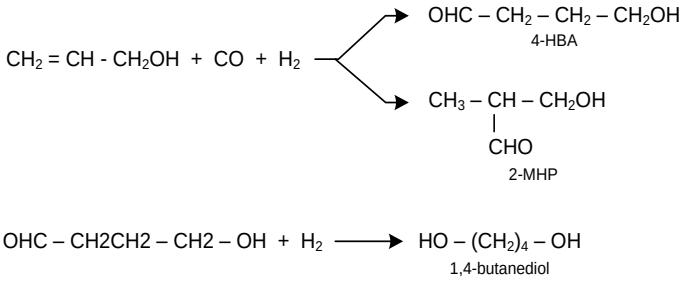

Fig. 7.Hydroformylation scheme of allyl alcohol [24]

Three phases are involved hydroformylation reactions: CO and H_2 are the gas phase, $HRh(CO)(PPh_3)_3$ is dissolved in both the organic phase and in water. The reaction follows the Model 1 (G-O/W). In this reaction, the catalyst allyl alcohol, which is soluble in the organic phase (n-heptanol), and water were introduced into the stirred tank reactor (autoclave) at 70 °C and 5 MPa for 5 h with CO/H_2 molar ratio of 1:1. The reaction occurs at the interface of the organic phase and the products then dissolve into the aqueous phase. The product and the organic phase, which contains the catalyst, are easy to separate and therefore the catalyst can be recycled with a new amount of allyl alcohol to start a new reaction. The use of a GLL system in this synthesis has proven good catalyst performance for the hydroformylation of allyl alcohol, leading to 91% yield. Another advantage is related to the product separation. However, the presence of aldehyde product in the organic phase will potentially trigger catalyst deactivation because aldehyde interacts with $HRh(CO)(PPh_3)_3$, which deactivates it.

1.3.2. Contacting scheme: model 2.

Some examples of multiphase reactions that follow model 2 are described in Table 2. They consist of hydroformylation of olefin compound, such as propylene and styrene, and the synthesis of pivalic acid from iso- and tert-butanol.

Table 2. Examples of gas-liquid-liquid reactions following model 2.

Gas-Liquid-Liquid Reactions	Apparatus	Operating Parameters	Result	Ref
Hydroformylation of olefin	Tubular reactor with static mixer	C_{cat}= 30 wt% TPPTS, 800 wt, ppm Rh; L_r= 3 m; D_{in}= 17.8 mm; V_r= 0.561 L; t_r= 5s;T_r=40 °C.	Selectivity= 99%. (model 2 (G-O/W))	[3]
Hydroformylation of styrenes	Mini channel	Molar ratio CO:H_2 = 1:1; P= 25 bars; T_r= 65 °C.	Conversion = 97%; Yield = 94%. (model 2 (G-O/W))	[5]
Carbonylation of benzylchloride	Stirred tank Reactor	T_r= 50 – 60 °C; P= 0.1 MPa using organo metallic phase transfer catalysis	Hydrolysis of phenyl acetyl complex is the rate determining step. (model 2 (G-W/O))	[33]
Carbonylation of azadienes	Stirred tank Reactor	T_r= 25 °C; t_r= 6 h; P= 1 atm using organo metallic phase transfer catalysis	Yield allyl amide= 65%. (model 2 (G-W/O))	[34]

1. Hydroformylation of olefin

Hydroformylation is defined as a reaction between olefin compounds with carbon monoxide and hydrogen to produce aldehyde compounds. The olefin compound is an unsaturated hydrocarbon compound having a double bond between the carbon atoms. The reaction has been applied at industrial scale (e.g. the Rhône-Poulenc process); typically, the industrial scale process is performed in a multistage stirred reactor with an efficient heat exchanger due to the high exothermic nature of the reaction. Several researchers have studied the synthesis of aldehyde by hydroformylation reactions in order to improve the process. Weise et al. [3] conducted experiments on the hydroformylation of olefins according the following chemical reaction using continuous flow equipment:

$$H_2 + CO + \text{olefin} \xrightarrow{\text{catalyst}} R - CHO$$

The reaction was performed in a tubular reactor filled with static mixers (Sulzer SMV) [3]. The olefin is partially miscible in water and the homogeneous catalyst solution used (30 wt% TPPTS, 800 wt. ppm Rh dissolved in pure water) is in excess with respect to the reactants. Firstly, the catalyst solution flow was fed into the olefin flow; this liquid-liquid flow was then mixed with the gas flow (H_2 and CO), which was fed into the reactor. The aldehyde product was purified from the catalyst using a settling process. Subsequently, the separated catalyst was directly recycled to the reactor to perform the chemical reaction again.

Purwanto and Delmas [4] performed a similar study on the hydroformylation of 1-octene compound (classified as higher olefin and alpha-olefin) using a catalyst [RhCl (1.5-COD)]$_2$/TPPTS in the aqueous phase. 1-octene is partially miscible in water with very low solubility and is the limiting step in this reaction process. The solubility of 1- octene in the homogeneous catalyst therefore needs to be increased before reacting with H_2 and CO gas, in order to obtain a satisfactory yield. Ethanol was therefore added as a co-solvent to enhance octene solubility in the aqueous phase (factor 104 compared with octane solubility without the

addition of the co-solvent). However, the presence of ethanol in the aqueous phase caused the formation of acetal, an undesired product. To prevent this, buffer solutions (Na_2CO_3 and $NaHCO_3$) were added to the homogeneous catalyst phase.

These hydroformylation reactions between olefin/1-octene, TPPTS and Rh in water, H_2 and CO gas follow the contacting Model 2 (G-O/ W). However, it should be noted that when the reaction is carried out at higher pressure, for example in an autoclave reactor, the solubility of hydrogen gas and carbon monoxide in the liquid phase increases; the gas is then partially dissolved in the continuous phase and the reaction stages will then follow the mechanism of Model 3 (G-O/W) (see Table 3).

The challenges in performing this reaction were related to the partial miscibility of the olefin in the water phase that contains the homogeneous catalyst (TPPTS and Rh), as well as the low solubility of hydrogen and carbon monoxide gas in the water phase [3][5][35]. Typically, in the previous works, reactions were performed in stirred tank reactors with gas-to-liquid or liquid-to-liquid mass transfer limitations.

For these reasons, Wiese et al. [3] and Purwanto and Delmas [4] attempt to obtain an optimal reaction product by carrying out the hydroformylation in a tubular reactor equipped with static mixer to increase the surface area between phases or in an autoclave reactor to increase in the solubility of CO and H_2 gas in solution.

2. Carbonylation of benzylchloride and azadienes

The carbonylation reaction, shown in Fig. 8, was performed using two types of solvent, including a non-polar organic solvent of diphenyl ether and an aqueous alkali ($NaCo(CO)_4$/Bu_4NBr/aq.NaOH) at 0.1 MPa and temperature 50–60 °C [33]. The reaction product was phenyl acetic acid compound soluble into the aqueous phase.

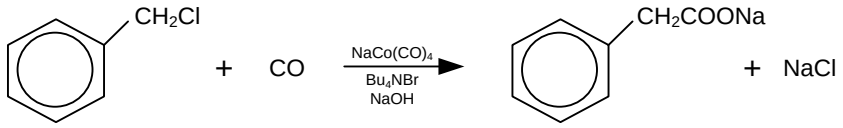

Fig. 8.Carbonylation of benzylchloride.

The catalyst is referred to a phase transfer catalyst (PTC) and plays an important role in facilitating the transport of cobalt carbonyl salt from the aqueous to organic phases. In the organic phase, cobalt was present as cobalt anion and the reaction between the cobalt anion, benzyl chloride and CO gas produced phenyl acetyl complex as an intermediate product. A hydrolysis of phenyl acetyl complex was then performed at the organic-aqueous interface forming phenyl acetyl acid as the final product. At the end of reaction, phenyl acetic acid moves from the organic phase to the aqueous catalyst phase. Based on the previous work, it was observed that the kinetics of the hydrolysis of phenyl acetyl complex is the rate determining step in the synthesis of phenyl acetic acid [33]. Three phases are involved in this synthesis: CO (gas phase), benzyl chloride (organic phase), and NaCo(CO)4/Bu4NBr/ aq. NaOH (aqueous phase). The reaction mechanism hence follows the mechanism of Model 2 (G-W/O).

Alper and Amaratunga [34] studied the carbonylation of azadienes with a phase transfer catalyst comprising benzene, water or aqueous NaOH, benzyltriethyl ammonium chloride and

cobalt carbonyl as a metal catalyst. The reaction took place in several steps. Firstly, CO gas flows into a mixture of distilled water, benzene and benzyltriethyl ammonium chloride (aqueous phase catalyst); secondly, cobalt carbonyl was added along with methyl iodide; thirdly, this mixture was stirred and azadiene was added with carbon monoxide. The reaction was able to produce allyl amide compound with 65% yield in 6 h at a temperature 25 °C and 1 atm pressure. A lower yield of 40% was obtained with a shorter reaction time (2 min) and a higher temperature (60 °C).

The three phases involved in this reaction are azadiene soluble in benzene (organic solvent), methyl iodide soluble in water, and CO gas. The carbonylation reaction takes place in the organic phase similar to the carbonylation of benzylchloride above but the reaction product is in the aqueous phase [34]; this reaction follows the mechanism of Model 2 (G-W/O).

1.3.3. Contacting scheme: model 3.

Several multiphase reactions following model 3, including hydrogenation reactions, peroxide hydrogen synthesis, hydrogen synthesis and carboxylation, are presented in Table 3.

Table 3: Examples of gas-liquid-liquid reaction following model 3.

Gas-Liquid-Liquid Reactions	Apparatus	Operating Parameters	Result	Ref
Hydrogenation of α,β-Unsaturated Aldehydes	Microchannel	D_{cp}=500, 750, 1000 µm; L_{cp}= 3, 6, 12 m; T_r= 60 °C; PH_2=1 – 2 MPa	Volume rate of catalyst phase affect the overall reaction rate & conversion. (model 3 (G-W/O))	[6]
Synthesis of H_2O_2 via anthraquinone method	Coupling process (Oxidation-extraction)-mini-channel	The dimension of flow channel was 15mm x 2 mm x 3 mm; micro filtration membrane D_{pore} =5 µm, thickness = 0.3 mm; T_r=50 °C; PO_2=200 & 300 KPa	Conversion= 100% in t< 6.5 s at T= 50 °C. Mass transfer rate significantly increases by the addition of gas phase. (model 3 (G-O/W))	[7]
Synthesis of H_2O_2 via anthraquinone method Coupling process (Oxidation-extraction)	Stirred tank Reactor	V_r= 1 L; Catalyst:anthraquinone working solution; T_r= 50 °C;PO_2= 1 atm; V_0/V_w= 200:450; $N_{agitation}$= 263 rpm; C_{EAQH2}= 218 mol.m^{-3}; batch system.	C_{H2O2} (product) = 93 mol m^{-3} in 100 min. (model 3 (G-O/W))	[8]
Synthesis of Hydrogen through H_2S splitting cycle	Stirred tank reactor	V_r= 300 ml; $N_{agitation}$= 100-200 rpm; T_r= 22 °C; C_{iodine}= 0.1462 mol/L; molar ratio toluene/water=80/0.7	effective interfacial area= 4.03 m^2 (at 100 rpm) (model 3 (G-O/W))	[9]
Carboxylation of olefins	Packed bed reactor	$C_{styrene}$= 4 M; T= 100 °C; t_r= 40 min;C_{cat}=2 mol%, C_{co-cat} = 10 mol%	Conversion= 100%. (model 3 (G-O/W))	[10]
Synthesis of Pivalic Acid from Iso- and tert-butanol	Stirred tank Reactor (autoclave)	gas-inducing system (ring); 6-blades Rushton turbine; P_{max}= 60 bars; $N_{agitator}$= 1800 rpm	Increasing %volume of 2nd liquid will increase in the yield (84%). (model 3 (G-O/W))	[36] [18]
Hydroformylation of 1-octene	Stirrer tank reactor (batch-autoclave)	V_r= 6x10^{-4} m^3; P_r= 1.5–2.5x10^{3}kPa, T_r= 333-343 K; $N_{agitation}$= 23.3 rps; cat= $[RhCl(1.5\text{-}COD)]_2$ with TPPTS in water.	Selectivity= 80%; first order reaction; reaction rate increased with the H_2 partial pressure. (model 3 (G-O/W))	[4]

1. Hydrogenation of α,β-unsaturated aldehydes

Onal et al. [6] carried out the hydrogenation of α, β-unsaturated aldehyde solution in aqueous multiphase catalysis Ru (II)-TPPTS using a microreactor with a diameter in the range of 500–1000 µm and length from 3.6 m to 12 m. The reaction took place according to the following reaction equation (Fig. 9):

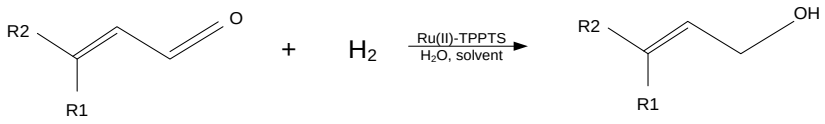

Fig.9. Hydrogenation of α,β – unsaturated aldehyde [6]

The three-phase system consists of an aqueous catalyst phase, an unsaturated aldehyde and hydrogen gas. To carry out the chemical reaction, unsaturated aldehyde and aqueous catalyst were fed through in T-junction resulting in dispersed liquid-liquid flow. At this point, hydrogen was not mixed with the liquid phases, but it was injected into liquid dispersion via a second T-junction. A multiphase dispersed flow pattern as shown in Fig. 10 was formed. The reaction took place at 60 °C and the partial pressure of the hydrogen gas (corresponding to the total pressure in the capillary tube) was in the range of 1.0–2.0 MPa.

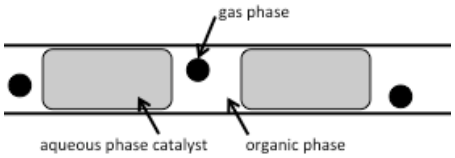

Fig. 10. Flow pattern of GLL in channel [6]

The main challenge for performing this reaction in a microreactor is related to the generation of a regular dispersion of the liquid and gas in the continuous phase [37][38]. The conversion rate was significantly low (around 10%) due to the short mean residence time (2–3 min).

Hydrogen gas has very low solubility in the aqueous catalyst phase but shows greater solubility in the organic phase [35]. Since the organic phase has a higher affinity for PTFE (micro channel material), the inner wall of the channel was completely wetted by the organic phase, not the aqueous phase. As a result, when hydrogen was fed to the liquid-liquid phase mixture it formed bubbles in the organic phase (Fig. 10). An increase in the volumetric flow rate of the aqueous phase increased the Reynolds number and the overall mass transfer coefficient [6]. Mass transfer rates at the G/L interface greatly determine the hydrogenation rate and are important to optimize the overall reaction rate. In their study, Onal et al. [6] revealed that an increase up to 1.4 ml.min−1 in the hydrogen flow rate enhanced the rate of the hydrogenation reaction, however beyond this value the reaction rate decreased. Beyond a certain value, an increase in hydrogen flow rate leads to an increase of gas bubbles in the organic phase and this reduces the effective reaction volume and mean residence time in the capillary tube. Another factor that emerges as a limiting step in this reaction is the low value of the activation energy (Ea) when the reaction temperature is high. This condition is triggered by

the limited mass transfer occurring in L/L interface, due to the low solubility of water in the organic phase (1.0 g.L–1).

This reaction follows the Model 3 (G-W/O), where the unsaturated aldehyde is the organic phase, the catalyst is in the aqueous phase and hydrogen is gas. The gas solubility in the organic phase is greater than in the catalyst phase, the bubble size therefore decreases and the reaction takes place in the bulk of organic phase.

2. Synthesis of H_2O_2 via anthraquinone method

Another example of a reaction following Model 3 is the synthesis of hydrogen peroxide. Hydrogen peroxide is one of the best 'green' oxidation reactants and it is widely used in the chemical industries and environmental protection.

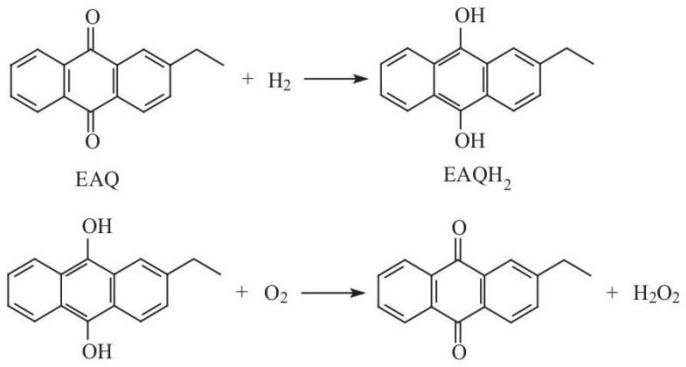

Fig.11. Two-stages of hydrogen peroxide synthesis [8]

Synthesis of hydrogen peroxide was performed via two steps (Fig. 11): firstly, 2-ethyl-anthraquinone (EAQ) dissolved in the organic solvent is hydrogenated to form 2-ethyl-anthra-hydroquinone ($EAQH_2$). This is followed by a reactive extraction process, whereby the oxidation of $EAQH_2$ and the extraction of hydrogen peroxide from the anthraquinone solution take place simultaneously. The three-phase system involved in the second step process included oxygen gas, organic solvent (anthraquinone working solution) and deionized water. The anthraquinone solution was a mixture of 2-ethylanthraquinone, trioctyl phosphate and an aromatic C_9–C_{10} compound with a concentration of 120 $g.l^{-1}$ anthraquinone and a volume ratio of C_9–C_{10} to the trioctyl phosphate of 3:1. The reaction rate is faster than the extraction rate, so the e ffects of both reaction and hydrogen peroxide mass transfer on the extraction rate are non-negligible [8]. A means for intensification is the integration of the chemical reaction and separation processes in a single unit. However, it is not easy to develop such integrated processes in industrial practice. The reaction and mass transfer between multiple phases (gas-liquid and liquid-liquid) play an important role in the rate limitations of the process [7][8]. The oxidation rate of $EAQH_2$ itself is strongly influenced by the mass transfer of oxygen through the liquid film and the rate of chemical reaction. Oxygen consumption also varies with volumetric ratios of anthraquinone solution to oxygen, stirring speed and initial concentration of $EAQH_2$. Tan et al. [7] explained that there are two main requirements to improve the efficiency of oxidation and extraction performance: prevent the partial pressure of O_2 from becoming too low and ensure significant residence time. This reaction was performed using a micro-dispersion system that employs a 5 µm pore size microfiltration membrane to disperse the

fluids. The contacting mechanism of the three phases involved in the reaction follow Model 3 (G-O/W). Oxygen gas and $EAQH_2$ are both partially soluble in the organic solvent [37], whilst the reaction between oxygen and the $EAQH_2$ occurs in the bulk of organic phase.

3. Synthesis of Hydrogen through H_2S splitting cycle

Li et al. [9] studied the effect of operating parameters (i.e. the volume ratio of toluene/water, stirring speed and temperature) on the synthesis hydrogen via the H_2S splitting cycle. The reaction scheme is as follows:

$$H_2S + H_2SO_4 \longrightarrow S + SO_2 + 2H_2O \qquad (H_2S \text{ Oxidation})$$
$$2H_2O + I_2 + SO_2 \longrightarrow H_2SO_4 + 2HI \qquad (\text{Bunsen reaction})$$
$$2HI \longrightarrow H_2 + I_2 \qquad (\text{HI decomposition})$$

The Bunsen reaction is performed at room temperature and the reaction starts with the appearance of two phases, which are poorly soluble. In the process, water is a solvent for the SO_2 gas to form a reducible bisulfate anion, however it is also used to ionize HI and H_2SO_4 compounds. Toluene is employed as an organic solvent for I_2. In the next step, SO_2 gas is fed into the reactor; the contact of SO_2 gas and the liquid triggers the dissolution of gas in both liquids, however the dissolved SO_2 concentration is greater in the aqueous phase than in the I_2-toluene solution. At the same time, I_2 is transferred from the I_2-toluene solution to the aqueous phase. The contact between SO_2 gas, which is dissolved in the aqueous phase and I_2 initiates the hydrogen producing reaction. Due to the very low solubility of water in toluene, the Bunsen reaction in toluene can be neglected. The Bunsen reaction mechanism in aqueous phase is shown as follows:

$$SO_2 + H_2O \rightleftharpoons H^+ + HSO_3^- \qquad (\text{step 1})$$
$$H^+ + HSO_3^- + I_2 + H_2O \rightleftharpoons H_2SO_4 + 2HI \qquad (\text{step 2})$$

This mechanism is supported by the results of: firstly, SO_2 was a stable gas with a small reducing capability; secondly, iodine consumption was not observed after contact with the SO_2 gas in the I_2- toluene solution; thirdly, the SO_2 gas dissolved in water, thereby generating the formation of H_2SO_4 or a hydrogen bisulphite solution, which has a stronger reduction ability.

The Bunsen reaction is largely determined by the mass transfer of SO_2 from the gas phase to the liquid phase. The reaction can be improved in several ways, including enhancement of the stirring process. Higher stirring rates have a positive impact on the reaction rate because it improves mass transfer between water and toluene, since it creates higher interfacial area between the phases. As a comparison, the reaction rate 1.5 times greater at a stirring speed of 300 rpm than with 100 rpm. Other ways to increase the reaction yield is by increasing the volume ratio of the toluene to liquid mixture, by increasing the partial pressure of SO_2, and by increasing the iodine concentration in the I_2- toluene solution.

The contacting mechanism between SO_2 gas, I_2-toluene solution and water in this synthesis follows Model 3 (G-O/W). SO_2 gas and I_2 are both partially soluble in water. The synthesis of hydrogen takes place in the bulk of continuous water phase.

4. Carboxylation of olefins

The synthesis of cyclic organic carbonate was performed via oxidation and carboxylation reactions [10]. Several possible reactions schemes exist for this synthesis as shown in Fig. 12; the sequential epoxidation-carboxylation (Fig. 12(a)) scheme is the most probable.

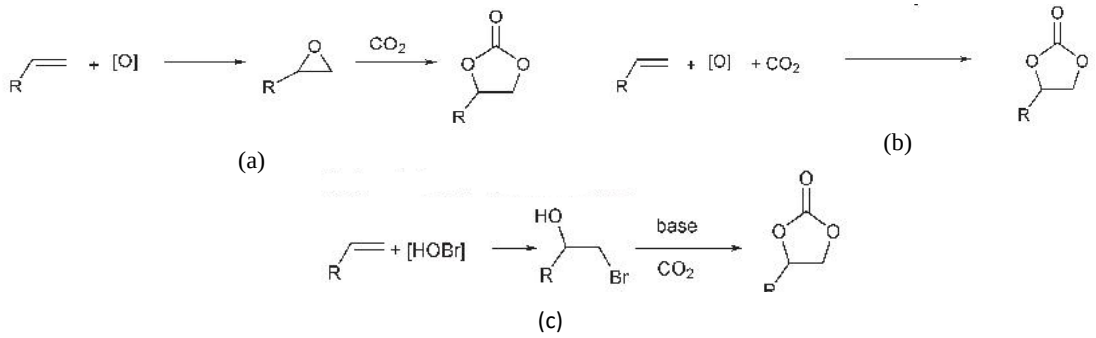

Fig.12. Reaction strategies for the synthesis of cyclic organic carbonate (a) Sequential oxidation and carboxylation, (b) Simultaneous oxidation and carboxylation, (c) Carboxylation via oxy-bromination [10].

The main challenge for performing both reactions simultaneously is related to the specific needs of each reaction. Hydrogen peroxide is usually chosen as an oxidant because epoxidation will produce water only as a by-product. However, hydrogen peroxide is not an appropriate oxidant for carboxylation, which typically requires a Lewis base as a catalyst. Moreover, the presence of water as a by-product in the system triggers a two-phase epoxidation reaction because olefin is hydrophobic. In order to reach sufficient reaction yield, a long reaction time is required due to the fact that CO_2 is completely soluble in water (2000 mg/L) [39] and therefore mass transfer, from water (aqueous phase) to olefin (organic phase), takes much longer. The rate of mass transfer in this stage is hence the limiting step. The reaction strategy chosen above involved methyltrooxorhenum (MTO) as a catalyst to epoxidize olefin (styrene) to styrene oxide, and then an amino trisphenolate complexed aluminum catalyst with a tetrabutyl ammonium iodide (TBAI) co-catalyst to convert styrene oxide into styrene carbonate. The study focuses on the carboxylation reaction involving a three-phase GLL system comprising a catalyst and co-catalyst that are soluble in the solvent, styrene oxide and CO_2 gas. As for the epoxidation reaction, carboxylation is conducted via the following steps: first, styrene and oxidant were introduced into the epoxidation reactor to produce the epoxide compound. The product was then separated from the excess of hydrogen peroxide entering the carboxylation reactor. The aqueous phase, which contains the hydrogen peroxide, and the epoxide product in the organic phase are then separated. Next, the organic phase is mixed with a Lewis base catalytic system; this solution is then mixed with CO_2 gas. A segmented gas liquid flow then entered the carboxylation reactor.

Sathe et al. [10] used a packed bed flow reactor, which offers enhanced interfacial area and also safer control of the reaction. It also eliminated the needs for a pressurized vessel to maintain constant pressure in headspace above the reaction mixture. The use of a flow reactor was an appropriate solution for the sequential carboxylation epoxidation using mutually incompatible reagents, which are introduced in the reactor at different points (spatially and temporally). This sequential operation enabled a yield of styrene oxide-to-styrene carbonate of 88% for a residence time of 30–40 min. This synthesis follows the contacting Model 3 (G-O/W)

between CO_2 gas, a Lewis base catalyst and an organic compound. The CO_2 gas and the Lewis base catalyst are partially soluble in the organic compound. The combination of the cyclic organic carbonates occurs in the bulk of the organic phase.

5. Synthesis of Pivalic Acid from Iso- and tert-butanol

The synthesis of pivalic acid is generally characterized by the presence of two liquid phases and a gas phase with a parallel/consecutive reaction scheme where both the main and side reactions are fast. The oligomerization side reaction and the consecutive reaction consists of isomerization, disproportionation and carbonylation, producing a higher acid product with a longer carbon chain.

In the Koch synthesis [36], pivalic acid can be produced from iso and tert-butanol with CO gas and water as reactants, using sulfuric acid as a catalyst. 2-methyl butanoic acid is the main by-product.

$$\underset{\text{Isobutanol}}{(CH_3)_2CHCH_2OH} + CO + H_2O \longrightarrow \underset{\text{2-methyl butanoic}}{(CH_3)_3CCO_2H}$$

Brilman et al. [36] used an autoclave reactor at high operating pressure to obtain a reaction yield of 84% for the synthesis of pivalic acid from iso- and tert-butanol. The use of the autoclave reactor pressurized up to 60 bars and equipped with a gas-inducing impeller at high stirring speed (1800 rpm) enabled an increase in mass transfer and improvement of gas solubility during the reaction. The selectivity of pivalic acid was increased by reducing acidity and temperature, and by increasing the pressure of CO.

The technological challenges related to this reaction are similar to the previous case and are related to the solubility of the three separate phases, which must be in contact for the reaction to occur. The droplets of iso- and tert-butanol dissolve partially in the continuous phase, however the gas does not dissolve in the droplets or the continuous phase. In Models 1, 2, and 3, it is assumed that there neither the dispersed or continuous liquid phases are soluble in the gas phase. In Model 3, the partial solubility of the liquid and gas phases in the continuous phase is the decisive step. It is therefore evident that by increasing the solubility of the dispersed phases in the continuous phase, the reaction occurring in the bulk continuous phase will be enhanced.

Brilman et al. [18] also studied the synthesis of pivalic acid/carboxylic acid using other reactants comprising CO gas, iso-butene, tertbutanol, catalyst solution and heptane, as a second immiscible liquid. This was carried out under pressure (40 bars) in an autoclave reactor for 1 h using an acid catalyst H_2SO_4 96 wt%. The CO gas, iso-butene and tert-butanol dissolved in heptane were firstly contacted with the H_2SO_4 catalyst. CO, iso-butene, and tert-butanol were then transported to the catalyst phase due to partial solubility. The reaction then took place in the catalyst phase and the product formed was extracted by heptane.

The effects of reactant feed rate, location of the gas injection, stirring rate and the presence of an immiscible liquid phase on the total acid yield and product distribution were studied. At low reactant flow rate, oligomer formation is suppressed and the selectivity of pivalic acid increases, whilst the selectivity of acid products with longer carbon chains decreases. The solubility of CO into the catalyst phase is still relatively low (1.5×10^2 mol/m^3 at 40 bars and 293 K) and therefore only yields 25% of pivalic acid. To achieve higher yields, two

points must be considered: the flow rates of CO gas and alkene, and the mass transfer of CO gas. In addition, acid yield will increase with increasing agitation speed. An alternative choice for the second liquid in the system also has positively impacts reaction yield. In this study, the yield and selectivity of pivalic acid both depend on the volume of heptane used; higher volumes of heptane enable an increased capacity of CO gas dispersion. Heptane was chosen as an immiscible organic liquid phase since CO solubility in heptane is 3.5 times greater than in the catalyst solution [35], and CO gas does not react with heptane. The reaction of carboxylic acid follows Model 3 (G-O/W) with CO as the gas phase, a hydrocarbon soluble in heptane as the organic phase and an acid catalyst as the aqueous phase.

1.4. Derivation of mass transfer equations

In gas-liquid-liquid systems, the volumetric mass transfer coefficient ($k_L.a$) is the important parameter for evaluating the performance of such multiphase reactors. Two models exist for describing the gas-liquid-liquid mass transfer mechanism, by taking the spreading coefficient, S into consideration. The spreading coefficient, S, for gas-oil-water is:

$$S= \sigma_{wg} - (\sigma_{og} + \sigma_{ow}) \quad (1)$$

where the term “oil” stands for the organic phase, “water” stands for the aqueous phase and σ represents interfacial tension. When the spreading coefficient (S) for gas-oil-water interaction is positive (S>0), the organic liquid has a tendency to form a thin film at the gas-liquid interface, and if the spreading coefficient is negative (S<0), the organic phase forms liquid droplets. In the later, there is no direct contact between gas and the organic liquid. The gas transport route occurs in series from the gas to aqueous phase and then to the organic phase [2].

The possible mass transfer equations for some gas-liquid-liquid contactors are developed in this section by assuming that the transport route takes place in series.
Refering to figure 13(a), the mass balance equation of component A in the bulk gaseous phase is given by:

$$Q_{Ag}.C_{Ag} = Q'_{Ag}.C'_{Ag} + V_{L1}.\frac{dC_{AL1}}{dt} \quad (2)$$

then, the mass balance equation of component A in the bulk liquid (L_1) is expressed:

$$Q_{AL1}.C_{AL1} + V_{L1}.\frac{dC_{AL1}}{dt} - V_{L1}.\frac{dC'_{AL1}}{dt} = Q'_{AL1}.C'_{AL1} \quad (3)$$

Refering to figure 13(b), the mass balance equation of component A in the bulk liquid (L_1) can be written as:

$$Q_{AL1}.C_{AL1} = V_{L2}.\frac{dC_{AL2}}{dt} + Q'_{AL1}.C'_{AL1} \quad (4)$$

and, the equation of component A in the bulk liquid (L_2) can be presented as:

$$Q_{AL2}.C_{AL2} + V_{L2}.\frac{dC_{AL2}}{dt} - V_{L2}.\frac{dC'_{AL2}}{dt} = Q'_{AL2}.C'_{AL2} \quad (5)$$

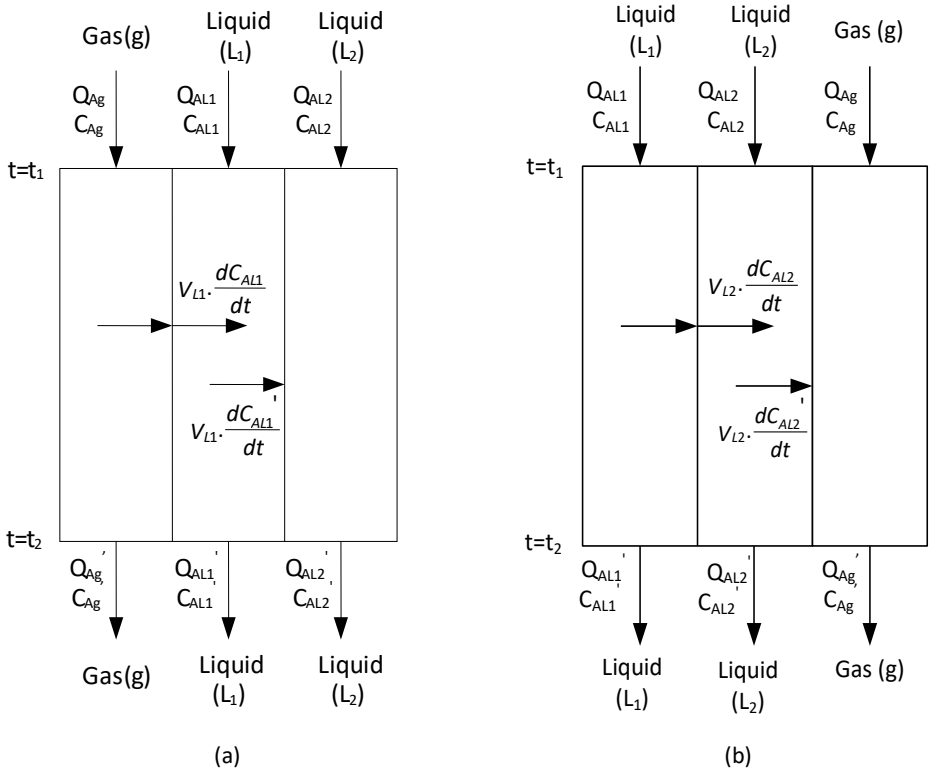

Figure 13. The mass transfer scheme between phases in reactor/contactor

Based on the two-film theory and refering to G-O/W or G-W/O systems, the overall mass transfer resistance is the sum of possible individual contributions: (1) mass transfer resistances in both films at the gas/water or gas/oil interfaces, (2) mass transfer resistances in both films at the water/oil or oil/water interfaces, (3) diffusion resistance in the oil droplets [21]. In this section, the mass transfer equation was derived for each possible route of gas-liquid-liquid reaction.

1.4.1. Mass transfer model 1: reaction at the L/L interface

The profile of the gas concentration in each phase is shown in figure 14. As mentioned previously, the mass transfer phenomena take place for two possible systems: G-O/W or G-W/O.

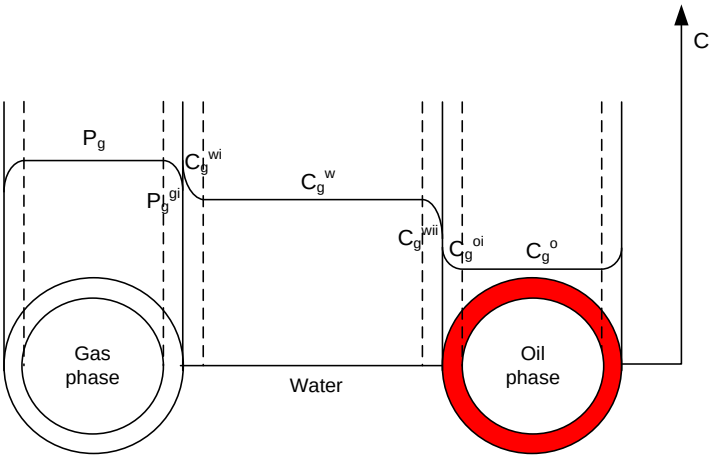

Figure 14. The concentration profile between phases for model 1

1. Mass transfer of gas from a bulk gaseous phase to bulk aqueous phase (G-O/W system)

The decrease in concentration to time at steady state condition over the gas phase to the aqueous phase can be described as follow:

$$\frac{dC}{dt} = k_g.a_g.(P_g - P_g^{gi}) = k_w.a_w.(C_g^{wi} - C_g^{w}) \tag{6}$$

According to Henry's law, on the interface of the gas-aqueous phases, P_g^{gi} can be given by:

$$P_g^{gi} = H.C_g^{wi} \tag{7}$$

where *H* is Henry's law constant of gas component. Substituting the value of P_g^{gi} in equation (2), and the concentration of gas in the aqueous film C_g^{wi} can be presented as:

$$C_g^{wi} = \frac{k_g.a_g.P_g + k_w.a_w.C_g^{w}}{k_w.a_w + H.k_g.a_g} \tag{8}$$

Then, by substituting equation (8) and (7) into equation (6), the mass transfer rate is written in the equation (9) below

$$\frac{dC}{dt} = k_g.a_g.(P_g - H.C_g^{wi}) = k_g.a_g.(P_g - \frac{H.k_g.a_g P_g + H.k_w.a_w.C_g^{w}}{H.k_g.a_g + k_w.a_w}) \tag{9}$$

Rearranging this equation and it can be presented as follow

$$\frac{dC}{dt} = \frac{1}{\frac{H}{k_w.a_w} + \frac{1}{k_g.a_g}}(P_g - H.C_g^{w}) \tag{10}$$

2. Mass transfer of dissolved gas in the bulk aqueous phase to oil phase interface

In this step, the soluble gas in the bulk aqueous phase diffuses and comes in contact with oil droplets. At the steady-state condition, the mass transfer rate of gas can be expressed as follow:

$$\frac{dC}{dt} = k_w.a_w.(C_g^{w} - C_g^{wii}) = k_o.a_o.(C_g^{oi} - C_g^{o}) \tag{11}$$

$$C_g^{oi} = K_e.C_g^{wii} \tag{12}$$

Then equation (12) is substituted to the equation (11),

$$\frac{dC}{dt} = k_w.a_w.(C_g^{w} - C_g^{wii}) = k_o.a_o.(K_e.C_g^{wii} - C_g^{o}) \tag{13}$$

and the value of C_g^{wii} can be written as the measurable parameter,

$$C_g^{wii} = \frac{k_w \cdot a_w \cdot C_g^w + k_o \cdot a_o \cdot C_g^o}{k_o \cdot a_o \cdot K_e + k_w \cdot a_w} \quad (14)$$

Substituting the equation (14) into the equation (13), the decrease in gas concentration with time can be presented as:

$$\frac{dC}{dt} = k_w \cdot a_w \cdot (C_g^w - \frac{k_w \cdot a_w \cdot C_g^w + k_o \cdot a_o \cdot C_g^o}{k_o \cdot a_o \cdot K_e + k_w \cdot a_w}) \quad (15)$$

Rearranging this equation, it can be written as follow:

$$\frac{dC}{dt} = \frac{1}{\frac{K_e}{k_w \cdot a_w} + \frac{1}{k_o \cdot a_o}} (K_e \cdot C_g^w - C_g^o) = \frac{K_e \cdot C_g^w}{\frac{K_e}{k_w \cdot a_w} + \frac{1}{k_o \cdot a_o}} \quad (16)$$

This model assumes that the chemical reaction takes place in the aqueous-oil phase interface, and that there is no gas in the bulk oil since the gas completely reacts at the interface, therefore the gas concentration in the bulk oil $C_g^o = 0$. These equations refer to the G-O/W system. For the G-W/O system, similar equations describing the mass transfer of gas from the gaseous phase to the oil phase can be derived and given as follows:

$$\frac{dC}{dt} = \frac{1}{\frac{H}{k_o \cdot a_o} + \frac{1}{k_g \cdot a_g}} (P_g - H.C_g^o) \quad (17)$$

and, the mass transfer of dissolved gas in the oil phase to the aqueous phase interface can be presented:

$$\frac{dC}{dt} = \frac{1}{\frac{K_e}{k_o \cdot a_o} + \frac{1}{k_w \cdot a_w}} (K_e \cdot C_g^o - C_g^w) = \frac{K_e \cdot C_g^o}{\frac{K_e}{k_o \cdot a_o} + \frac{1}{k_w \cdot a_w}} \quad (18)$$

1.4.2. Mass transfer model 2: reaction at the G/L interface

This model describes the different mass transfer phenomena of first model (reaction at the L/L interface). The concentration profile of oil is shown in figure 15.

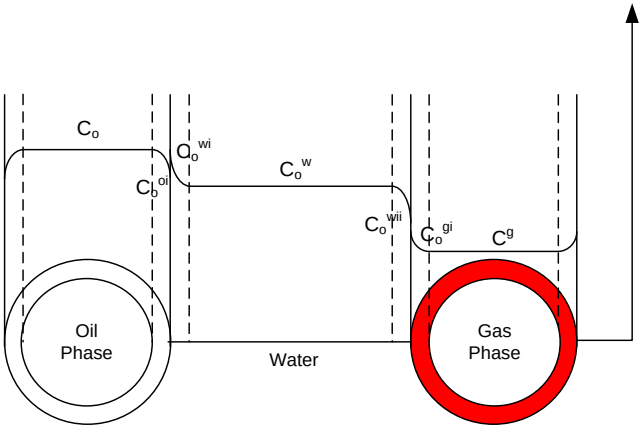

Figure 15. The concentration profile between phases for model 2

1. Mass transfer of oil from the bulk oil phase to aqueous phase (G-O/W system)

The mass transfer rate is given as follow:

$$\frac{dC}{dt} = k_o . a_o . (C_o - C_o^{oi}) = k_w . a_w . (C_o^{wi} - C_o^{w}) \tag{19}$$

The concentration of oil in the oil film is in equilibrium with the concentration of oil in the water film given in equation (20):

$$C_o^{wi} = K_e . C_o^{oi} \tag{20}$$

The value of C_o^{oi} can then be expressed as below:

$$C_o^{oi} = \frac{k_o . a_o . C_o + k_w . a_w . C_o^{w}}{k_w . a_w . K_e + k_o . a_o} \tag{21}$$

Rearranging equation (19) the mass transfer rate of oil from the bulk oil phase to the bulk aqueous phase is shown by the following equation:

$$\frac{dC}{dt} = k_o . a_o . (C_o - \frac{k_o . a_o . C_o + k_w . a_w . C_o^{w}}{k_w . a_w . K_e + k_o . a_o}) \tag{22}$$

$$\frac{dC}{dt} = \frac{1}{\frac{K_e}{k_o . a_o} + \frac{1}{k_w . a_w}} . (C_o . K_e - C_o^{w}) \tag{23}$$

2. Mass transfer of oil from the bulk aqueous phase to the gaseous phase

In this step, the oil is dissolved in the aqueous-gaseous interface, and the reaction between the oil phase and the gas phase takes place at this interface. The mass transfer rate at aqueous-gaseous interface can be presented as follow:

$$\frac{dC}{dt} = k_w . a_w . (C_o^{w} - C_o^{wii}) = k_g . a_g . P_g^{gi} \tag{24}$$

The reaction completely reacts in the interface. Therefore there is no oil in the bulk of the gaseous phase, and the oil concentration in the side of the aqueous film is in equilibrium with gas pressure in gaseous film,

$$P_g^{gi} = H . C_o^{wii} \tag{25}$$

The value of C_o^{wii} can be expressed by the measurable parameter as below

$$C_o^{wii} = \frac{k_w . a_w . C_o^{w}}{k_g . a_g . H + k_w . a_w} \tag{26}$$

Then, the mass transfer rate of oil from the bulk aqueous phase to the gaseous phase can be presented in the equation as follows:

$$\frac{dC}{dt} = k_w . a_w . (C_o^{w} - \frac{k_w . a_w . C_o^{w})}{k_g . a_g . H + k_w . a_w}) \tag{27}$$

$$\frac{dC}{dt} = \frac{1}{\frac{H}{k_w . a_w} + \frac{1}{k_g . a_g}} . (H . C_o^w) \quad (28)$$

Similar to the previous explanations, these equations can be derived for G-W/O system. In the G-W/O system, the mass transfer rate of the bulk aqueous phase to the bulk oil phase is expressed as follow:

$$\frac{dC}{dt} = \frac{1}{\frac{K_e}{k_w . a_w} + \frac{1}{k_o . a_o}} . (C_o^w . K_e - C_o) \quad (29)$$

The mass transfer rate of the aqueous phase dissolved in the oil phase to the oil-gaseous phase interface can be presented the following equation:

$$\frac{dC}{dt} = \frac{1}{\frac{H}{k_o . a_o} + \frac{1}{k_g . a_g}} . (H . C_o) \quad (30)$$

1.4.3. Mass transfer model 3: reaction in the continuous liquid phase

This model describes gas and oil phases that are partially soluble in the continuous aqueous phase. The dissolved gas and oil come in contact with each other, and the reaction between the soluble gas and oil takes place in the continuous phase. The concentration profile in both phases for G-O/W system are shown in figure 16.

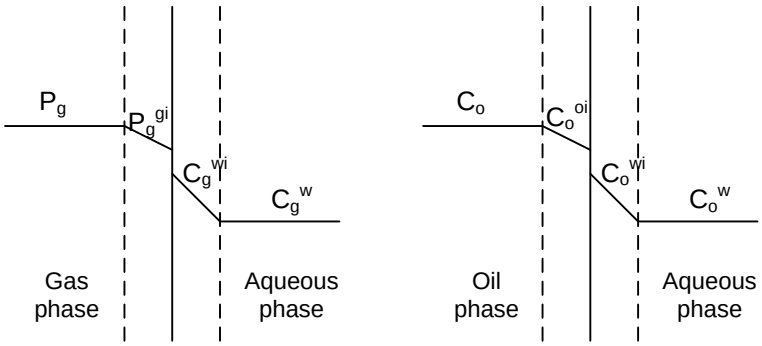

Figure 16. The concentration profile between phases for model 3

1. Mass transfer of gas from a bulk gaseous phase to the aqueous phase

$$\frac{dC}{dt} = k_g . a_g . (P_g - P_g^{gi}) = k_w . a_w . (C_g^{wi} - C_g^w) \quad (31)$$

$$\frac{dC}{dt} = \frac{1}{\frac{H}{k_w . a_w} + \frac{1}{k_g . a_g}} . (P_g - H . C_g^w) \quad (32)$$

2. Mass transfer of oil from the bulk oil phase to the aqueous phase

$$\frac{dC}{dt} = k_o \cdot a_o \cdot (C_o - C_o^{oi}) = k_w \cdot a_w \cdot (C_o^{wi} - C_o^{w}) \tag{33}$$

$$\frac{dC}{dt} = \frac{1}{\frac{K_e}{k_o \cdot a_o} + \frac{1}{k_w \cdot a_w}} \cdot (K_e \cdot C_o - C_o^{w}) \tag{34}$$

The identical equations for the G-W/O system can be derived from these equations with slight modification. The mass transfer rate of gas from the bulk gaseous phase to the oil phase can then be expressed as follows:

$$\frac{dC}{dt} = \frac{1}{\frac{H}{k_o \cdot a_o} + \frac{1}{k_g \cdot a_g}} \cdot (P_g - H \cdot C_g^{o}) \tag{35}$$

The mass transfer rate of the aqueous phase to the bulk oil phase is given by the following equation:

$$\frac{dC}{dt} = \frac{1}{\frac{K_e}{k_w \cdot a_w} + \frac{1}{k_o \cdot a_o}} \cdot (K_e \cdot C_w - C_w^{o}) \tag{36}$$

From the mass transfer equations above, it is essential to know which film is the controlling the mass transfer rate. For the gas/liquid transfer, the gas-side resistance can be neglected because the volumetric mass transfer coefficient for gas is significantly greater than that for the liquid phase. A possible resistance in gas/liquid mass transfer can therefore only be at the aqueous or oil film side. Table 4 below summarizes the mass transfer resistance in the models explained above.

Table 4. The mass transfer resistances for the proposed models

Mass Transfer Model	G-O/W System	G-W/O System
Model 1	Mass transfer of gas from a bulk gaseous phase to bulk aqueous phase: $K_{L1} = \frac{1}{\frac{1}{k_g \cdot a_g} + \frac{H}{k_w \cdot a_w}}$	Mass transfer of gas from a bulk gaseous phase to bulk oil phase: $K_{L1} = \frac{1}{\frac{H}{k_o \cdot a_o} + \frac{1}{k_g \cdot a_g}}$
	Mass transfer of dissolved gas in the bulk aqueous phase to oil phase interface: $K_{L2} = \frac{1}{\frac{K_e}{k_w \cdot a_w} + \frac{1}{k_o \cdot a_o}}$	Mass transfer of dissolved gas in the bulk oil phase to aqueous phase interface: $K_{L2} = \frac{1}{\frac{K_e}{k_o \cdot a_o} + \frac{1}{k_w \cdot a_w}}$
Model 2	Mass transfer of oil from the bulk oil phase to the bulk aqueous phase:	Mass transfer of aqueous from the bulk aqueous phase to the bulk oil phase:

	$K_{L1} = \frac{1}{\frac{K_e}{k_o \cdot a_o} + \frac{1}{k_w \cdot a_w}}$	$K_{L1} = \frac{1}{\frac{K_e}{k_w \cdot a_w} + \frac{1}{k_o \cdot a_o}}$
	Mass transfer of oil from the bulk aqueous phase to gaseous p $K_{L2} = \frac{1}{\frac{1}{k_g \cdot a_g} + \frac{H}{k_w \cdot a_w}}$	Mass transfer of aqueous from the bulk oil phase to gaseous phase: $K_{L2} = \frac{1}{\frac{H}{k_o \cdot a_o} + \frac{1}{k_g \cdot a_g}}$
Model 3	Mass transfer of gas from a bulk gaseous phase to aqueous phase: $K_{L1} = \frac{1}{\frac{1}{k_g \cdot a_g} + \frac{H}{k_w \cdot a_w}}$	Mass transfer of gas from a bulk gaseous phase to oil phase: $K_{L1} = \frac{1}{\frac{H}{k_o \cdot a_o} + \frac{1}{k_g \cdot a_g}}$
	Mass transfer of oil from the bulk oil phase to aqueous phase: $K_{L2} = \frac{1}{\frac{K_e}{k_o \cdot a_o} + \frac{1}{k_w \cdot a_w}}$	Mass transfer of aqueous from the bulk aqueous phase to oil phase: $K_{L2} = \frac{1}{\frac{K_e}{k_w \cdot a_w} + \frac{1}{k_o \cdot a_o}}$

1.5. Discussion

1.5.1. Effect of hydrodynamics and choice of technologies

Since mass transfer between the gas-liquid phases and liquid-liquid phases is directly related to the interfacial surface area, the size of the gas bubbles and the droplets has a significant effect on the efficiency of the process. Generally, all systems that lead to a decrease in the characteristic size of the bubbles and drops will be beneficial to reaction efficiency. However, a simple decrease in bubble or drop size is not the only factor that may influence the reaction performance. Several other competing phenomena may also occur, e.g. the diffusion of a reactant at the interface and the chemical reaction. The relative rates of the competing phenomena control where the reaction takes place and therefore it is of major importance that the different phenomena occurring in the considered reaction be identified. The Hatta number (Ha) [40] expresses the relative magnitudes of rate of reaction and the rate of physical mass transfer, and in particular, the rate of reaction in an interfacial film to the rate of diffusion of species through the film. Practically, it enables identification of where the chemical reaction occurs in a heterogeneous medium.

$$Ha = \left(\frac{\text{Rate of reaction of A in the film per unit surface area}}{\text{Rate of mass transfer of A through the film per unit surface area}}\right)^{1/2}$$

The literal expression of Ha depends on the kinetics and interfacial models used, however three regimes can be identified.

- For Ha < 0.3, the reaction is much slower than mass transfer of the species from the dispersed phases, so the reaction takes place in the continuous bulk;
- For Ha > 3.0, the reaction is much faster than mass transfer of the species from the dispersed phases, so the reaction takes place at the interface;
- For 0.3 < Ha < 3.0, the reaction rate is of the same order of magnitude as the rate of mass transfer from the dispersed phases, so the reaction may take place in both the bulk and at the interfaces.

Although Ha was initially defined for reactive gas-liquid systems, it can also be used for two-phase liquid-liquid reactions. In the case of reactive GLL systems, Ha can be defined with respect to the species that must be transported through the gas-liquid and liquid-liquid interfaces to react, i.e. reactant C, which is initially present in the gas phase, and the reactant present in the dispersed liquid phase (A for G-W/O system or B for G-O/W system).

In the case of GLL reactions, Ha will control the reaction depending on the reaction system. For reactions following Model 1, the limiting step is the diffusion of the reactant in the dispersed liquid phase and therefore Ha at the liquid-liquid interface will control the reactive system. For those that follow Model 2, the limiting step is the diffusion of the gas into the liquid so Ha at the gas-liquid interface controls the system. Finally, for Model 3 reactions, the rates of diffusion of the reactants from both the dispersed gas and liquid phases are of the same order of magnitude and therefore Ha can be calculated for both the gas liquid and liquid-liquid interfaces. From the above, it is clear that for each GLL reaction, the appropriate physical model that correctly defines the limiting steps must firstly be identified. Following this, specific process equipment and operating conditions can then be chosen such that they are adapted to the reaction requirements. Stirred tank reactors can be a pertinent equipment choice for many reactions provided they are fitted with appropriate impeller types and correctly designed (e.g. use of baffles, correct choice of off-bottom impeller clearance, liquid height). For continuous processes, stirred tanks remain a good choice, even if packed columns or tubes equipped with static mixers are also well adapted for fast reactions and low coalescing systems. Continuous miniaturized flow reactors are also an alternative to the traditional stirred tank reactor for reactions that are highly limited by heat and/or mass transfer, or that employ hazardous products. In such continuous flow equipment, the residence times are generally short and therefore are better adapted to fast reactions. Due to the high surface to volume ratio (and therefore increased surface effects) of such equipment, the continuous phase is often determined by the wettability of the reactor wall by the liquids. Model 1 describes a system where the reaction takes place at the liquid-liquid interface. In this case, the Hatta number is small (Ha < 0.3) and therefore the reaction is fast compared with the solubility of the reactant (initially contained in the drops) in the continuous liquid phase. Due to the consumption of the reactants by the chemical reaction, an acceleration of mass transfer at the liquid-liquid interface is expected. It is therefore important to generate small drops such that the surface area for mass transfer is maximized. Moreover, in order to renew the liquid at the drop interface and increase mass transfer, turbulent flow conditions are required. For batch or continuous processes, a stirred tank equipped with a high shear impeller, e.g. rotor-stator, which will promote drop breakup, in combination with an axial flow impeller, which will ensure global circulation in the tank, would be well adapted. The dissolution of the gas in the continuous liquid phase is generally simple to achieve and therefore the means in which the

gas is injected in the liquid has little influence; a simple ring sparger is typically used in stirred tanks. One of the examples described in section 3 “Application to Gas-liquid-liquid reactions” shows that an increase in stirrer rotational speed induces an increase in reaction yield (ozonolyse reaction [21]). This is due to the impact of the rotational speed, which promotes the creation of smaller droplets and also increases turbulence, both of which enhance mass transfer.

In Model 2, the reaction occurs at the gas-liquid interface. This configuration corresponds to a high value of the Hatta number (Ha > 3) and the success of the process is strongly linked to the bubble size. Since the solubility of the liquid droplet into the continuous phase is not a problem, the size of the droplets is not a limiting factor. Small bubbles can be generated by the use of disc turbines, e.g. Rushton turbines or concave blades turbines (which enable improved gas handling), and by correctly choosing and implementing the gas sparger. Different sparger types exist, including ring and flat geometries; a simple tube sparger is not however recommended. If the reaction kinetics are slow, it is important to increase the residence time of the gas phase by using a stirred tank with a height much larger than the diameter of the tank. In this case, multiple impellers on the shaft should be used. The turbulence created in the tank will also promote the reaction by renewing the gas liquid interface. For this model, as well as for Model 1, the location of the agitator at the beginning of the operation is crucial since, depending on the range of interfacial L/L tension and viscosities of the system, it may determine which phase will be dispersed in the other (O/W or W/O). Generally, the agitator should initially be located in the phase that is expected to be the continuous one. In the case where the dispersed phase is fed into the continuous phase, it should be added at the surface if it is denser than the continuous phase or in the impeller outflow if it is lighter than the continuous phase.

In Model 3, the solubility of the gas and of the dispersed liquid in the continuous phase is high. Furthermore, the reaction is slow and occurs in the continuous phase, corresponding to intermediate Hatta numbers (0.3 < Ha < 3). In this case, the residence time is the controlling parameter of the process and the influence of the bubble and drop size is less important than in the other two models. A stirred tank reactor is well adapted to this scenario. The recommended impeller type for such an operation would be a disc turbine or pitched blade turbine since these are effective for bubble and drop generation (see for example the synthesis of pivalic acid [37]), as well as for global mixing of the system. Gas should be fed into the system through a ring or plate sparger.

1.5.2. Effect of the pressure

Increasing the pressure of the reacting system is particularly interesting when the solubility of the gas in the continuous phase is the limiting step. Gas solubility increases with pressure and therefore the reaction yield can be enhanced by operating under pressure. For example, in the hydroformylation reaction that was carried out in an autoclave reactor [4], an increase in the partial pressure of hydrogen increased the solubility of hydrogen and carbon monoxide in the continuous liquid phase and reaction contacting mechanism changed from Model 2 to Model 3. Other examples of reactions that report the effect of the pressure on the yield of reactions are given in [10] and [36].

1.6. Conclusion

To effectively perform a GLL reaction, the contacting mechanism responsible for its enhancement should be known. In this analysis, three phase contacting models that represent the contacting mechanisms between phases for water-in-oil or oil-in-water systems with a gas have been presented. The proposed models are based on mass transfer that can occur between the three different phases.

From the reaction mechanisms illustrated by the contacting models, it is obvious that the gas-liquid-liquid reactions will proceed if the inter-phase mass transfer is effective. Mass transfer occurs from the dispersed gas phase to the continuous liquid phase and/or from the dispersed liquid phase to the continuous liquid phase and can be promoted by employing correctly adapted process equipment and the associated operating conditions, such that the phases are dispersed in the right manner and interfacial area and turbulence are increased. However, depending on the contacting mechanism required by the reaction type, different equipment and operating conditions should be chosen to enhance reaction performance. Model 1 corresponds to fast reactions that occur at the liquid-liquid interface. In this case, it is important to promote mass transfer by increasing the surface area of the droplets and create turbulent flow conditions in order to renew the liquid-liquid interface. Model 2 corresponds to GLL systems where by the solubility of the dispersed liquid in the continuous phase is high and the reaction takes place at the gas/liquid interface. In this case, bubble size is the parameter that limits mass transfer so it is important to choose equipment and conditions that promote high gas/liquid interfacial areas and bubble breakup. Model 3 corresponds to slow reactions occurring in the continuous liquid phase in which the solubility of the dispersed gas and liquid phases is high. In this case, the residence time (or the operating time) is the controlling parameter for reaction performance, whilst the size of the bubbles and droplets in less important.

Literature

[1] J. Wiley and K. Hepburn, *Chemical Reaction Engineering - Boston.* 1982.

[2] R. Kaur and M. Ramakrishna, “ROLE OF DISPERSED PHASE IN GAS-LIQUID.”

[3] K. D. Wiese, O. Möller, G. Protzmann, and M. Trocha, “A new reactor design for catalytic fluid-fluid multiphase reactions,” *Catal. Today*, vol. 79–80, pp. 97–103, 2003.

[4] P. Purwanto and H. Delmas, “Gas-liquid-liquid reaction engineering: hydroformylation of 1-octene using a water soluble rhodium complex catalyst,” *Catal. Today*, vol. 24, no. 1–2, pp. 135–140, 1995.

[5] S. Kasinathan *et al.*, “Syngas-mediated C-C bond formation in flow: Selective rhodium-catalysed hydroformylation of styrenes,” *Synlett*, no. 18, pp. 2648–2651, 2011.

[6] Y. Önal, M. Lucas, and P. Claus, “Application of a capillary microreactor for selective hydrogenation of α,ß-unsaturated aldehydes in aqueous multiphase catalysis,” *Chem. Eng. Technol.*, vol. 28, no. 9, pp. 972–978, 2005.

[7] J. Tan, C. Dong, Y. C. Lu, J. H. Xu, and G. S. Luo, “Coupling process of oxidation and extraction in a gas-liquid-liquid microdispersion system for H 2O 2 synthesis,” *Ind. Eng. Chem. Res.*, vol. 51, no. 4, pp. 1834–1845, 2012.

[8] S. Lu, L. Wang, Y. Wang, and Z. Mi, “Kinetic Model of Gas-Liquid-Liquid Reactive Extraction for Production of Hydrogen Peroxide,” *Chem. Eng. Technol.*, vol. 34, no. 5, pp. 823–830, 2011.

[9] J. Li, A. Moniri, and H. Wang, “Apparent kinetics of a gas-liquid-liquid system of Bunsen reaction with iodine-toluene solution for hydrogen production through H2S splitting cycle,” *Int. J. Hydrogen Energy*, vol. 40, no. 7, pp. 2912–2920, 2015.
[10] A. A. Sathe, A. M. K. Nambiar, and R. M. Rioux, “Synthesis of cyclic organic carbonates via catalytic oxidative carboxylation of olefins in flow reactors,” *Catal. Sci. Technol.*, vol. 7, no. 1, pp. 84–89, 2017.
[11] T. M. Baber, D. Graiver, C. T. Lira, and R. Narayan, “Application of catalytic ozone chemistry for improving biodiesel product performance,” *Biomacromolecules*, vol. 6, no. 3, pp. 1334–1344, 2005.
[12] A. Lundstedt, M. J. Webb, and H. Grennberg, “Ozonolysis of polycyclic aromatic hydrocarbons in participating solvents,” *RSC Adv.*, vol. 7, no. 10, pp. 6152–6159, 2017.
[13] M. F. Díaz, F. Hernández, O. Ledea, J. A. Gavín Sazatornil, and J. Moleiro, “1H NMR study of methyl linoleate ozonation,” *Ozone Sci. Eng.*, vol. 25, no. 2, pp. 121–126, 2003.
[14] L. Riadi, A. Y. Widianto, E. Purwanto, A. Pono, and R. Theresia, “Synthesis of biodiesel from waste cooking oil by two steps process transesterification and ozonation,” *J. Chem. Pharm. Res.*, vol. 7, no. 9, pp. 17–21, 2015.
[15] L. Riadi, E. Purwanto, H. Kurniawan, and R. Oktaviana, “Effect of Bio-based Catalyst in Biodiesel Synthesis,” *Procedia Chem.*, vol. 9, pp. 172–181, 2014.
[16] L. Riadi, E. Purwanto, and Y. Chandra, “Ash Base-Catalysed in Promoting Ozonolysis of Used Cooking Oil,” *Int. J. Eng. &Technology*, vol. 12, no. 06, pp. 87–90, 2012.
[17] A. Wegmann, J. Melke, and P. Rudolf von Rohr, “Three phase liquid-liquid-gas flows in 5.6 mm and 7 mm inner diameter pipes,” *Int. J. Multiph. Flow*, vol. 33, no. 5, pp. 484–497, 2007.
[18] D. W. F. Brilman, M. J. V. Goldschmidt, G. F. Versteeg, and W. P. M. Van Swaaij, “Heterogeneous mass transfer models for gas absorption in multiphase systems,” *Chem. Eng. Sci.*, vol. 55, no. 15, pp. 2793–2812, 2000.
[19] A. Ładosz, E. Rigger, and P. Rudolf von Rohr, “Pressure drop of three-phase liquid–liquid–gas slug flow in round microchannels,” *Microfluidics and Nanofluidics*, vol. 20, no. 3. pp. 1–14, 2016.
[20] Z. Wen, X. Yu, S. T. Tu, J. Yan, and E. Dahlquist, “Intensification of biodiesel synthesis using zigzag micro-channel reactors,” *Bioresour. Technol.*, vol. 100, no. 12, pp. 3054–3060, 2009.
[21] A. Kornmüller and U. Wiesmann, “Ozonation of polycyclic aromatic hydrocarbons in oil/water-emulsions: Mass transfer and reaction kinetics,” *Water Res.*, vol. 37, no. 5, pp. 1023–1032, 2003.
[22] A. G. Panda, S. R. Jagtap, N. S. Nandurkar, and B. M. Bhanage, “Regioselective hydroformylation of allylic alcohols using Rh/PPh 3 supported ionic liquid-phase catalyst, followed by hydrogenation to 1,4-butanediol using R11/PPh3 supported ionic liquid-phase catalyst,” *Ind. Eng. Chem. Res.*, vol. 47, no. 3, pp. 969–972, 2008.
[23] R. V. Chaudhari, A. Seayad, and S. Jayasree, “Kinetic modeling of homogeneous catalytic processes,” *Catal. Today*, vol. 66, no. 2–4, pp. 371–380, 2001.
[24] R. M. Deshpande, S. S. Divekar, B. M. Bhanage, and R. V. Chaudhari, “Activity of HRh(CO)(PPh3)3 catalyst in hydroformylation of allyl alcohol: Effect of second immiscible liquid phase,” *J. Mol. Catal.*, vol. 75, no. 1, pp. 19–22, 1992.
[25] S. Rakovsky, M. Anachkov, M. Belitskii, and G. Zaikov, “Kinetics and mechanism of the ozone reaction with alcohols, ketones, ethers and hydroxybenzenes,” *Chem. Chem. Technol.*, vol. 10, no. 4s, pp. 531–552, 2016.
[26] Q. Dai, L. Chen, S. Zhou, and J. Chen, “Kinetics and mechanism study of direct ozonation organics in aqueous solution,” *RSC Adv.*, vol. 5, no. 31, pp. 24649–24654, 2015.
[27] H. Lawrence Clever, R. Battino, H. Miyamoto, Y. Yampolski, and C. L. Young, “IUPAC-

NIST Solubility Data Series. 103. Oxygen and Ozone in Water, Aqueous Solutions, and Organic Liquids (Supplement to Solubility Data Series Volume 7)," *J. Phys. Chem. Ref. Data*, vol. 43, no. 3, 2014.
[28] Bińi, "Ozone Solubility in Liquids.pdf" 2006. .
[29] P. Dowideit and C. Von Sonntag, "Reaction of ozone with ethene and its methyl- and chlorine-substituted derivatives in aqueous solution," *Environ. Sci. Technol.*, vol. 32, no. 8, pp. 1112–1119, 1998.
[30] S. Toby and F. S. Toby, "Reactivity of the ozone-ethane system," *J. Phys. Chem. A*, vol. 102, no. 24, pp. 4527–4531, 1998.
[31] B. E. Krisyuk, A. V. Maiorov, and A. A. Popov, "Kinetics and mechanism of ozone addition to olefins and dienes," *Kinet. Catal.*, vol. 57, no. 3, pp. 326–332, 2016.
[32] J. Sadowska, B. Johansson, E. Johannessen, R. Friman, L. Broniarz-Press, and J. B. Rosenholm, "Characterization of ozonated vegetable oils by spectroscopic and chromatographic methods," *Chem. Phys. Lipids*, vol. 151, no. 2, pp. 85–91, 2008.
[33] L. Cassar and M. Foa, "Phasetransfer carbonylation catalysis in cobalt-catalyzed of benzyl halides," *Org. Synth.*, vol. 134, pp. 5–6, 1977.
[34] H. Alper and S. Amaratunga, "The regiospecific phase transfer catalyzed reductive carbonylation of azadienes," *Can. J. Chem.*, vol. 61, no. 6, pp. 1309–1313, 1983.
[35] U. J. Jáuregui-Haza, E. J. Pardillo-Fontdevila, A. M. Wilhelm, and H. Delmas, "Solubility of hydrogen and carbon monoxide in water and some organic solvents," *Lat. Am. Appl. Res.*, vol. 34, no. 2, pp. 71–74, 2004.
[36] D. W. F. Brilman, N. G. Meesters, W. P. M. Van Swaaij, and G. F. Versteeg, "Mass transfer effects in the H2SO4 catalyzed pivalic acid synthesis," *Catal. Today*, vol. 66, no. 2–4, pp. 317–324, 2001.
[37] V. M. Rajesh and V. V. Buwa, "Experimental characterization of gas-liquid-liquid flows in T-junction microchannels," *Chem. Eng. J.*, vol. 207–208, pp. 832–844, 2012.
[38] J. Yue, E. V. Rebrov, and J. C. Schouten, "Gas-liquid-liquid three-phase flow pattern and pressure drop in a microfluidic chip: Similarities with gas-liquid/liquid-liquid flows," *Lab Chip*, vol. 14, no. 9, pp. 1632–1649, 2014.
[39] Praxair, Carbon Dioxide Safety Data Sheet P-4574, Octobre (2016).
[40] S. Hatta, Technological Reports of Tôhoku University 10 (1932), pp. 613–622.

Nomenclature

G	gas	L_{cp}	capillary pipe length (m)
L	liquid	N	stirring speed (s^{-1})
O	oil	P	pressure (Pa)
W	water	Q	flow rate ($m^3.s^{-1}$)
C	concentration (mol %)	T	temperature (°C)
D	diameter (m)	t	time (s)
H	high (m)	V	volume (m^3)
L_r	reactor length (m)		

Chapter 2

Reactors Technologies for Gas-Liquid-Liquid Phase Contacting

Contents

2.1. Introduction

One of the challenges of chemical engineering going forward is to find a flexible industrial design allowing a product adjustment to market developments. Continuous efforts through in-depth studies have been carried out to find alternative processes/systems/ operating units that aimed at improving economically the processes used and reducing negative impacts on the environment. Economics and the sustainability of the processes used are crucial factors in making decisions for business/trading activities at present. Some critical criteria considered in making decisions are a capital investment over entire plant, efficient use of raw materials, and the overall impact on the environment. Efforts to develop sustainable technology, which consumes far less energy, have been carried out for the last three decades. This approach is referred to as processes which are precisely defined as "Chemical Engineering Development" that generates something substantially cleaner, as well as consuming energy efficiently" [1]. For Chemical Process Industry, this process is an essential tool for achieving economic improvement, reducing the impact on the environment, and completing the ultimate goal of sustainability.

The gas-liquid-liquid (GLL) environment has been applied in unit operations of chemical engineering that involves the processes of mixing, extraction, absorption, and mainly chemical reactions as a focused review in this section. Reactors for carrying out three-phase reactions have a unique design. The design is adjusted to the amount of mass transfer between gas and liquids phases, which can be represented by the value of the mass transfer coefficient (k_g), (k_L), and in the transfer processes, the information about the determinant phase of mass transfer resistance is important. These characteristics become an essential consideration in determining of the feeding system design for each phase, especially gas, which can be dispersed into the solution/liquid mixtures in several ways, such as the spray, and the bubble model.

The developed GLL reactor types in the last decade include tubular reactors with static mixers, jet loop reactors, RSR (Rotor Stator reactor)-STR (Stirrer Tank reactor) tandem reactors. The reactors were designed in such a way as to improve their performances in supporting the continuity of three-phase reactions more effectively and efficiently by combining reaction and separation processes in one cycle, replacing conventional mixing with other devices like a static mixer, combining the performance of two reactors as well as the development of an intensified reactors design that has been much studied lately. In principle, the efforts taken are intended to enlarge the contact surface area between phases [2][3] and determine the stages of the contact mechanism of each phase involved in the process [4]. Alternatively, in some cases, specific chemical compounds are often added into the solution to decrease in surface tension and promoting the formation of micro-emulsions, that bringing these active species always be kept in contact effectively [5]. Conversely, the efforts through the catalyst activity improvement are not enough since the active species in GLL systems are easily restricted by the mass transfer rate. With all its advantages and disadvantages, the use of a GLL reactor requires a good understanding of the working system, contact mechanism, and the three-phase dispersion method within a reactor.

Since $k_{L.a}$ is one of the essential parameters for mass transfer process within the reactor, the derivation of mass balance equation for each mass transfer model might perform, as the three models elucidated in chapter 1, will be able to provide a detail illustrations about the mass transfer resistance mainly the dominant phases resistance. This information is important, and it is considered in choosing the appropriate reactor type.

The numerous investigations have a passion for developing chemical processes involving gas-liquid and liquid-liquid systems. However, there is very less information available on chemical processes involving three-phase gas-liquid-liquid systems especially dealing with chemical reactors, whereas reactor system is one of the core processes in chemical industries, e.g., hydrogenation, hydroformylation, carbonylation, coupling process, etc. [6][7][8][9][10][11]. On the other side, over the last few years, it has been developed the intensified reactors systems, which have substantial implications in enhancing the mass transfer rate between phases. Its huge potential as a three-phase reactor has attracted many researchers to explore further the performance of intensified reactors. Limitations in terms of the product quantities and the determination of operating parameters for specific reactions, including temperature, pressure, flow rate, and residence time, are studied and developed continuously to achieve optimal results. Since its small dimensions, this reactor exhibits different behavior compared to conventional reactors types that have been widely studied.

Therefore, the utilization of an appropriate reactor, choosing the properly operating variable is vital for a three-phase system with the more complex characteristics, since, for three-phase, it is relatively more difficult in realizing maximum yield and conversion. Therefore, the main objectives of this chapter are to present the gas-liquid-liquid reactor's performance and its applications, understanding the strength and weaknesses of each reactor, as well as understanding the stages in selecting the appropriate reactor type for a particular chemical reaction.

2.2. Reactor-Technologies for Gas-Liquid-Liquid

The selection of a suitable reactor for a specific system requires many aspects to be considered. A reaction can also be combined with a separation process in the reactive separator equipment. However, some specific aspects should not be ignored when reactor performance is compared. These aspects are volumetric throughput, volume reactor, residence time distribution, catalyst usage effectiveness, mass transfer rate, pressure, and temperature constraints in the reactor [12].

The selection and proper use of reactors for chemical reactions significantly affect the reaction product's formation and deal with yield, reaction conversion, and selectivity, primarily for chemical reactions restricted by mass transfer. The application of reactors capable of supporting the creation of a high surface area for mass transfer is the reactor type that will deliver the reaction products with better yield, conversion, and selectivity. Table 1 shows four types of reactors that have been used for gas-liquid-liquid reactions in the past 15 years.

Table 1. Gas-liquid-liquid reactors application from literature

Reaction	Type of Reactor	Remark	Ref
Coupling process of oxidation and extraction for H_2O_2 synthesis	Minichannel	The size of the flow channel was 15mm x 2 mm x 3 mm, using microfiltration membrane D_{pore}=5 µm, thickness 0.3 mm; T=50 °C; PO_2=200 & 300 KPa.	[11]
Hydrogenation of α,β-Unsaturated Aldehydes	Microreactor	$D_{capillaries}$=500, 750, 1000 µm; lengths of capillaries= 3, 6, 12 m; T= 60 °C; PH_2=1 – 2 MPa	[13]

Hydroformylation of propene	Tubular reactor filled with Sulzer SMV static mixers	Reactor length= 3 m, D_{in}= 17.8 mm; internal volume= 0.561 litre; residence time= 5 S; Sulzer SMV static mixers	[6]
Hydroformylation of propene	Jet loop reactor	The reactor has an outer tube, an inner tube, and a nozzle. Height diameter of vessel = 10 m, the height to diameter ratio = 8, reactor volume = 108 m^3	[10]
Hydroformylation of styrenes	Minichannel	Tube-in-tube gas flow reactor Z m AF-2400; CO:H_2 ratio is 1:1, P= 25 bar, T= 65 °C	[7]
Hydroformilation of cyclododecatriene	Minichannel	Reactor volume= 3 ml, channel dimension: 2 mm x 2 mm (square channel), liquid flow rate= 15 ml/min, ratio of CO:H_2= 1:1, gas flow rate= 440 N ml/min, pressure= 30 bar.	[9]
Oxidation of 2,3,6-trimethylphenol (TMP)	Rotor-Stator Reactor (RSR)-Stirred Tank Reactor (STR) tandem	Outer diameter of RSR= 200 mm, axial length of RSR= 62 mm, volume of STR= 250 ml, T-reaction= 75 °C, P= 1 bar, stirring speed= 600 rpm	[14]

Five aspects were elucidated as the basis for comparing the performance these rectors, included of general description/characteristics, hydrodynamic, applications, advantages and disadvantages.

2.2.1. Tubular Reactor with Static Mixers

The tubular reactor is widely applied for multiphase reactions such as gas-liquid-liquid reactions. Principally, the reactor consists of a cylindrical column filled with the static mixer. The gas and liquid reactants, as well as the liquid phase homogeneous catalyst, are introduced into the reactor. Contact between phases in the reactor occurs with the help of the static-mixer. The presence of the static mixer and a circulating pump in the tubular reactor successfully breaks down the gas-liquid mixture into droplets and the fine bubbles gas to form a surface area of mass transfer for gas-liquid-liquid reactions. The tubular reactor operates continuously. It offered a simple design with no moving parts, the flow and mixing are easily controlled, and uniform residence time inside the reactor.

Static mixers, also known as motionless mixers, have become standard equipment in the process industries. However, new designs are being developed, and new applications are being explored. Static mixers are employed inline in a once-through process or in a recycle loop where they supplement or even replace a conventional agitator. Commercial static mixers have a wide variety of basic geometries and many adjustable parameters that can be optimized for specific applications. Sulzer SMV mixer is one of static mixer type used for various chemical processes that mainly intended to disperse one phase in another or to increase the coefficient of mass transfer between phases; therefore, its application related to the liquid-liquid, gas-liquid, or solid-liquid phase. This type also includes applications for multiphase-coupled reactions with separation processes [15].

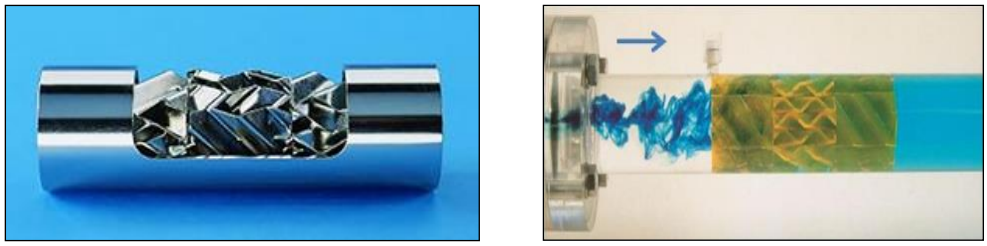

Figure 1. Sulzer SMV mixer (Koch-Glitsch Inc.) [15]

As an illustration, the typical data of dimensions and operating parameters in the previous work [6][16] consists of the reactor length 3 m, diameter 17.8 mm, filled with Sulzer SMV mixers, and internal volume of reactor about 0.56 liter. Then, catalyst mass flow rate up to 400 $kg.h^{-1}$, propene mass flow rate up to 3 $kg.h^{-1}$, synthesis gas flow rate up to 1 $kg.h^{-1}$. Its means that with the total fluid velocity up to 0.6 $m.s^{-1}$, the fluids would have a residence time of about 5 s for the chemical reaction [6].

The tubular reactor has been applied to perform hydroformylation, one of the three-phase reaction types involving the gas-liquid-liquid phase. This reaction synthesized aldehyde from propene using a homogeneous catalyst (30 wt.% TPPTS, 800 wt. Ppm Rh in pure water), which is known as Ruhrchemie–Rhône/Poulenc process and has been realized on a commercial scale. Among many GLL reactions, hydroformylation has attracted much attention, especially for catalysts recycling. This reaction is also becoming more attractive for industrial applications since energy consumption and environmental impact can be dramatically lowered by applying the new process design [13]. The biggest challenge for conducting this reaction is the reaction yields are substantially restricted by the mass transfer of propene [6]. This obstacle could be solved with a tubular reactor since the use of this reactor type was able to increase the space-time yield up to 10 fold of that obtained from the same reaction in stirred tank reactor. Further, olefins compound up to 1-octene could be converted to aldehyde lead acceptable time-space yield and high reaction selectivity using this reactor. In a stirred tank reactor, these achievements are not easily realized [6].

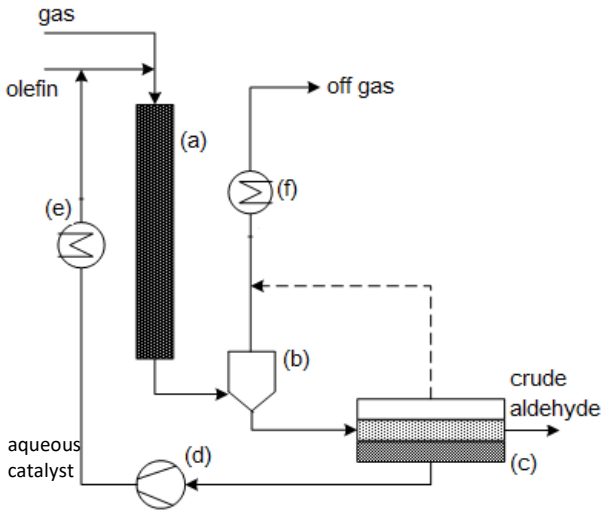

Figure 2. Schematic of hydroformylation mini plant: (a) tubular reactor, (b) gas flash, (c) settler, (d) circulating pump, (e and f) heat exchangers [6].

The use of homogeneous catalysts during this time faces constraints related to the separation between catalysts and reaction products. Conventionally, the separation of the catalyst was carried out by distillation, whereas, at thermal pressure, the catalyst is very susceptible to decomposition. Separation in this way poses a high risk of losing the mass of catalyst, which is undoubtedly a considerable loss economically in a large-scale process in the industry. However, this risk could be prevented by utilizing the tubular reactor system, as shown in Fig. 2. Fig. 2 shows that the reaction product, which is still mixed with the catalyst, is separated from the un-reacted residual gas. Furthermore, the product and aqueous catalyst solution are separated using decantation, and the aqueous solution containing catalyst flows back into the reactor (recycle). In this case, the selection of decantation as a separator is suitable for the density of aldehyde and the type of homogeneous catalyst used where the density of aldehyde is 788 kg/m^3, and the density of aqueous catalyst is 1000 kg/m^3. Besides simple in design, this separator is also easy operationally.

Concerning heat removal, it has been known that hydroformylation is a very exergonic reaction process. In a stirred vessel with a longer space-time than a tubular reactor, the longer space-time potentially encourages side reactions with undesired products. Therefore, the conventional processes usually utilize an internal heat exchanger to reach and maintain the reaction temperature. The different heat removal system could be found in tubular reactors. Considering that the mass flow rate of catalyst in this system could also significantly serve as a heat-conducting fluid, the heating system could be installed externally, leading to a simple reactor design.

The application of this system for hydroformylation reaction is able to overcome the problem of separation of homogeneous catalysts, prevent catalyst loss, and prevent undesirable side reactions. Furthermore, effectiveness, as well as efficiency of the process, is possible to reach.

Further, the use of a static mixer in continuous processes is an attractive alternative to conventional agitation since similar and sometimes better performance can be achieved at a lower cost. Motionless mixers typically have lower energy consumptions and reduced maintenance requirements because they have no moving parts. They offer a more controlled and scalable rate of dilution in fed-batch systems and can provide homogenization of feed streams with a minimum residence time [15]. A static mixer within a tubular reactor allows a large specific surface area to appear for CO, H_2, and propene in better contact, as well as the reaction takes place with consideration these chemical compounds have a partial soluble characteristic in the catalyst phase.

Table 2. Potential advantages of static mixer compared to mechanically agitated vessels [15]

Static mixer	Agitation
Small space requirement	Large space requirement
Low equipment cost	High equipment cost
No power required except pumping	High power consumption
No moving part except pump	Agitator drive and seals
Small flanges to seal	Small flanges plus one large flange to seal
Short residence times	Long residence times
Approaches plug flow	An exponential distribution of residence times

Good mixing at low shear rates	Locally high shear rates can damage sensitive materials
Fast product grade changes	Product grade change may generate waste
Self-cleaning, interchangeable mixers or disposable mixers	Large vessels to be cleaned

However, the static mixer also has several significant disadvantages that are needed higher pressure drop in its operational, more significant potential for fouling, the relative difficulty for cleaning, and higher cost as well as it just suitable for continuous operation [17].

2.2.2. Microreactor and Minichannel Reactor

2.2.2.1. General description

Microreactors are miniaturized and continuous devices. It is often comprised of several channels of different sizes and shapes with dimensions of the order less than 1000 µm [2][13][18], whereas minichannel reactors physically have a greater dimension of more than 1000 µm until several mm [19]. Multiphase flow in microdevices has become a focus of researchers in the last decade because the microdevices have great potential in the intensification of gas-liquid-liquid reactions such as hydrogenation, hydroformylation, and carbonylation [4]. Due to its small volume, it has highly promising characteristics for several chemical process applications, including separation and purification, chemical and biological screening, fine chemicals, and materials synthesis [20]. Microreactors are able to deliver a regular gas-liquid-liquid segmented flow in the regime laminar where the flow behaviors within the channel were strongly influenced by several factors such as a channel diameter, type of materials for microchannel, solubility, and operating conditions such as liquid/gas flow rate, temperature, and pressure.

2.2.2.2. Hydrodynamic

The dynamics of bubble/slug formation in small diameter pipes <1000 µm are very different from those in conventional plug flow reactors. In this capillary pipe the gas-liquid-liquid segmented flow generated emerged shear forces in the opposite direction to the flow direction caused by friction, which could not be ignored, and the effect will be getting greater in the smaller capillary pipe diameter. The shear force triggers the internal circulation in the droplet liquid and the liquid slug. In some cases, the mixing process is governed by the bubble velocity, the drop liquid dispersed velocity, and the slug length. Therefore, one reason for implementing gas-liquid-liquid segmented flow in many microreactor applications is that the recirculation motion within the drop liquid dispersed and the liquid slug is able to enhance the mass transfer between gas and liquid-liquid phase dramatically. Because of highly intense and effective contact in a small channel, some specific reactions which require a high operating temperature could perform well at a lower temperature.

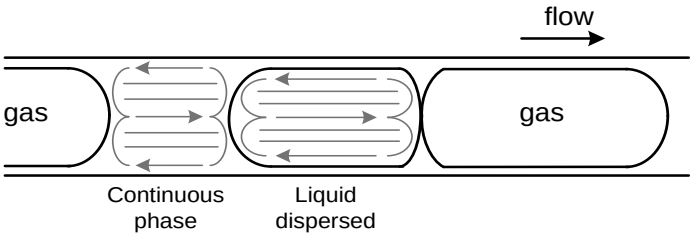

Figure 3. Internal recirculation in drop liquid dispersed and liquid slug

It may thus be considered that the gas-liquid-liquid mass transfer also depends on those parameters. The idea of correlating the kLa-value to the hydrodynamic characteristics of the flow was later readopted in the model developed by R. Kaur [21].
Their approach distinguishes three contributions to the mass-transfer from gas-liquid-liquid segmented flow, including mass transfer gas to continuous phase and dispersed phase, as well as mass transfer occurring between the continuous phase and dispersed phase.

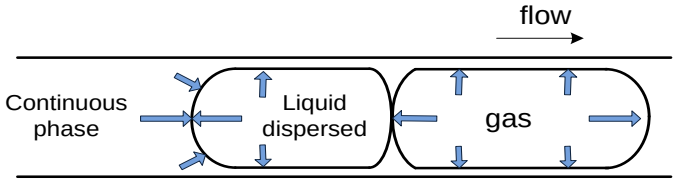

Figure 4. Mass transfer direction of three-phase flow within the microreactor

Three-phase segmented flow can be generated either in a simple flow-focusing device or in a combined junction, i.e., double T-junction [22]. The feeding system of gas and liquid-liquid phase reactants involves two types of T-mixers with three kinds of inlet sequences: O_1-W_2-G_3, O_1-G_2-W_3, and W_1-G_2-O_3 as shown in Figure 5 where oil is a continuous phase, whereas water and gas is a dispersed phase, respectively [22]. Experiments using these configurations elucidated that the first two types (see figure 5(a),(b)) are able to generate stable flows with uniform water droplets and gas bubbles. Conversely, the different results have been illustrated for the third configuration (W_1-G_2-O_3), whereas unstable flow patterns were generated, indicated by the irregular bubble lengths throughout the tube. The flow instability was caused by the low wetting properties of pure water to the channel wall thoroughly. The poor of wetted channel wall bring a direct contact of gas and channel wall, and then, gas filled totally T-junction area, which is more difficult for liquid water to scrape the bubble neck and cut it off. This phenomenon leads to the formation of very long bubbles and irregular bubbles length. Therefore, the third feeding configuration is not a preferable operation.

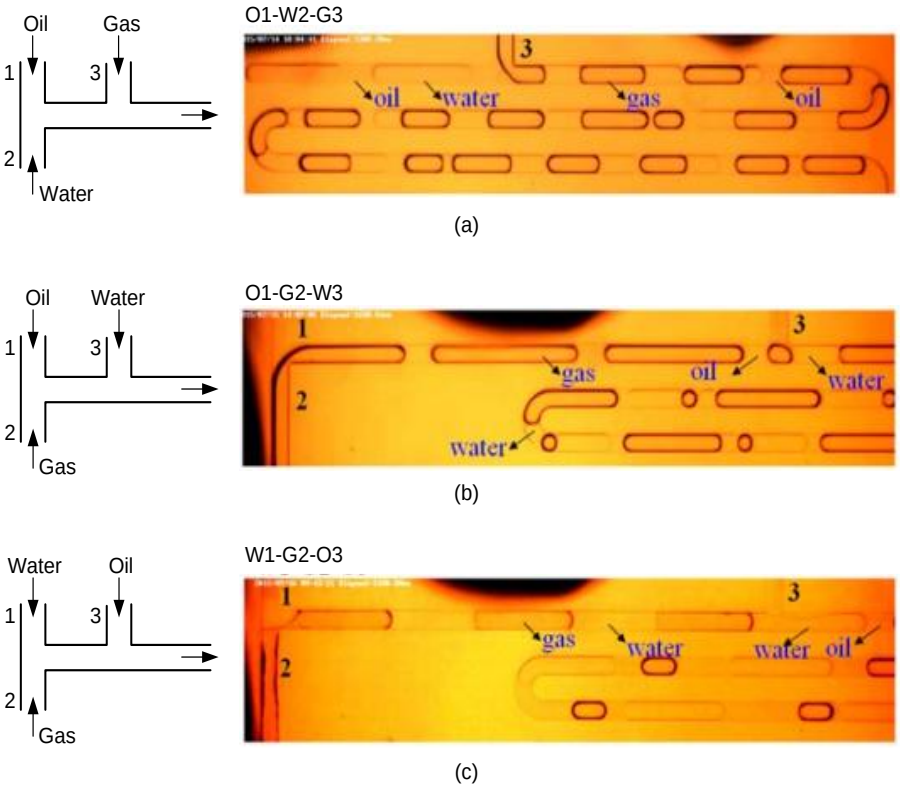

Figure 5. Three types of feeding configurations for gas-water-oil phases (G = gas, W = water, O = oil) [22]

A study on the dynamics of bubble, droplet, and slug formation involving water, paraffin, and air in the pipes of 5.6 mm and 7 mm inner diameters of minichannel has also been reported Wegmann et al. 2007. The pipe was made from glass (Schott Duran) with a total length of 5 m divided into five sections, each of which has a length of 1 m to ensure better pressure and temperature control of the pipeline flow.

The experimental had detected four types of flow dynamics that emerged in the tube, i.e., stratified, intermittent, dispersed, and annular flow patterns. The dynamics of bubble, droplet and slug formation in the mini-channel must be known well to determine optimum operating conditions such as temperature, pressure, and inter-phase contact mechanisms occurring within microchannel [8].

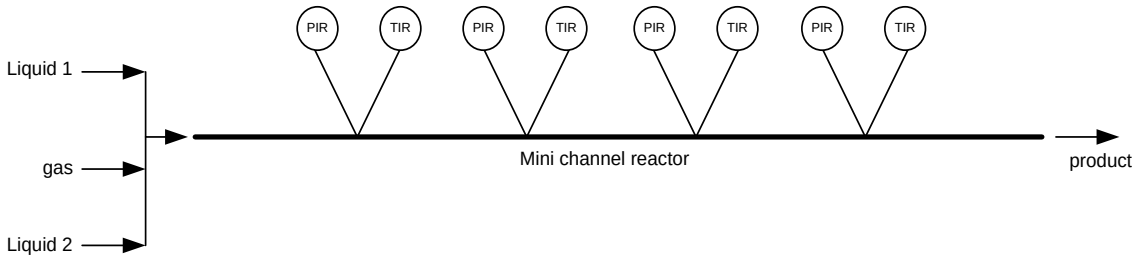

Figure 6. Schematic diagram of the mini-channel reactor [8]. PIR = Pressure Indicator Recorder, TIR = Temperature Indicator Recorder.

2.2.2.3. Applications

Microdevices in the range diameter <1000 µm are a promising topic for the pharmaceutical and fine chemical industry, mainly intended for the processes involving many different phases like gas-liquid-liquid. Hydrogenation α, β-unsaturated aldehyde is one example of a three-phase reaction that has been performed in three types of a microreactor with an internal diameter of 500, 750, and 1000 µm and capillary pipe lengths of 3, 6, and 12 m. The microreactor used is made of PTFE material to visualize fluid dynamics within the microreactor, which can operate up to a maximum pressure limit of 3 MPa. To ensure the hydrogenation lasting effectively into the reaction system was added the homogeneous Ru (II) -TPPTS catalyst, which was highly soluble within the aqueous phase [13]. The hydrogenation experimental tool scheme using a capillary microreactor is shown in figure 7.

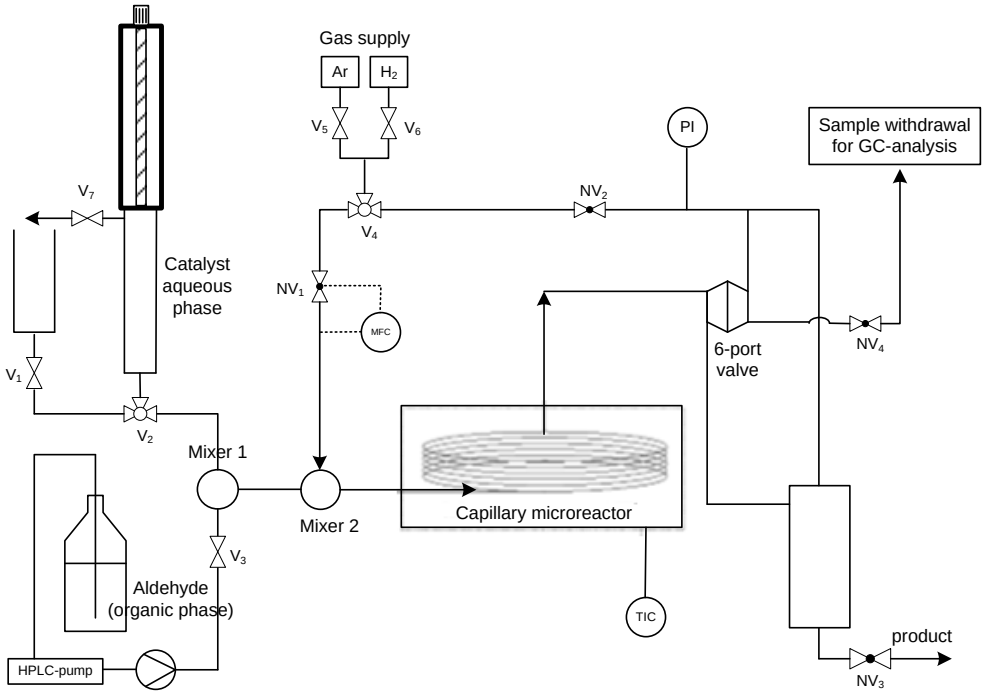

Figure 7. The scheme of a capillary microreactor for Hydrogenation α, β-unsaturated aldehyde [13]

The dynamics of bubble, droplet, or slug formation that appears in the capillary tube can be described in Figure 8. Since the organic phase has a higher affinity for PTFE, the capillary inner walls are thoroughly closed by the organic phase (continuous phase), and the aqueous phase is never in direct contact with capillary walls. Therefore hydrogen gas injected into the L/L mixture is only in the organic phase.

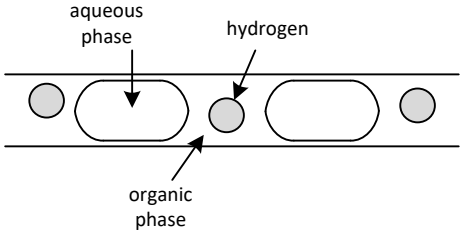

Figure 8. The flow dynamic formed within capillary microreactor [13]

The studies on hydrogenation reactions indicate that the use of a capillary microreactor is influenced by several operating parameters, one of them related to the catalyst phase. In determining the effect of the catalyst, the experiment was carried out by varying the volumetric flow rate of the aqueous phase containing a homogeneous catalyst where the hydrogenation reaction is expected to take place, whereas the organic phase and hydrogen gas flow rates are kept constant at 250 µL / min and 2800 µLn / min. The reaction temperature of 50 °C and hydrogen pressure in the capillary pipe of 2 MPa is selected. Under these conditions, the conversion and reaction rates observed show a tendency to increase. An increase in the catalyst's volumetric flow rate has been shown to result in an increase in dimensionless numbers of Reynolds Number and mass transfer coefficient overall. The overall mass transfer efficiency is directly related to the Reynolds Number.

In this context, as most multiphase reactions involve gas and liquid-liquid, the rate of mass transfer in the G/L-phase boundary is one of the controlling factors. However, it does not mean to obtain a large product yield into the liquid phase that must be injected hydrogen gas with a tremendous flow rate, but conversely, the optimum yield can be achieved by only a relatively small hydrogen gas flow rate of 1.4 mLn/min. The use of hydrogen flow rates of more than 1.4 mLn/min will actually reduce the reaction rate due to at high hydrogen flow rates, hydrogen gas bubbles occupying the organic phase (Figure 7) as a continuous phase are getting more so that it has an impact on reducing the effective volume of reaction and the average residence time within a capillary pipe.

Another parameter of interest in this experiment is the temperature. In this work, the selection of a high reaction temperature has a potential of decrease in activation energy because, at high temperature, the mass transfer rate in L/L phase boundary decreases as a result of low hydrogen solubility in water (~ 1.0 g/L) [13] as a catalyst medium. In this case, the optimum reaction rate still might be reached by reducing the droplet size, which leads to an increase in the specific surface area. It may be done by reducing the internal diameter of the capillary tube.

Dan I. Enache et al. (2007) performed a hydroformylation study on cyclododecatriene (CCDT) (olefin type) using a homogeneous catalyst in a square channel reactor (HEx) under dimensions of 2 mm x 2 mm. In this work, the concentration of the catalyst of 0.3 mol% was dissolved in cyclododecatriene (without solvents) under temperature in the range of 50-85 °C, and 30 bar pressure constant with a backpressure regulator and supported by pressure transducers and a manometer with 0.1 accuracies [9].

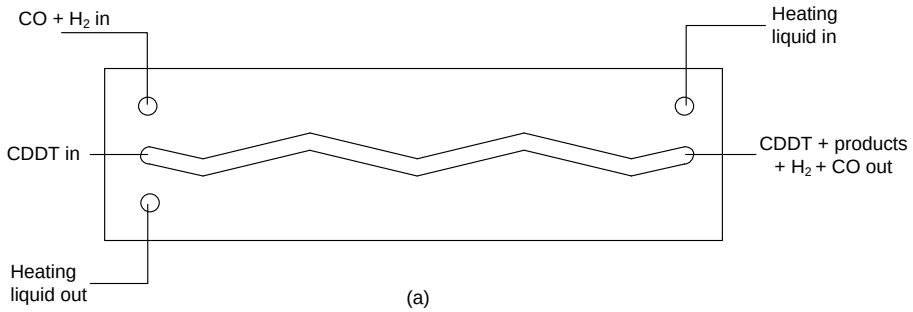

(a)

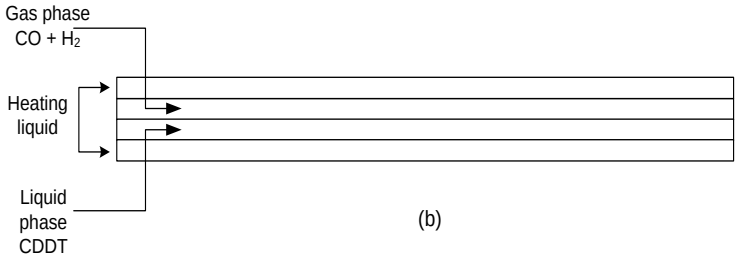

Figure 9. Schematic diagram of HEx reactor. CDDT = cyclododecatriene [9]

The most interesting section of this work is the integration of channel-reactor and heat exchanger. The intensification process brings consequence an increase in the heat transfer load required by a reactor unit. However, the heat requirement can easily be met by this heat exchanger. Therefore, hydroformylation might perform at the setting temperature desired, then unwanted side reaction can be prevented. The HEx reactor can produce a high selectivity of monoaldehyde products; moreover, this reactor has a simple design, no moving parts, give a better possibility in controlling flow and mixing process, stable flow, and uniform residence time can be achieved within throughout the reactor.

2.2.2.4. Advantages/disadvantages

The small dimensions of microreactor offer many advantages in chemical processes, i.e., improving the process safety, mainly for the chemical processes under high risk operating parameters such as high temperature and pressure [7]. In case of reactions with high hazard potential, small volume generates a low impact of possible runaway reactions, as well as a favorable ratio of surface area to volume for heat/mass transfer rate and controllable phase dispersion to ensure stable operation and production, that allowing a high reaction yields achieved [8]. Besides purposed for homogeneous catalysts, microreactors also accommodate heterogeneous catalyst systems by applying microstructured plate coated catalysts with an appropriate method. The fluid reacting components flow through a microreactor, and a multiphase reaction takes place on the plate's coated catalyst.

One disadvantage of preparing G/L/L multiphase flow using microfluidic devices is the low production rate, which greatly restricts this technology's wide application. Thus, designing a novel micro-structured device and further developing a droplet swarm is necessary to realize the application of multiphase flow in chemical reaction and separation processes. One feasible solution achieving scale-up is operating several microfluidic devices in parallel [23].

2.2.3. Jet Loop Reactor

Jet loop reactor can be described as a hybrid reactor unit between continuous stirred tank reactor (CSTR) and tubular reactor (PFR), which combines many appropriate attributes of both reactor concepts. Based on the mixing process, the large specific internal surfaces achieved are able to create the different mass transfer of convective and diffusion. The fine dispersion of the reacting components in the reactor can also distribute heat evenly to achieve better reaction selectivity. Also, the residence time in the reactor that can be controlled makes it flexible for fast and slow chemical reaction applications.

Wide application of this reactor for various catalysts reactions has covered jet loop reactor down-flow and up-flow systems. The appropriate utilization of down-flow and up-flow reactor systems should consider the physical properties of chemicals involved in fluid density. The schematic of the jet loop reactor down-flow and up-flow for the different fluid densities is shown in figure 10. The density (ρ_1) is the density of the continuous phase, and ρ_2 is the dispersed phase density.

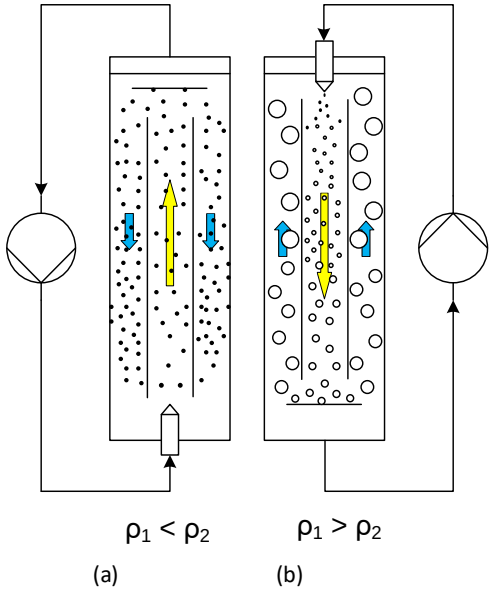

Figure 10. The schematic of jet loop reactor, (a) up-flow system by placing a nozzle at the bottom, (b) down-flow with a nozzle at the top [24].

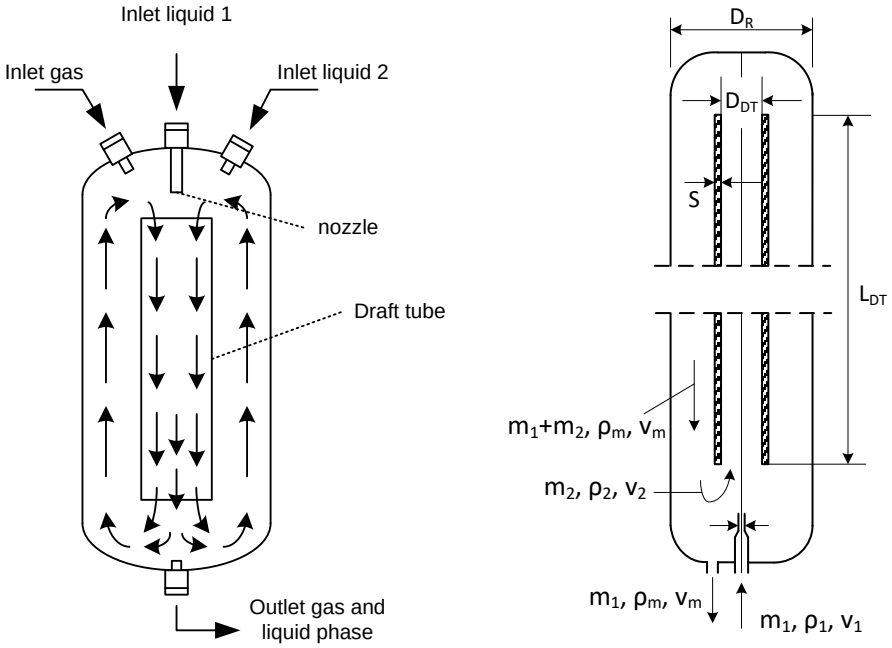

Figure 11. Schematic of jet loop reactor down-flow and up-flow, D_R = reactor diameter, D_{DT} = draft tube diameter, S = draft tube wall thickness, L_{DT} = length of draft tube, v = flow rate, m = mixture; 1, 2 = component 1, 2.

Jet loop reactor mainly consists of an outer tube, an inner tube, and a nozzle installed in the draft tube (Figure 11). Nozzle serves to introduce feeding flow supported by pump work that enables mixing processes to take place well and eliminates the utilization of a mechanical mixer inside the reactor. That's why a large-capacity pump is a critical item in this design. Gas-phase is fed to the reactor as per the consumption via a pressure regulator. This reactor type is an efficient contactor and mixer for the gas and liquid phase due to the rotation of the liquid phase catalyst carrying unconverted gas raw material into the reactor. The recycled liquid phase is introduced to the draft tube using a nozzle and forming the jet flows. This circulation takes place in several flow cycles, and it can be adapted to the processing needs.
The circulation number (n) can be determined by calculating the ratio between the total mass flow rate ($m_1 + m_2$) to the throughput mass flow (m_1) of the reactor, as can be seen in figure 12.

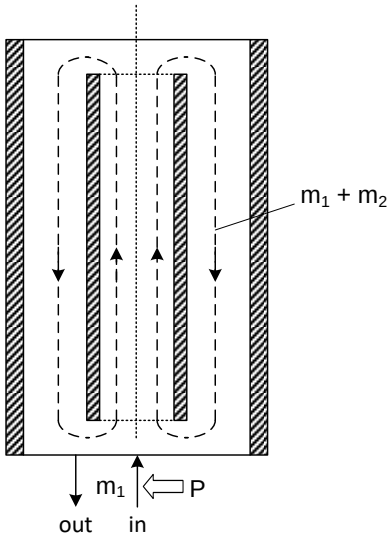

Figure 12 Schematic of a loop reactor within and outgoing stream and internal circulated stream induced by power P [24].

$$n = \frac{m_1 + m_2}{m_1} \quad (1)$$

Hydrodynamic of jet loop reactor resembles CSTR in series with the same reactor volume. High numbers indicate strong back mixing and, therefore, a performance closer to a CSTR, while low numbers lead to a plug flow-related flow regime ($n \geq 20$ approximate CSTR, $n = 0$ approximate PFR) [24]. The jet flows to enable the formation of very fine gas-liquid dispersions, which can enhance a large surface area between phases for the mass transfer process. Since yields product for multiphase reactions is primarily determined by mass transfer rate, thus the use of a jet loop reactor is an appropriate decision for various applications of gas-liquid-liquid reactions. The jet loop reactor is also adequate to provide high Reynold numbers in generating a high intensity of reactants mixing. It also has shown the opportunity to reduce the space-time, increase in selectivity, as well as require low energy consumption in its operation [10][25][26][27].

Then, for measuring the mass transfer rate within a reactor, an appropriate model should be determined at first. Among the existing model, the mass transfer model for the multiphase system inside the reactor could be elucidated using two-film theory. Some general trends related

to the value of mass transfer coefficient within Jet Loop Reactor: (1) The mass transfer coefficient increase with increasing the gas and liquid flow rate. (2) The volumetric mass transfer coefficient is 11-13% higher in the square draft tube than in the cylindrical draft tube. (3) The addition of salt or coalescence suppressing substances like isopropyl alcohol leads to fine bubbles in the gas/liquid system. Therefore, it can produce a higher mass transfer coefficient.

Moreover, Jet loop reactor also offers advantages such as a simple design, no moving parts, the flow and mixing are easily controlled, the inlet section of the liquid/gas phase could be modified adjusted to the reaction system referenced. Furthermore, the jet loop reactor is characterized by a mixing control and bubble size that is better than conventional bubble columns. The mass transfer rate is highly affected by the reactant flow rate and jet stream velocity within the reactor. For that reason, Jet loop reactor was already used for several chemicals, and biochemical catalyzed reactions consist of homogenous and heterogeneous catalysts and biocatalysts [25].

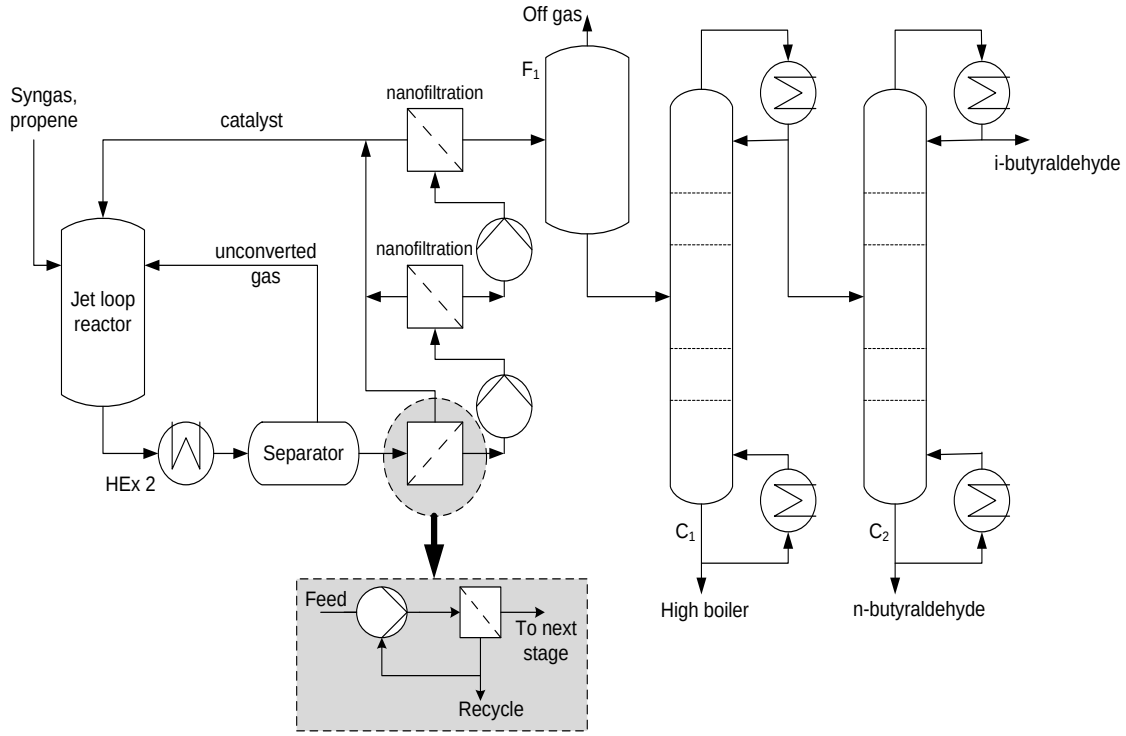

Figure 13. Flowsheet of Hydroformylation of propene with Jet Loop Reactor [10]

Tim Seifert et al. (2014) studied hydroformylation of propene to synthesis butyraldehyde, which was carried out using a jet loop reactor as a new design and a bubble column reactor, a conventional design comparing both reactors performances. The proposed new design consists of a jet loop reactor followed by an external heat exchanger and a separator unit to separate the unconverted gas from the product mixtures containing catalyst. The catalyst and product were separated in the next process in the multistage organophilic nanofiltration unit, and then, the separated catalyst flowed back into the reactor. An attractive design aspect is applying an external heat exchanger behind the reactor unit adequate in providing a flexible surface area needed for the heat transfer process. Further, the high flexibility in the jet loop reactor unit can be easier realized.

Butyraldehyde is widely applied as a vulcanization accelerator, synthesis resin, and plasticizer. The developed process designs follow the "Ruhrchemie process" scheme under operating parameters: the reaction temperature of 110 °C and 21 bar pressure, 20 min residence time, and the reaction conversion attain 75% with a selectivity of propene to butyraldehyde was 97% [10]. Besides propene was transformed into the n-/iso-butyraldehyde, other reactions that took place consisted of a side reaction and the consecutive reaction 1 and 2. In these 2 consecutive reactions, the butyraldehyde products were transformed into butanol and 2-ethyl-2-hexenal.

Main reaction : $\text{Propene} + CO/H_2 \xrightarrow{\text{catalyst}} \text{n-/iso-butyraldehyde}$

Side reaction : $\text{Propene} + H_2 \longrightarrow \text{Propane}$

Consecutive reaction 1: $\text{Butyraldehyde} + H_2 \longrightarrow \text{Butanol}$

Consecutive reaction 2: $\text{2-Butyraldehyde} \longrightarrow \text{2-ethyl-2-hexenal} + H_2O$

Unlike a jet loop reactor, the conventional process applied a bubble column reactor for conducting hydroformylation in a more complicated design and larger reactor in size and higher energy consumption mainly for stirring and compressor/pump to drain gas/liquid. In a conventional system using a bubble column, the reactor has a high to diameter ratio of around 2.5, and a stirrer is used to disperse gas to a liquid phase. Then, a flash separator unit followed the reactor, which is operated at 1 bar pressure. The liquid mixture containing catalyst and solvent is recycled into the reactor, and the main product leaves for the separator unit to obtain a high purity of the final product.

The current works on hydroformylations using a jet loop and bubble column reactor showed that propene's selectivity to butyraldehyde could be improved 1%, the reaction conversion significantly increased from 75% to 90% in the same operating conditions applying jet loop reactor [10]. These improvements undoubtedly reduce raw material and utility consumption by almost 7%, which has an economic impact on operational costs compared to the hydroformylation processes in bubble columns.

2.2.4. Rotor-Stator Reactor (RSR) + Stirred Tank Reactor (STR) Tandem Process

Unlike other reactors, the tandem reactor integrates two kinds of continuous reactors and separators in one process cycle. The continuous reactors involved in this section are the rotor-stator reactor (RSR) and the stirred tank reactor (STR). The RSR unit utilizes the rotor's rotation between the stator to create intensive contact between phases involved in a reaction, i.e., the gas phase and the liquid-liquid phases. A similar mixing principle was found in the second type of reactor (stirrer tank reactor). In the STR, gas, and liquids phases come into contact due to stirring activities like the rotor's function at the RSR. Next, after contacting processes between phases in the second reactor, the gas will be separated from the liquids mixture and exit through a condenser. The separation is possible to occur, even though the STR works at atmospheric temperature, because of the very small gas solubility in the liquid phase; even if the STR works at the higher temperatures, the separation of gas will be easier to take place. In the flow cycle described in Figure 15, the liquid phase is recycled into the RSR in several cycles. This cycle allows liquids reactants which have not reacted yet in the previous period to carry out the chemical reactions both with liquids reactants and fresh gas reactant. Therefore, utilizing the tandem reactor is capable of increasing yield and reaction conversion of three-phase gas-liquid-liquid reactions.

In this section, it is described a rotor-stator reactor with the detail specification is shown in table 3. The RSR is composed of rotor rings that act as the rotating component, and stator rings are the disturbing component with 6 and 5 pieces, respectively. The rotor ring is attached to the rotor seat while the stator ring is concentrically mounted on the cover cap. Rotor rings and stator rings are arranged alternately in the radial direction. Part of the rotor has many perforations with a diameter of 4 mm as a fluid channel besides open space between rotor and stator. The rotor's high rotation speed and strength by the presence of perforations in the rotor field can break gas bubbles and liquid droplets in tiny sizes and create the violent turbulence of fluids that drove the formation of a large surface area-interface for mass transfer. The high gravity level produced in the RSR is one to three orders of magnitude larger than the gravitational acceleration [28], resulting in intense mass transfer and micromixing effects.

Table 3. The specification of RSR [28]

Remark	Value
Layer number of rotor rings	6
Layer number of stator rings	5
Number of perforations in the rotor rings	180, 240, 294, 348, 408,
Number of pins in the stator rings	462
The diameter of perforations in the rotor rings (mm)	12, 16, 20, 24, 24
The diameter of pins in the stator rings (mm)	4
The inner diameter of rotor rings (mm)	5
The inner diameter of stator rings (mm)	70, 94, 118, 142, 166,
The inner diameter of RSR (mm)	190
Height of rotor rings (mm)	80, 104, 128, 152, 176
Height of stator rings (mm)	300
Height of RSR (mm)	61
	60
	65

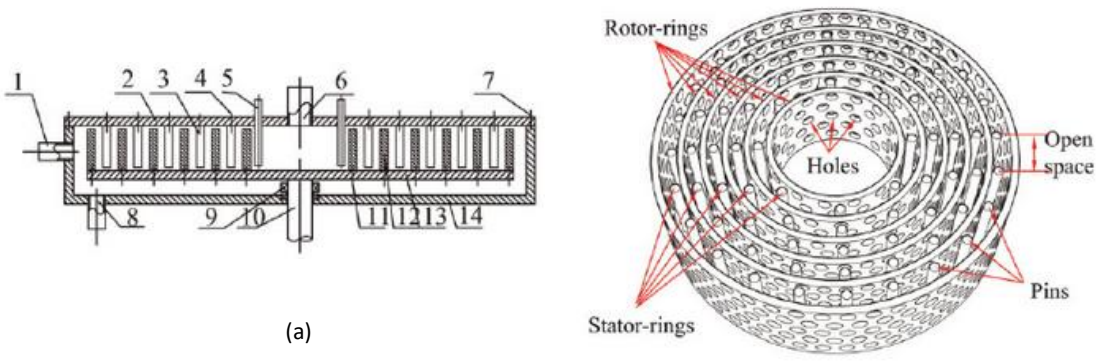

(a) (b)

Figure 14. Schematic diagram of RSR. (a) Structure of RSR. (b) 3D diagram of rotor rings and stator rings: (1) gas inlet; (2) cover cap; (3) stator; (4, 7, 11) bolts; (5) liquid distribution; (6) gas outlet; (8) liquid outlet; (9) seal; (10) shaft; (12) rotor; (13) rotor seat; (14) casing [28].

The second reactor involved a stirred tank reactor (STR) under 250 ml volumes and a condenser as the main components. Oil batch and circulation thermostatic batch are adopted to maintain RSR and STR's operating temperature at specific temperatures.

Figure 14 shows a detail schematic diagram of RSR. The operating stages of RSR are as follows: first, the liquids mixture is pumped into the RSR through a liquid inlet and jetted into the cavity of the RSR via a liquid distributor installed in the middle near the shaft. The liquids mixture then flowed radially outwards through the fluid channels in the rotor-stator arrangement. It was fragmented into tiny liquid droplets under the influence of centrifugal force generated by the rotating rotor rings at a specified rotation speed. Simultaneously, the gas-phase was introduced into the RSR from a gas inlet and flowed inwardly through the fluid channels; counter-current contact takes place with the liquids mixture. Then, excess gas was stripped out of the liquids mixture, and they were flown out the RSR via the gas and liquid outlet, respectively, toward stirred tank reactor (see Figure 15). In a short processing time, only in minutes, a specific volume of the liquid mixture product was removed from STR.

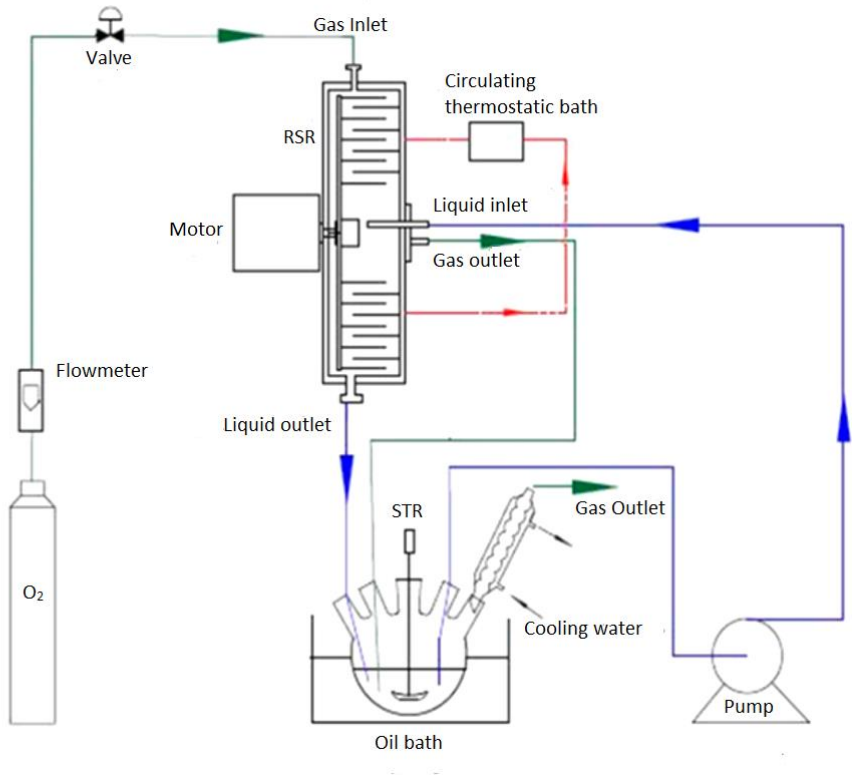

Figure 15. Schematic of RSR+STR tandem process [14]

However, this reactor has a more complicated design than other types of reactors and higher energy consumption, and it becomes more significant as the reactor capacity. Besides that, this reactor needs supporting equipment. It has moving parts, it requires maintenance regularly to avoid the risk of wear, and periodically, it needs to change the moving parts to keep the reactor's performance.

The synthesis of 2,3,5-trimethyl-1,4-benzoquinone (TMQ) is carried out through a catalytic oxidation reaction of 2,3,6-trimethylphenol (TMP) in a three-phase gas-liquid-liquid in a reactor system that combines a rotor-stator (RSR) and a conventional stirred tank reactor (STR) [14]. The 2,3,5-trimethyl-1,4-benzoquinone (TMQ) is an essential intermediate compound in the synthesis of vitamin E. Vitamin E is a necessary nutrient for humans to resist oxidation and slow down aging. The need for it increases up today.

$$\text{2,3,6, -trimethylphenol} + O_2 \xrightarrow{CuCl_2} \text{2,3,5-trimethyl-1,4-benzoquinone} + H_2O$$

Conventionally, TMQ is generated through a sulfonation reaction of TMP with H_2SO_4, followed by an oxidation reaction using manganese dioxide. Since TMQ-products synthesized through this reaction are often contaminated by water and inorganic salt, so this process is gradually not used anymore and replaced by TMP catalytic oxidation, which is the primary method for industrial production for TMQ at present by considering simple in the process, environmentally friendly, generate a high purity product. The process is capable of producing high yield TMQ. Generally, the industry chooses CuCl2 as the primary catalyst and oxygen/H_2O_2 as an oxidation agent to realize the catalytic oxidation TMP to TMQ in STR. As to GLL three-phase reaction, this reaction is restricted by the mass transfer process; therefore, their study tried to intensify mass transfer efficiency as a condition for achieving yield and optimum reaction conversion by utilizing high gravity technology and involving the influence of centrifugal force.

The various operating parameters, including the rotational speed of RSR, volumetric gas flow rate, liquid volumetric flow rate, water volume fraction in the liquid phase, reaction temperature, on TMQ yield, were systematically examined. Results reveal that the high conversion could be achieved at the RSR rotor rotational speed of 600 rpm, and the optimal temperature for safety is 75 °C. The use of gas flow rates up to 80 L/h tends to deliver a stable TMP conversion because, at a low gas flow rate, gas has a little effect on liquid-liquid mixing in RSR where the mixing is a very crucial process for TMP activation that triggered by the contact between $CuCl_2$ catalyst and TMP. The contact between gas and liquid in RSR is the cause of this phenomenon due to the liquid dispersion in RSR will face a gas resistance at too high a gas volumetric flow rate. A similar result was found out by raising the water fraction contained $CuCl_2$ catalyst. Water in this reaction system is a solvent for the $CuCl_2$ catalyst. The use of water up to 0.98 fraction increases the solubility of CuCl2 in liquid water, facilitating the TMP activation.

These results elucidate that the increase in TMQ synthesis in the RSR + STR tandem reactor results from an intensive process involving liquid-liquid mixing, gas-liquid mass transfer, and oxidation reactions in RSR [14].

The performance of gas-liquid-liquid reaction in the developed reactors is shown in Table 4.

Table 4. Reactors performance in gas-liquid-liquid reactions

Gas-liquid-liquid Reaction	Operating Parameters					
	Residence time	Yield	Conversion	Temperature/ pressure	Type of Reactor	Reff
Hydrogenation of α,β-Unsaturated Aldehydes	2-3 minutes	-	-	60 °C / 2 MPa	Microreactor	[13]
Coupling process of oxidation and extraction for H_2O_2 synthesis	6.5 sec	-	100% & Murphree eff = 90%	50 °C / 300 KPa	Minichannel	[11]
Hydroformylation of styrenes	58 min	94%	97%	65 °C / 25 bar	Minichannel	[7]

Hydroformylation of propene	5 sec	Selectivit = 99%	-	40 °C	Tubular reactor with static mixers	[6]
Hydroformilation of propene	1200 s	Selectivit y = 97%	90%	110 °C/ 21 bar	Jet loop reactor	[10]
Hydroformilation of cyclododecatriene	6 min	Selectivit y = 99%	30%	85 °C/ 30 bar	Minichannel	[9]
Oxidation of 2,3,6-trimethylphenol (TMP)	10 min	20%	86.9%	75 °C/ 1 atm	RSR-STR tandem	[14]

2.3. Reactor Selection

GLL multiphase reactions have unique characteristics involving immiscible gas and liquid-liquid phases under a higher complexity compared to the reactions involving reactants with the same phase and two different phases [23][29]. The overall rate of gas-liquid-liquid reactions would depend on the following parameters: (1) Intrinsic kinetics of the reaction steps, (2) Solubility of gases in two liquid phases, (3) Gas-liquid and liquid-liquid mass transfer coefficient, (4) Drop size of the dispersed phase, (5) Bubble size of the gas phase, and (6) liquid-liquid equilibrium properties for the reactants and products [21]. Gas-liquid-liquid reactions in their applications take place in several diffusion stages. The diffusion resistance might be a serious burden if it is not facilitated by selecting the right process system and the fluid contact strategy.

The basic concept of the chemical process in a multiphase reactor involves the diffusion resistances removal at various process stages to bring up a high mass transfer rate and the maximum productivity that can be realized. The developed mass transfer models (see table 4, chapter 1) have described the transfer's possible route. The derived equations for mass transfer resistance in each model show a similar form for the gas-liquid route (gas to oil and gas to water) and liquid-liquid route (oil to water and water to oil). Transfer rate increases with a decrease in gas or liquid resistance, which can be realized by enhancing the mass transfer coefficient (k_g, k_L), and surface area contact (a). There are some possible strategies for improving mass transfer between phases:

- First, reducing the droplets sizes of gas bubbles and or liquid. Reducing sizes will be able to create high surface area contact and a smaller distance of diffusion. Enhancing the surface area contact can be reached through good mixing/agitation.
- Second, increase in the partial pressure of the gas. Higher partial pressure reduces the value of Henry's law constant.
- Third, enhancing the concentration of gas / liquid solute and lowering the liquid-liquid equilibrium constant.

Therefore, selecting appropriate gas-liquid contactors becomes a critical step in realizing a high mass transfer rate. Some aspects that should be considered in determining gas/liquid contactor [30]:

1. Contacting pattern. The contacting method through the flowing gas and liquid phase resembles a plug flow in a contactor with the largest mass transfer driving force. In contrast, the contacting method corresponds to a mixed flow with the smallest mass transfer driving force. As we shall see in figure 20, towers have the most extensive mass transfer driving force

and, in this respect, have an advantage over tanks. Agitated tanks have the smallest driving force. Figure 20 shows the approximate plug G/plug L, bubble tanks approximate plug G/mixed L, agitated tanks approximate mixed G/mixed L.

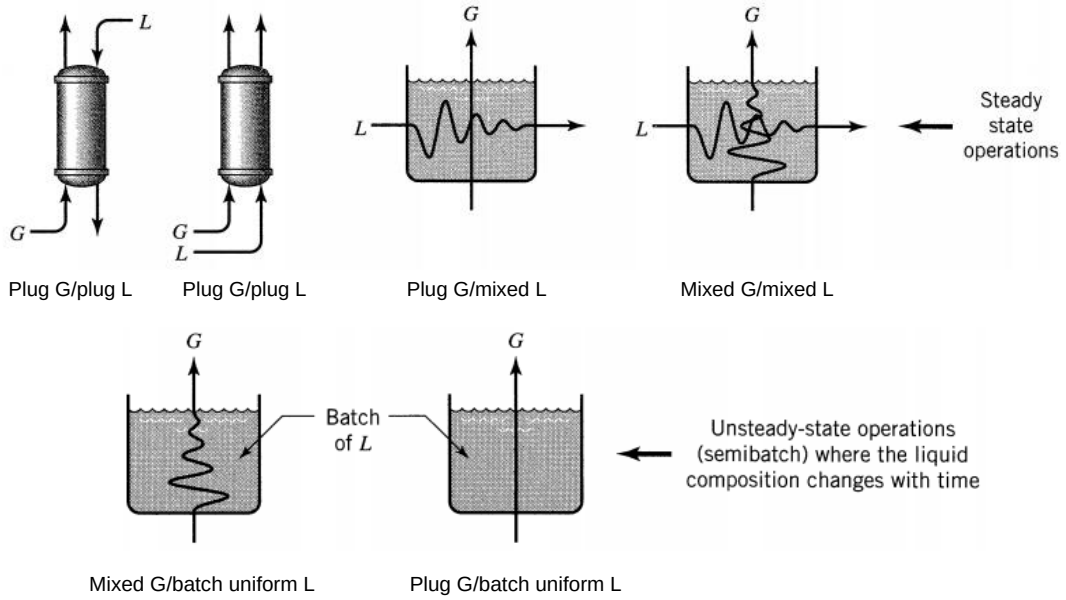

Figure 20. Contacting pattern between gas and liquid phase in G/L contactors [30]

2. k_g and k_L. Liquid droplets in gas give a high k_g and low k_L. Conversely, gas bubbles rising in the liquid have a low k_g and high k_L.

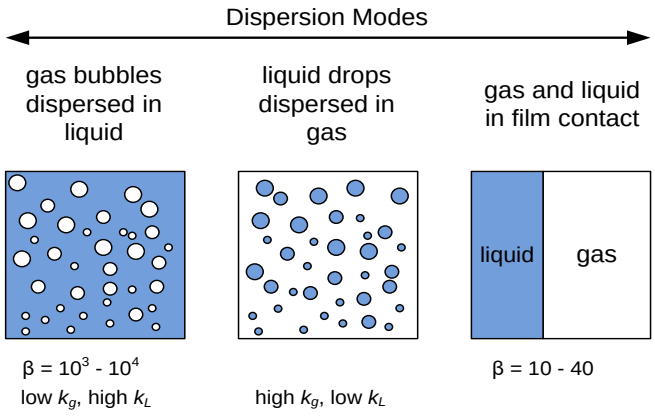

Figure 21. Three dispersion modes for gas-liquid-liquid systems.

β is the ratio of liquid-phase volume to diffusion layer volume. β = $\frac{\varepsilon_L}{\delta_L . a}$, where ε_L the fractional hold-up of liquid-phase; δ_L is the thickness of liquid phase diffusion; and a is interfacial area per unit reactor volume.

3. Flow rates. The packed-bed contactor and the similar one have the best performance under relative flow rates of about F_L/F_g = 10 at 1 bar. Other contactors are more flexible, and they work well in a wider range of F_L/F_g values.
4. Solubility. For highly soluble gas in a liquid, the small value of Henry's law constant, gas film control, it should avoid bubble contactor. For low soluble gas in a liquid, the high value of

Henry's law constant and liquid film control, it should avoid the use of spray tower.

5. The mass transfer resistance is in the gas phase and or liquid film. If the liquid film resistance is dominant, stay away from the spray contactor, and contrary, if the gas film resistance dominates, stay away from the bubble contactor.

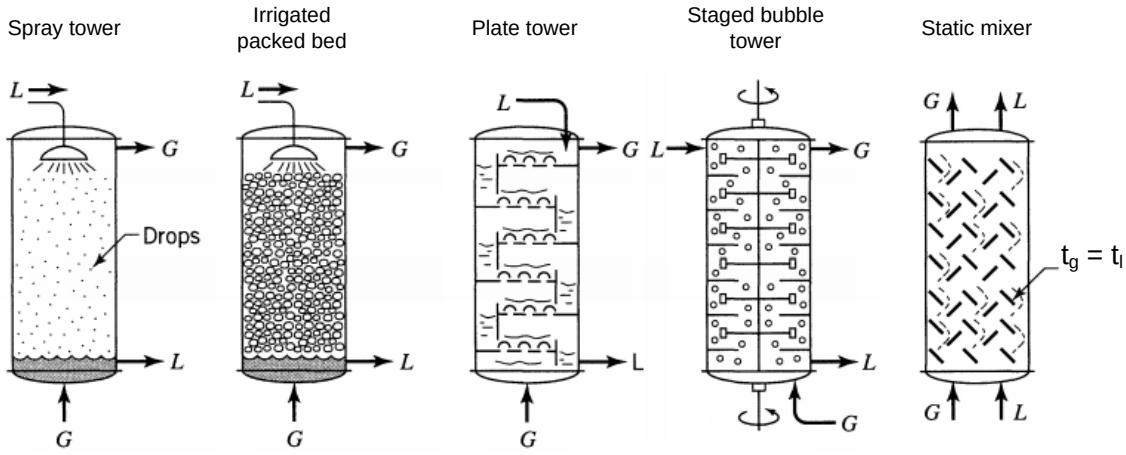

Figure 22. Tower contactors for G/L reactions [30]

Based on the explained aspects above, the characteristic of the developed reactors for GLL applications described in this chapter can be classified in table 5.

Table 5. Characteristics of each reactor for GLL applications

Contactor/ Reactor	Contacting pattern	Level of Driving Force	k_g or k_L	F_L/F_g	Mass Transfer Resistances	Solubility
Tubular with a static mixer	Mixed G/mixed L	low	Down flow: high k_g low k_L. Up flow: low k_g high k_L	Max 10 at 1 bar	Down flow: suitable for the dominant k_g. Up flow: suitable for the dominant k_L.	Down flow: suitable for highly soluble gas in liquid. Up flow: suitable for slightly soluble gas in liquid.
Microreactor	Plug G/plug L	High	Low k_g and high k_L	Flexible	Model bubble, suitable for the dominant k_L.	Suitable for slightly soluble gas in liquid
Jet loop (down flow & up flow)	Plug G/plug L	High	Low k_g and high k_L	Flexible	Model bubble: suitable for the dominant k_L.	Down flow: suitable for highly soluble gas in liquid. Up flow: suitable for slightly soluble gas in liquid
RSR+STR tandem	RSR: mixed G/mixed L. STR: plug G/mixed L	Medium	RSR: low k_g high k_L and high k_g low k_L (flexible). STR: low k_g high k_L	Flexible	RSR: flexible. Suitable for high k_g or high k_L STR: suitable for the dominant k_L.	RSR: flexible STR: suitable for slightly soluble gas in liquid.

Each reactor has advantages and disadvantages. The use of a specific reactor type should be adapted to the reacting components' physical/chemical properties. It could be found an appropriate reactor for performing gas-liquid-liquid reactions in realizing an optimum reaction yield by adequate consideration. Further, a better process will generate a small volume of waste, lower pollution impact on the environment, and finally, reduce operational costs.

2.4. Conclusion

The developed four reactor technology in this chapter is intended for GLL applications. Each reactor shows a unique design, adapted to its function as a medium to carry out a chemical reaction, enabling a mass transfer between phases to perform optimally. Three-phase GLL reactions are also a unique system that involves immiscible gas and liquid-liquid phases with specific physical and chemical characteristics. That's why knowing about the chemical reactant behavior in contact is principally necessary to determine a reactor design appropriately. Some parameters were known to govern the overall reaction rate, consist of intrinsic kinetic of the reaction steps, the solubility of gases in two immiscible liquids, gas-liquid and liquid-liquid mass transfer coefficient, drop size of the dispersed phase, bubble size of gas, and liquid-liquid equilibrium properties for all phases involved. Therefore, a selected contactor should generate a contacting pattern that triggers a high driving force for mass transfer and generates liquid droplets and gas bubbles, which have a high mass transfer coefficient. In many cases, the specific contactor was chosen by considering which film layer will control the transfer process, gas/liquid film. Finally, a reactor design should be able to provide a large surface area for transfer between phases. The appropriately selected reactor will facilitate the efforts to realize a high yield and conversion.

Literature:

[1] V. G. Pangarkar, "Process intensification in multiphase reactors: From concept to reality," *Chem. Eng. Process. Process Intensif.*, vol. 120, no. May, pp. 1–8, 2017.

[2] J. B. Powell, "Application of multiphase reaction engineering and process intensification to the challenges of sustainable future energy and chemicals," *Chem. Eng. Sci.*, vol. 157, pp. 15–25, 2017.

[3] Z. Qiu, L. Zhao, and L. Weatherley, "Process intensification technologies in continuous biodiesel production," *Chem. Eng. Process. Process Intensif.*, vol. 49, no. 4, pp. 323–330, 2010.

[4] A. Y. Widianto, J. Aubin, C. Xuereb, and M. Poux, "Gas-liquid-liquid reactions: Contacting mechanisms and effective process technologies," *Catal. Today*, no. November 2018, 2019.

[5] T. M. Baber, D. Graiver, C. T. Lira, and R. Narayan, "Application of catalytic ozone chemistry for improving biodiesel product performance," *Biomacromolecules*, vol. 6, no. 3, pp. 1334–1344, 2005.

[6] K. D. Wiese, O. Möller, G. Protzmann, and M. Trocha, "A new reactor design for catalytic fluid-fluid multiphase reactions," *Catal. Today*, vol. 79–80, pp. 97–103, 2003.

[7] S. Kasinathan *et al.*, "Syngas-mediated C-C bond formation in flow: Selective rhodium-catalysed hydroformylation of styrenes," *Synlett*, no. 18, pp. 2648–2651, 2011.

[8] A. Wegmann, J. Melke, and P. Rudolf von Rohr, “Three phase liquid-liquid-gas flows in 5.6 mm and 7 mm inner diameter pipes,” *Int. J. Multiph. Flow*, vol. 33, no. 5, pp. 484–497, 2007.

[9] D. Dumas *et al.*, "Intensification of the solvent-free catalytic hydroformylation of cyclododecatriene: Comparison of a stirred batch reactor and a heat-exchange reactor," *Catal. Today*, vol. 128, no. 1–2, pp. 18–25, 2007.

[10] T. Seifert *et al.*, "Intensified hydroformylation as an example for flexible intermediates production," *Chem. Eng. Process. Process Intensif.*, vol. 85, pp. 1–9, 2014.

[11] J. Tan, C. Dong, Y. C. Lu, J. H. Xu, and G. S. Luo, "Coupling process of oxidation and extraction in a gas-liquid-liquid microdispersion system for H 2O 2 synthesis," *Ind. Eng.*

Chem. Res., vol. 51, no. 4, pp. 1834–1845, 2012.
[12] F. Visscher, J. van der Schaaf, T. A. Nijhuis, and J. C. Schouten, “Rotating reactors - A review,” *Chem. Eng. Res. Des.*, vol. 91, no. 10, pp. 1923–1940, 2013.
[13] Y. Önal, M. Lucas, and P. Claus, "Application of a capillary microreactor for selective hydrogenation of α,ß-unsaturated aldehydes in aqueous multiphase catalysis," *Chem. Eng. Technol.*, vol. 28, no. 9, pp. 972–978, 2005.
[14] J. Chen *et al.*, "Study on the Synthesis of 2,3,5-Trimethyl-1,4-Benzoquinone by an RSR+STR Tandem Process," *Ind. Eng. Chem. Res.*, vol. 57, no. 40, pp. 13381–13386, 2018.
[15] R. K. Thakur, C. Vial, K. D. P. Nigam, E. B. Nauman, and G. Djelveh, "Static mixers in the process industries - a review," *Chem. Eng. Res. Des.*, vol. 81, no. 7, pp. 787–826, 2003.
[16] E. L. Paul, V. A. Atiemo-obeng, and S. M. Kresta, *HANDBOOK OF INDUSTRIAL MIXING Edited by*. 2003.
[17] A. Ghanem, T. Lemenand, D. Della Valle, and H. Peerhossaini, "Static mixers: Mechanisms, applications, and characterization methods - A review," *Chem. Eng. Res. Des.*, vol. 92, no. 2, pp. 205–228, 2014.
[18] V. M. Rajesh and V. V. Buwa, "Volume-of-fluid simulations of gas-liquid-liquid flows in minichannels," *Chem. Eng. J.*, vol. 345, no. July 2017, pp. 688–705, 2018.
[19] P. S. Saljoshi and A. T. Autee, “Experimental investigation of two-phase flow patterns in minichannels at horizontal orientation,” *Heat Mass Transf. und Stoffuebertragung*, vol. 53, no. 9, pp. 2799–2811, 2017.
[20] J. Yue, E. V. Rebrov, and J. C. Schouten, "Gas-liquid-liquid three-phase flow pattern and pressure drop in a microfluidic chip: Similarities with gas-liquid/liquid-liquid flows," *Lab Chip*, vol. 14, no. 9, pp. 1632–1649, 2014.
[21] R. Kaur and M. Ramakrishna, "ROLE OF DISPERSED PHASE IN GAS-LIQUID."
[22] C. J. Gommes, S. Blacher, J. H. Dunsmuir, and A. H. Tsou, "Practical Methods for Measuring the Tortuosity of Porous Materials from Binary or Gray-Tone Tomographic Reconstructions," *AIChE J.*, vol. 55, no. 8, pp. 2000–2012, 2012.
[23] Z. Chen, J. Xu, and Y. Wang, "Gas-liquid-liquid multiphase flow in microfluidic systems – A review," *Chem. Eng. Sci.*, vol. 202, pp. 1–14, 2019.
[24] H. Warmeling, A. Behr, and A. J. Vorholt, "Jet loop reactors as a versatile reactor set up - Intensifying catalytic reactions: A review," *Chem. Eng. Sci.*, vol. 149, pp. 229–248, 2016.
[25] W. Ludwig, R. G. Szafran, A. Kmiec, and J. Dziak, "Measurements of flow hydrodynamics in a jet-loop reactor using PIV method," *Procedia Eng.*, vol. 42, no. December, pp. 1157–1168, 2012.
[26] W. Chao-hai, W. Wen-xiang, D. Zhi-yi, and W. Chao -fei, "Characteristics of high-sulfate wastewater treatment by two-phase anaerobic digestion process with Jet-loop anaerobic fluidized bed," *J. Environ. Sci.*, vol. 19, no. 3, pp. 264–270, 2007.
[27] Z. DENG, C. WEI, and X. ZHOU, "Start-up and Performance of a Novel Reactor—Jet Biogas Inter-loop Anaerobic Fluidized Bed," *Chinese J. Chem. Eng.*, vol. 16, no. 1, pp. 143–150, 2008.
[28] R. L. Phase, "Mass Transfer Characteristics in a Gas – Liquid," no. March. 2009.
[29] M. Schrimpf, J. Esteban, T. Rösler, A. J. Vorholt, and W. Leitner, "Intensified reactors for gas-liquid-liquid multiphase catalysis: From chemistry to engineering," *Chem. Eng. J.*, vol. 372, no. March, pp. 917–939, 2019.
[30] J. Wiley and K. Hepburn, *Chemical Reaction Engineering - Boston.* 1982.

Symbols:		**Subscript/ superscript:**	
C	Concentration (mol.L^{-1})		
C_g^{wi}	Gas concentration in water at interface gas/water	*g*	Gas
C_g^{w}	Dissolved gas concentration in water	*o*	Oil

D	Diameter (m)	w	Water
T	Temperature (K)	i	interface
P	Pressure (atm)	L	Liquid
Q	Volumetric flow rate ($m^3.s^{-1}$)	L_1	Liquid 1
V	Volume (m^3)	L_2	Liquid 2
t	Time (s)		
k	Mass transfer coefficient ($m.s^{-1}$)		
a	Specific interfacial area (m^{-1})		
$k_L.a$	Volumetric liquid-side mass transfer coefficient (h^{-1})		
H	Henry coefficient (dimensionless)		
K_e	Equilibrium constant (dimensionless)		
K	Overall mass transfer coefficient		

Chapter 3

Hydrodynamics of gas-liquid flow in microtube

Contents

3.1. Introduction

Gas-liquid flow in microchannels can develop in different flow regimes. Gas-liquid flow patterns in microfluidic devices can vary from bubbly to annular flows based on the change in the volumetric flow rate of gas to a liquid. These two extreme conditions of gas-liquid flow are characterized by low and high void fractions, respectively. All flow regimes in the microchannel can be divided into three groups: regimes dominated by capillary forces; regimes dominated by inertial forces; and transitional regimes, where both of these forces are significant. The topology of the interface depends on fluid properties, operating conditions, as well as the geometry of the channel. Much work has been dedicated to the development of flow pattern maps that define the transition between the following regimes (figure 3.1):

- Bubbly flow, characterized by a number of tiny bubbles, smaller than the inside diameter of the channel;
- Slug flow or Taylor flow, characterized by bubbles that are longer than the characteristic dimension of the channel and separated from the walls by a thin liquid film;
- Annular flow, characterized by a continuous core of gas surrounded by a thin liquid film;
- Churn flow is between annular and bubbly flow, where the gas core breaks into tiny bubbles [1][2].

Many previous researchers have conducted a study of the two-phase flow pattern in the microchannel. Triplet et al., study a two-phase flow pattern in the channel with an inside diameter 1.09; 1.1; 1.45 mm. The observed flow patterns are slug, bubbly, churn, slug annular, and annular [1][3].

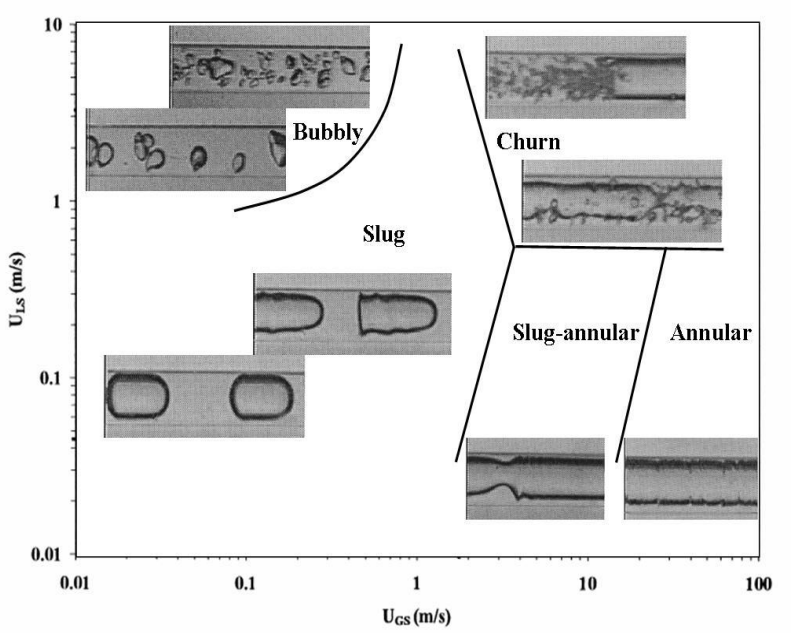

Figure 3.1. Gas-liquid flow pattern (using air and water) in micro-channel with inside diameter 1.097 mm; U_{LS} = superficial liquid velocity; U_{GS} = superficial gas velocity

Using gas and liquid superficial velocity on the range of 0.1 to 100 $m.s^{-1}$, and 0.01 to 10 $m.s^{-1}$, respectively, John W. Coleman (1999) described some flow pattern observed; bubble, dispersed, elongated bubble, slug, stratified, wavy, annular-wavy, and annular flow patterns. This study used the horizontal round and rectangular tubes with hydraulic diameters ranging from 5.5 to 1.3 mm and using air as a gas phase and water as a liquid phase [4]. Akimi Serizawa (2002) visualized the gas-liquid two-phase flow pattern in circular tubes of 20, 25, and 100 µm inside diameter with air-water as a gas and liquid phase, and for steam-water flow in a 50 µm inside diameter circular tube. The distinctive flow pattern, namely, dispersed bubbly flow, gas slug flow, liquid ring flow, liquid lump flow, annular flow, frothy annular flow, rivulet flow, and liquid droplets flow [5]. Then, the study using the superficial velocity of air and water lower than 0.1 m/s was conducted by Puccetti (2015). The flow pattern of Taylor slug and Taylor annular regimes only can be produced at the exit of the T-junction [6]. P.S. Saljoshi (2017), his experiment was conducted using a circular pipe with an inside diameter 1.1 mm and a total length of 650 mm. Five different two-phase flow patterns were identified, including bubbly, dispersed bubbly, slug, slug annular, and annular flow. The parameters affecting most of these patterns and their transition are channel size, superficial phase velocity (air and water), and surface tension [7].

Two dimensionless groups are introduced to characterize the two-phase flow. The related dimensionless number is the Reynold number and Capillary number. These dimensionless numbers are defined as in the following equation:

$$R_{e,L} = \frac{d_{ch}.U_{LS}.\rho_L}{\mu_L} \qquad R_{e,G} = \frac{d_{ch}.U_{GS}.\rho_G}{\mu_G} \tag{1}$$

$$C_a = \frac{\mu_{L.}U_{LS}}{\sigma} \tag{2}$$

where $R_{e,L}$, and $R_{e,G}$ are Reynold number for liquid and gas phase respectively; d_{ch} is the channel diameter; U_{LS} and U_{GS} are the liquid and gas superficial velocity; ρ_L and ρ_G are the density of liquid and gas; μ_L and μ_G are the viscosity of liquid and gas, and σ is the surface tension of liquid phase.

Reynold number represents a ratio between inertial forces and viscous forces, whereas the Capillary number expresses a ratio between viscous forces and surface tension.

3.1.1. Length of bubble

Hydrodynamic gas-liquid flow in the microfluidic with a low Reynold number has been well characterized by Garstecky et al., 2006 [8]. The flow pattern in the microfluidic generally has a characteristic low Reynold number. For $R_{e,L}$ and $R_{e,G}$<<1, the flow system will be dominated by viscous stresses and pressure gradients, whereas the effect of inertia is minimal, and it can be neglected.

In his study, the bubble length can be predicted by equation $L = d(Q_{gas}/Q_{liquid}) + w$, where L = the bubble length produced in a T-junction, Q_{gas} is the rate of gas inflow to the main channel given by $Q_{gas} = p/R$, where R is the flow resistance and p is the pressures drop between the inlet gas and the outlet of the main channel, located the length L_{ch} downstream from the T-

junction. Q_{liquid} is the liquid phase rate, d is the diameter of the bubble neck in T-junction, and w is the width of the main channel. Therefore the length of droplet and bubble is a function of several parameters (1) rate of continuous fluid, (2) viscosity of continuous fluid, (3) rate of discontinuous fluid or applied pressure of discontinuous fluid, (4) whether the surface-active additive, (5) geometry dimension of devices [8].

If L_s denotes the distance between the two consecutive bubbles, so the bubble length L_b increases while L_s decreases with the flow rate ratio Q_{gas}/Q_{liquid}. Changing the gas and liquid flow rate can achieve different bubble length. It was found at a fixed liquid flow rate; the bubble length increases with the gas flow rate. That is because, with a higher flow rate, the gas has a more significant force to push the liquid and resist the liquid pressure at the neck, so both the expansion and collapse time t_e and t_c increase, which leads to a longer bubble. On the contrary, at a fixed gas flow rate, L decreases with the liquid flow rate. When Q_{gas}/Q_{liquid} is very small, L is almost constant. The increasing liquid momentum cuts the neck quickly and shortens the time of expansion and collapse, which results in a bubble with a short length.

The average value of the air bubble length is a function of the liquid superficial flow velocity. The bubble length decreases in a logarithmic way, increasing the liquid superficial flow velocity [6]. Therefore the same conclusion can be obtained in terms of measured void fraction: void fraction experimentally measured decreases linearly with the superficial liquid velocity. On the contrary, the measured void fraction is weakly dependent on the air superficial flow velocity.

3.1.2. Pressure drop two-phase

In a two-phase gas-liquid system, the flow patterns formed along a microtube could not be separated from the pressure drop that arises. In a tube with a micro dimension and very long, the pressure change from the fluid inlet section is very different from the outlet section. Because the system observed involves a gas phase where the gas is very responsive to the changes in pressure, then, the design of a micro-device intended for a gas-liquid system must consider these pressure changes. The influence of pressure drop on the formation of gas-liquid flow patterns in a channel should be a focus-study that should not be ignored.

The pressure drop in the observed channel could be calculated by using Kreutzer's model. Kreutzer et al. proposed an expression of pressure drop along the channel based on Bretherton's analysis. Bretherton analysis is valid for vanishing liquid film thickness and for $Ca_b \rightarrow 0$. For $Ca_b \rightarrow 0$, the liquid film thickness approaches zero, and the cross-sectional area of the bubble approaches the channel cross-sectional area A [9]. The pressure drop over a unit length of the channel –(dP/dz)c, is then given by:

$$-\left(\frac{dP}{dz}\right)_c = \frac{\Delta P_{uc}}{L_b + L_s} = \frac{1}{L_b + L_s}\left(\frac{32\mu_l(U_g + U_l)}{D_c^2}(L_s + \delta) + 7.16\frac{\sigma(3Ca_b)^{2/3}}{D_c(1 + 3.34Ca_b^{2/3})}\right) \quad (3)$$

ΔP_{uc} = pressure drop over a unit cell, L = length, b = bubble, s = slug, σ = surface tension, D = diameter, c = channel, U = velocity, δ = correction of bubble length.

The equation (3) is integrated and rewrite, as shown in the equation below [9]:

$$\Delta P = 32.\mu_l.\frac{(U_g + U_l)}{D_c^2}.\left(\frac{L_s}{L_b + L_s}\right).\Delta z \quad (4)$$

At a steady-state, gravitational force and temperature difference are neglected, as well as the phases are in the equilibrium state have the uniform pressure [8]. Therefore, equation (4) can be applied to calculate the bubble length in the outlet section of the tube using Boyle's law:

$$P_1.V_1 = P_2.V_2 \quad (5)$$

P = gas pressure, V = bubble volume.

3.1.3. Superficial velocity

Gas and liquid superficial velocity U_{GS},U_{LS} are defined as follow:

$$U_{GS} = \frac{Q_{air}}{A_{ch}} \qquad U_{LS} = \frac{Q_w}{A_{ch}} \quad (6)$$

$$U_{TP} = \frac{Q_{air}}{A_{ch}} + \frac{Q_w}{A_{ch}} = U_{GS} + U_{LS} \quad (7)$$

Where U_{TP} is two-phase superficial velocity, A_{ch} is the cross-sectional area of the microchannel, and Q_{air} and Q_w are the imposed volumetric flow rate of gas and liquid, respectively [6]. U_{GS} and U_{LS} contribute to the magnitude of pressure in the inlet air before T-junction. Pressure monotonically increases when U_{GS} and U_{LS} are increased. The gas pressure established along the gas inlet branch of the T-junction when the steady-state condition is reached increases when the liquid superficial velocity is larger than the gas superficial velocity ($U_{GS}/U_{LS} < 1$) [6]. While average bubble velocity is defined as a function of the total superficial flow velocity of the liquid and gas, the average velocity of the bubble increases with the increase of the liquid and gas superficial velocity.

3.2. Experimental apparatus and method

The experimental device detailed in this section and illustrated in figure 3.2 allows gas-liquid flows to be generated and the bubble dispersion to be studied in terms of flow profile, bubble/slug length, and velocity. The experimental rig comprises:

- Microtube
- The feeding equipment to provide controlled gas and liquid flow rates (syringe pump, compressor, indicator, and regulator gas flow)
- Lighted observation board and camera

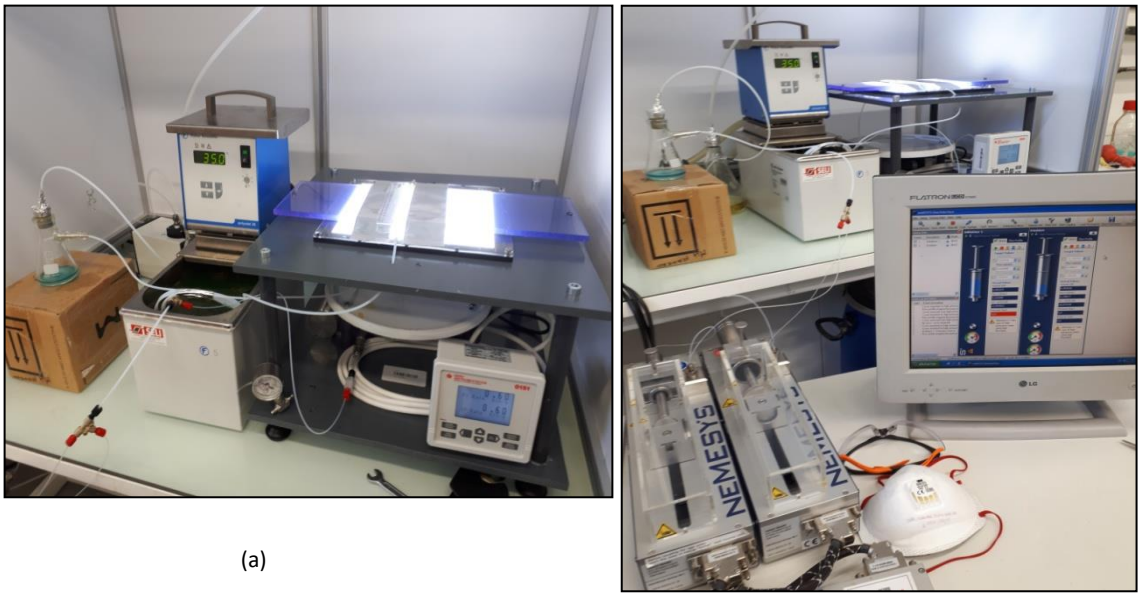

(a) (b)

Figure 3.2. Experimental apparatus for the observation of gas-liquid flow in a microtube. It seems there is the two Nemesys pump for flowing liquid, the observation field with the lamp, tube reactor, and the gas flow meter.

The observations are made based on the image shadows that appear due to evenly distributed irradiation of lamp on the microtube passed over the transparent plane as an observation field, allowing the detection of interfaces between gas bubbles and liquid can be observed well. The visible shadow flows as a representative of the gas bubble recorded using a camera. Flow characteristics that included flow patterns formed in the microtube, bubble/slug length, and the influence of superficial gas/liquid velocity on bubble length are studied.

3.2.1. Micro-tube design

3.2.1.1. Materials

The tube used to study the hydrodynamics of gas-liquid flow is a circular microtube in Poly tetra-fluoro-ethylene (PTFE) with the cross-section as seen in figure 3.3. PTFE presents the advantages of being transparent for visualizations.

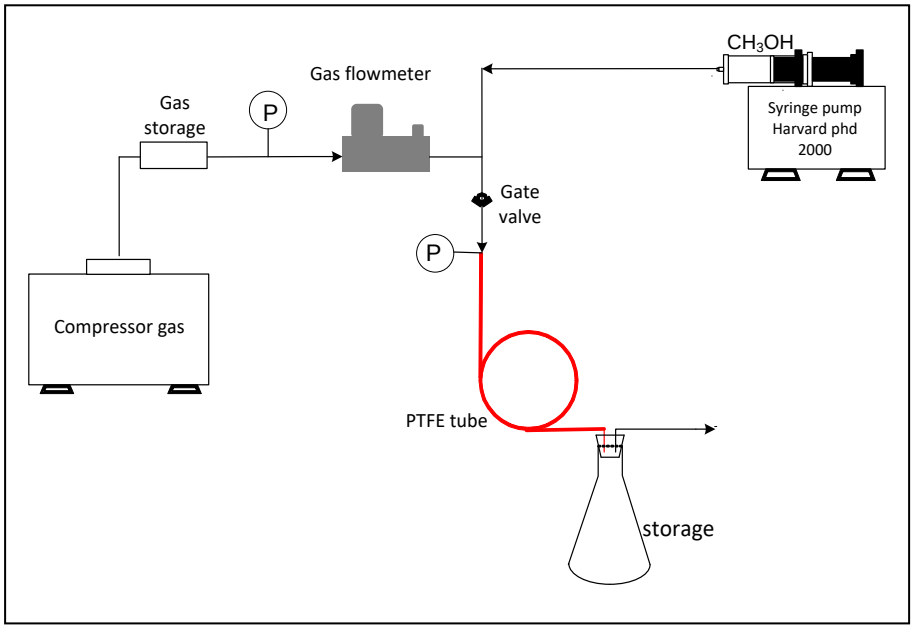

Figure 3.3. Scheme of experimental set up (P = pressure indicator, CH_3OH = methanol, air, PTFE = Poly tetra fluoro ethylene)

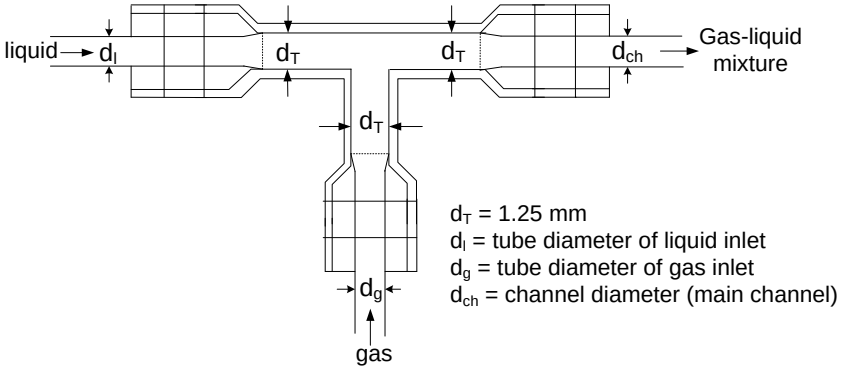

Figure 3.4. The cross-section of T-junction for gas and liquid phase contacting. The value of d_l, d_g, and d_{ch} was varied in these experiments.

Gas and liquid are mixed in the T-junction made from PTFE with a uniform inside diameter (d_T = 1.25 mm) in all branches.

3.2.1.2. Tube dimensions

The tube that observed a two-phase flow pattern has an inside diameter of 1 mm and a length of 20 and 30 m long. As a comparison, in these studies, a tube with an inner diameter 1.5 mm and 6 m length was also used. The use of several diameter sizes and tube lengths is to study the flow phenomenon/flow stability of liquid and gas when methanol and gas come into contact inside the tube at specific flow rates. These observations didn't use the smaller tubes than 1 mm with the consideration the utilization of the smaller tube diameter has a huge potential for blockage. At the same time, the tube length was chosen regarding the residence time needed to carry out the reaction by setting the appropriate gas and liquid flow rate.

3.2.1.3. Field of observations

The appeared flow pattern inside the microtube was observed by passing through the microtube at the top of the observation field's surface area that was made of frosted glass, as seen in Figure 3.2 and Figure 3.5. To facilitate these observations, a high-intensity lamp was installed at the bottom of this area.

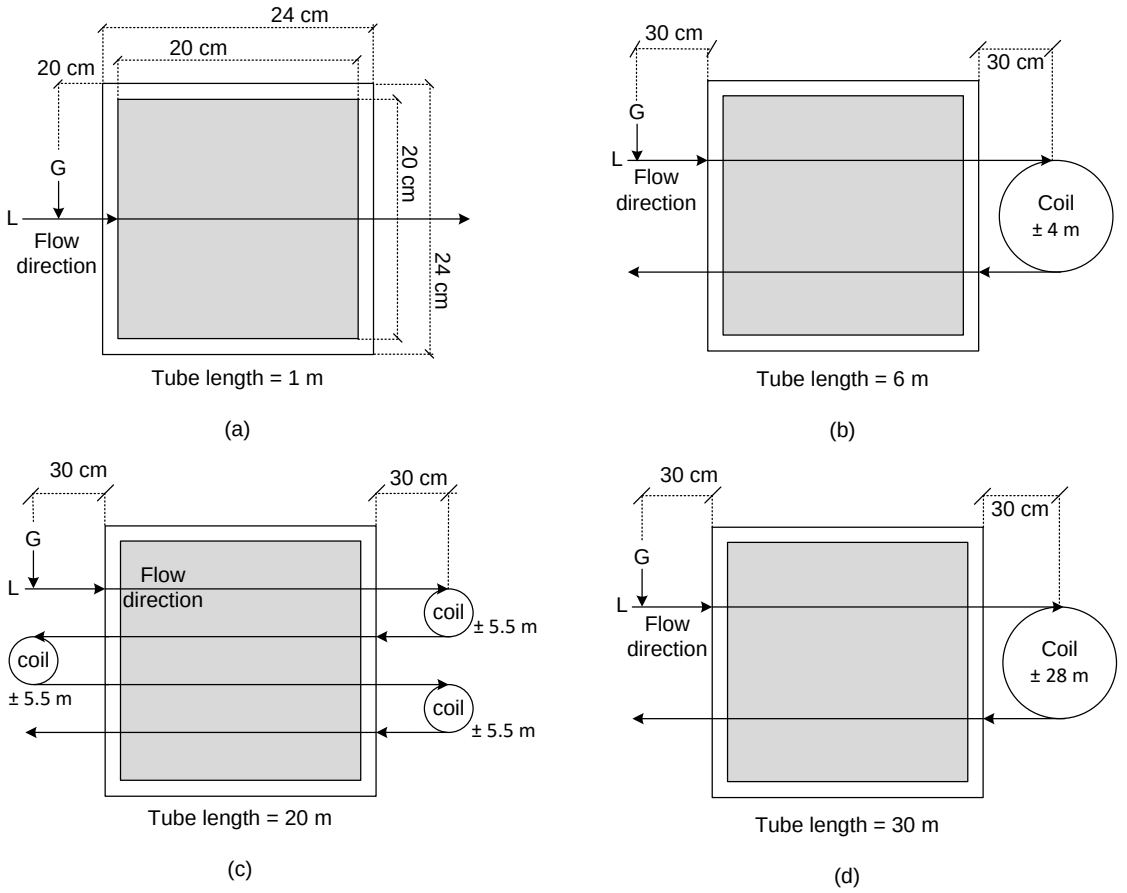

Figure 3.5. Field of observations of flow pattern inside microtube, (a) tube length = 1 m, (b) tube length = 6 m, (c) tube length = 20 m, (d) tube length = 30 m. Symbol G = gas, L = liquid.

3.2.2. Flow control

The scheme of the experimental set-up was given in figure 3.3. Air is supplied from a pressurized vessel and controlled employing SERV INSTRUMENTATION 0151B, which allows flow rates ranging from 0.00 to 20 Ncm^3/min gas with a maximum gas pressure 1.5 bars abs.

Concerning the liquid methanol, to ensure the stability of liquid flow throughout the tube length, a syringe-pump (HARVARD Apparatus PHD 2000) is used. This pump can flow liquid with the minimum and maximum flow rate in the range 0.0001 µl/hr (with 0.5 µl syringe) to 220.82 ml/min (with 140 ml syringe). In certain observations, especially for the observation using a longer tube (20 and 30 m), to flow methanol along the tube was required the higher power of the pump, and for this purposes, the observation used NEMESYS high-pressure syringe pump type NEM-B203-01 B that could work at high pressure. This pump can flow liquid

with the minimum and maximum flow rate in the range 171.0 nl/min – 825 ml/min, maximum pumping pressure 12 bars for 100 ml syringe; and the liquid flow rate in the range of 42.7 nl/min-206 ml/min with maximum pumping pressure around 50 bars for syringe 25 ml.

All observation was conducted at room temperature and 1 atm pressure. The gas inlet pressure was set and controlled before contact to ensure a constant gas flow rate in the tube.

3.2.3. Fluid properties

For conducting the preliminary experiment, methanol was used as a liquid phase and air as a gas phase. The properties of gas and liquid significantly contributed to the bubble formation within the microtube. The following are the properties of gas and liquid used for the observation at 20 °C.

Table 3.1. The properties of air and methanol

Fluid	ρ (kg/m^3)	μ ($kg/m.s$)	σ (N/m)
Air	1.2041	1.82E-05	-
Methanol	792	5.90E-04	2.27E-02

ρ = density, μ = viscosity, σ = surface tension

3.2.4. Experimental method

For conducting the observation, air and methanol flow rate were set in the range of 2.75 to 6 ml/min for air, and 2 to 6 ml/min for methanol with a constant gas inlet pressure was 1.2 bars. By using these variations, the two-phase flow has a dimensionless number in term of Reynold number gas in the range of $2.47 < Re_G < 5.39$; $36.45 < Re_L < 109.34$; and $0.000706 < Ca < 0.002117$. For the bubble-length measurement, a transparent tube was installed on the observation field illuminated by light from the bottom, and a ruler was put closest to the tube observed.

Taking pictures using a digital camera was done after a steady-state flow condition reached was indicated through the stable air and methanol flow rates in the microtube system; air-methanol flows smoothly without congestion. Then, bubble length was obtained by calculating the distinction of number designation on the ruler between the nose and tail of the bubble (Figure 3.6). The calculation is done with an approach of up to ml units.

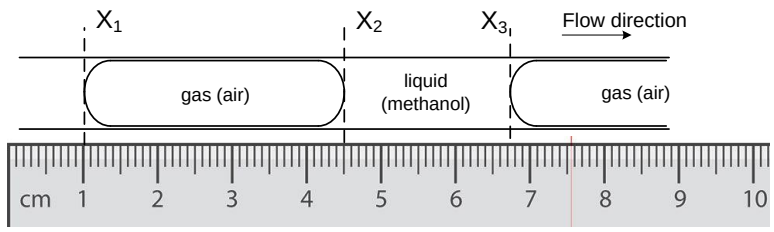

Length of bubble = $\Delta X = X_2 - X_1$; Length of slug = $\Delta X = X_3 - X_2$

Figure 3.6. Bubble length measurement method (X_1, X_3 = bubble tail; X_2 = bubble head).

3.3. Gas-liquid flow in micro-tube

Gas-liquid two-phase flow patterns in the microchannel are different from the flow patterns in a tube with a larger dimension. On a macro scale, the flow system works with several types of forces; one is the gravitational as a dominant force and a little influence of surface tension, whereas tube diameter can be negligible. However, in a microchannel with a dimension in the range of some μm until a few mm, surface tension, viscosity, inertia forces, and tube diameter play an essential role in determining flow patterns flow transition between them [1][3].

The flow characteristics in this experiment were indicated with the Reynolds number and Capillary number as shown in the section of 3.1.4 ($2.47 < Re_G < 5.39$; $36.45 < Re_L < 109.34$; and $0.000706 < Ca < 0.002117$). Reynolds number more than one indicates that in the flow system, inertia forces more dominant than viscous forces. Furthermore, the Capillary numbers less than 1 (Ca<<< 1) means the surface tension has a greater influence compared to viscous forces. Therefore, the effect of forces on the two-phase flow in these observations can be written in order as follows:

Surface tension > inertia forces > viscous forces

3.3.1. Stability and flow pattern description

The flows that appeared inside the channel during the observations included stable and unstable flow. Generally, the stable flow is defined as a flow that moves smoothly in regular flow rate/velocity and has the same bubble/slug dimension every time during the observation. In contrast, the unstable flow appears with the opposite characteristic of the stable flow. In the unstable flow, the bubble's length varied to time, and the bubble velocity changed during observation.

In this study, the flow patterns observed on the 20 and 30 m tube length, 1 mm inside diameter is slug flow or Taylor flow following the previous work [1][3], as seen in the figure below:

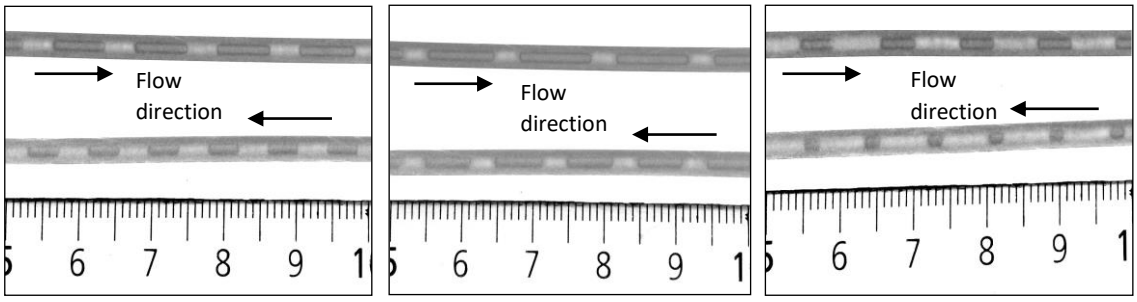

Q_{liquid} = 3 ml/min; Q_{gas} = 3 ml/min Q_{liquid} = 2 ml/min; Q_{gas} = 3 ml/min Q_{liquid} = 6 ml/min; Q_{gas} = 2.75 ml/min

(a)

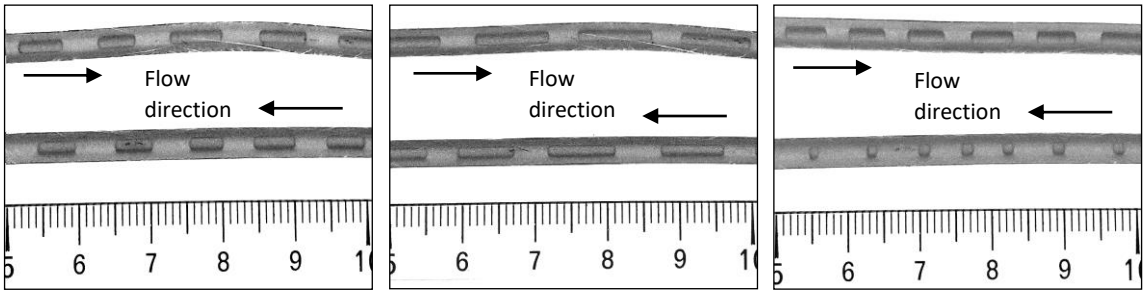

Q_{liquid} = 3 ml/min; Q_{gas} = 3 ml/min Q_{liquid} = 2 ml/min; Q_{gas} = 3 ml/min Q_{liquid} = 6 ml/min; Q_{gas} = 2.75 ml/min

(b)

Figure 3.7. Air-methanol flow pattern in micro-tube (the closest tube to the ruler is inlet tube section, and another is outlet tube section). (a) for 30 m tube length, (b) for 20 m tube length.

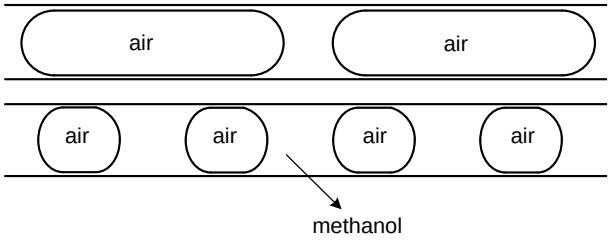

Figure 3.8. The flow models formed inside the tube with different bubble lengths

The bubbles appeared inside the tube (figure 3.8) with methanol wrapped around it. Methanol has the characteristic of a wetting tube wall; therefore, methanol formed a thin film on the surface close to the tube wall so that the bubbles and the tube wall never in contact. The bubbles are inside the tube flow, like slipping between thin layers of methanol. Generally, these bubbles flow at a similar velocity, even though the fluctuations sometimes appeared.

The bubbles have a length more than the tube diameter (> 1 mm) in the range of flow rate observed. The length at the inlet and the outlet section is different. This phenomenon has a relation to the magnitude of pressure drop across the tube. When the tube length was getting longer, the two-phase pressure drop throughout the tube also increased. Therefore, the length of the bubble will decrease as the pressure of the two-phase flow increase.

Flow pattern stability inside the tube for different inside diameter and tube length is shown in figure 3.9.

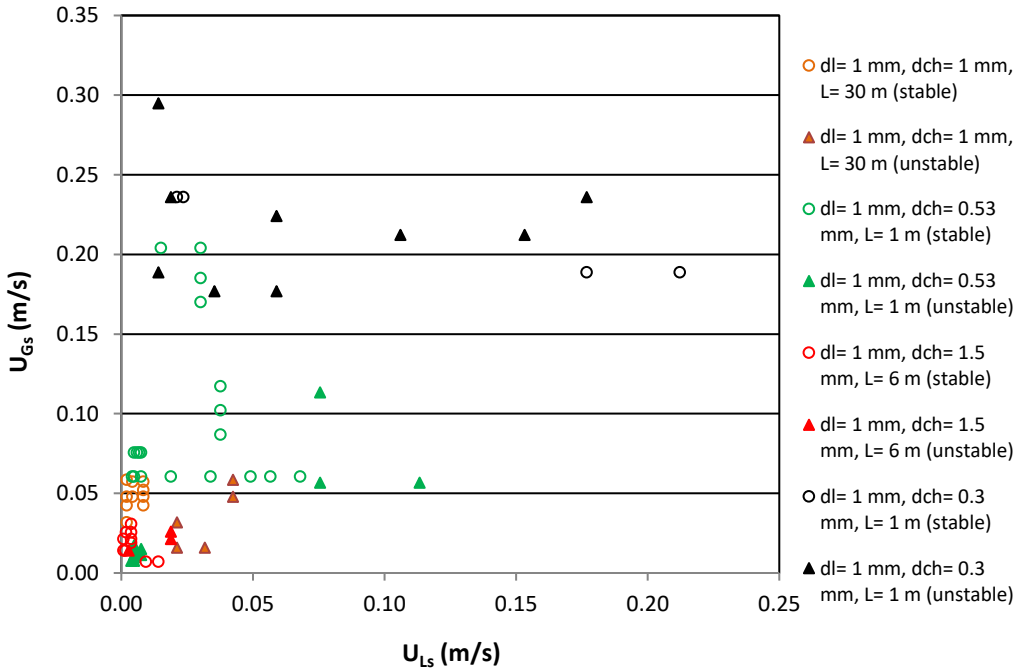

Figure 3.9. Flow pattern stability in the tube with the different inside diameter and tube length (d_l= diameter of a liquid inlet section, d_{ch} = channel diameter, L = the length of tube).

Figure 3.9 shows that stable two-phase flow could be found at the two-phase velocities, which tend to low. Then, in order to bring up stable flow, the liquid velocity has a more dominant influence than the gas velocity. When compared, at the liquid velocity, which tends to low and the constant gas velocity, the two-phase flow shows higher stability rather than that at the contra condition, i.e., at the low gas velocity and the constant liquid velocity. Furthermore, the two-phase flow pressure drop is getting bigger with increasing tube length with pressure drop. Therefore, to reach the end of the tube, the liquid pressure in the entrance section of the tube should be high, and it could be reached only by an increase in the liquid flow rate. However, at a specific liquid flow rate, the liquid pressure might become higher than the gas pressure. This condition triggered a part of the liquid phase to enter the gas tube and block the gas flow to the main channel. Therefore it should be avoided. If this phenomenon took place, the observed flow in the main channel would be mono-phase flow with the gas bubbles sometimes emerge inside the tube.

Some reasons, as the cause of unstable flows comprising the pulsation introduced by pump, which is triggered by the unstable flow of liquid velocity; formation and detachment of bubbles at the entry section (T-junction); and the plating of bubbles at the outlet of the canal [10].

3.3.2. Pressure drop gas-liquid Taylor flow

One of the essential parameters to be considered in a microchannel design is a pressure drop due to gas-liquid flow inside microchannel influenced by the interaction of some of the works comprising gravitational, interfacial, inertia, and viscous force. If the pressure drop is a significant fraction of the channel inlet pressure, the expansion of the gas phase along the

channel cannot be ignored [9]. Therefore, the pressure profile needs to be known for adequately determining the device's performance.

This study has observed the pressure drop characteristic of an air-methanol system to grasp how much influence it on the flow pattern formed in the microchannel, focusing on the bubbles lengths. The pressure drop in the observed channel could be calculated using Kreutzer's equation (4) section 3.1.2. Setting the outlet pressure is equivalent to the atmospheric pressure (1 atm). The channel inlet pressure can be determined by adding the outlet pressure with the pressure drop along the channel. Use equation (5) section 3.1.2, the bubble volume in the outlet section (V_2) can be calculated, and the bubble length can be derived from this volume. It corresponds to the theoretical bubble length on the exit tube ($L_{b,out}$-theoretical).

Figure 3.10 elucidates that the observed bubble length along the channel changed due to the more significant pressure drop with an increase in channel length. The bubble length theoretical ($L_{b,out}$-theoretical) in every microtube configuration is shown by the data points that form a straight line obtained by the calculation that was explained in the previous paragraph. On the other side, outside of the straight line, the data points indicate the exit tube's bubble length from the experiment ($L_{b,out}$-experiment). If both values are compared, $L_{b,out}$-experiment show a deviation from the theoretical value, and even, for longer bubble length, the deviations that occur are getting bigger. For a similar inside diameter and length of the tube, the pressure drop depends on the volumetric flow rate of air. Therefore, the bubble length increases with an increase in the ratio of air superficial velocity to methanol superficial velocity. In section 3.1.1, it has been explained the correlation between the bubble length to the superficial velocity ratio of both phases. It means that an increase in the superficial velocity ratio of both phases (UGs/ULs) would produce Lb,out which is getting bigger, and the deviation of the value of $L_{b,out}$–experiment, which is also more prominent due to sometimes the bubbles coalescence phenomena occurring. Besides that, the air compressor's performance is less stable for flowing air to the tube might cause these deviations that triggered the flow fluctuation during certain intervals time of observation. The bubble length experiment in figure 3.10 was an average length during observation.

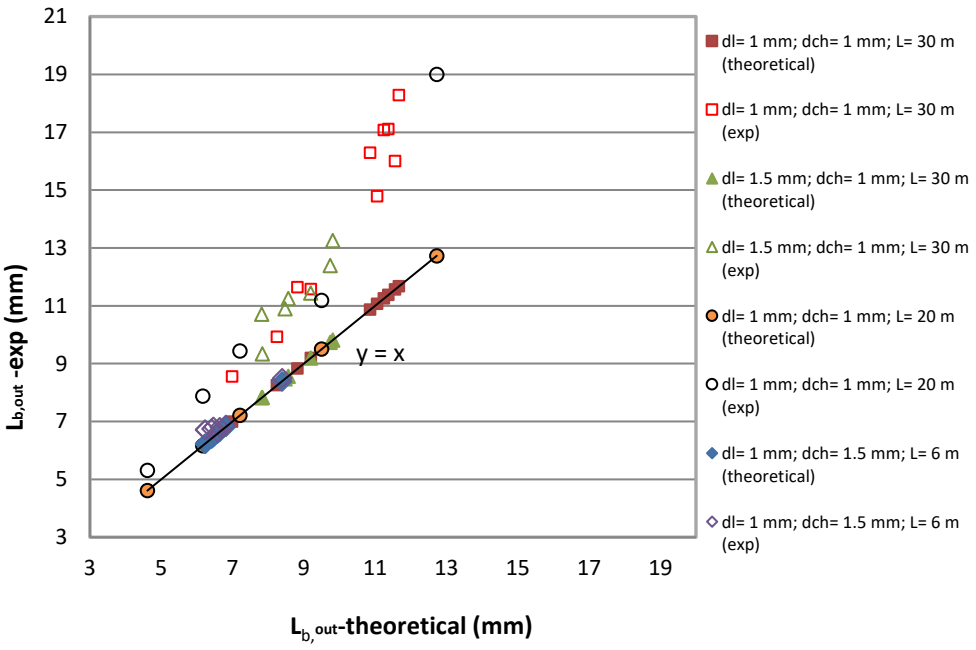

Figure 3.10. The pressure-drop air-methanol influence the bubble length between the entrance and the end of the channel. (d_l = tube diameter of inlet liquid; d_{ch} = tube diameter of the main channel).

$L_{b,out}$ theoretical in figure 3.10, refers to the calculation of the bubble length outside with bubble length measured at the inlet by taking into account the total pressure drop that arises between the entrance and the end of the microtube. Plot a curve from the theoretical value versus the experiment value would produce $L_{b,\,out}$ (exp).

3.3.3. Effects of gas and liquid superficial velocity to bubble length

The two-phase flow velocity is the sum of superficial air velocity, and methanol superficial velocity is shown in equation (7) section 3.1.3.

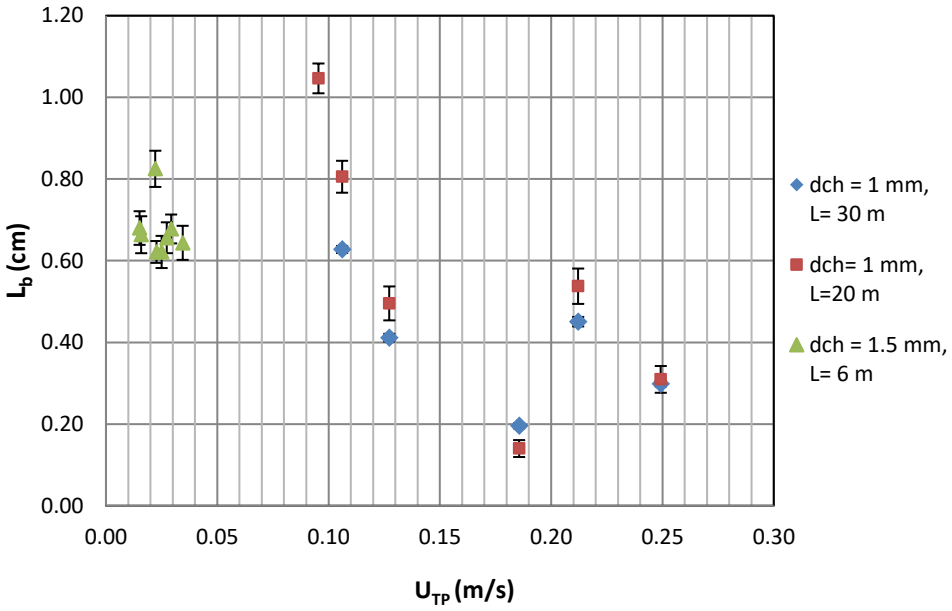

Figure 3.11. The effect of air-methanol superficial velocity on the length of bubbles for three types of tube dimensions. Lb was measured in a 20 cm long inlet tube, which was 30 cm from T-junction (see figure 3.5 (b), (c), (d))

Since the two-phase velocity is the total of the superficial air and methanol velocity, each phase's superficial velocity contributes to determining the length of the bubble in the tube. In the observations, an increase in two-phase flow velocity (U_{TP}) caused a decrease in the bubbles' length shown in figure 3.11. Two factors could explain this phenomenon: first, at higher flow rates, the inertia forces worked in the system getting bigger. Inertia forces served as the breaker for gas penetration at the bubble formation in the T-junction and released gas bubbles to the main channel. Secondly, at higher flow rates, the gas has a shorter penetration time than that for a lower flow rate.

By deeper analysis in figure 3.11 and table 3.2, it would be found that methanol superficial velocity gives a more significant effect than air superficial velocity. Small changes occurring in U_{Ls} provide a considerable impact, as indicated by the sharp decrease in bubble length. Moreover, conversely, in the greater U_{Gs}, bubble length decreases more gently.

Table 3.2. The influence of air-methanol velocity on the bubble's length formed inside the tube (dch = 1 mm, L = 30 m). Lb was measured in a 20 cm long inlet tube, 30 cm from T-junction (see figure 3.5 (d)).

U_{Ls} (m/s)	U_{Gs} (m/s)	U_{TP} (m/s)	U_{Gs}/U_{Ls}	L_b (cm)
0,0424	0,0636	0,1061	1,50	0,628
0,0636	0,0636	0,1273	1,00	0,411
0,0848	0,1273	0,2121	1,50	0,451
0,1220	0,1273	0,2492	1,04	0,299
0,1273	0,0583	0,1856	0,46	0,196

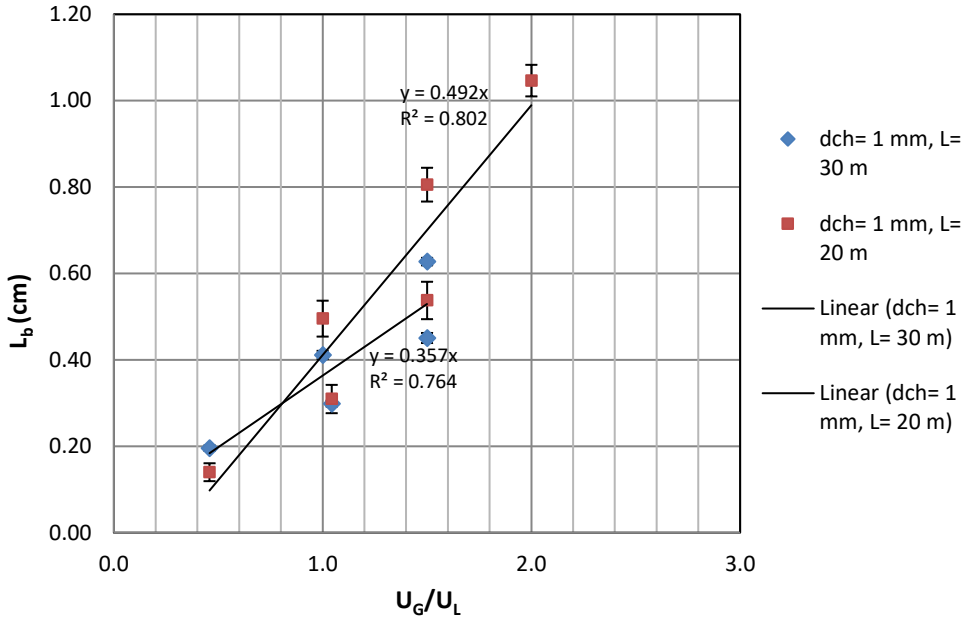

Figure 3.12. The influence of air-methanol superficial velocity ratios on the length of bubbles for two types of tube dimensions. Lb was measured in a 20 cm long inlet tube, which was 30 cm from T-junction (see figure 3.5 (c), (d)).

The change of air to methanol superficial velocity ratio promoted a shift in bubble length in the microtube with a linear correlation (Figure 3.12).

Figure 3.12 also confirmed that both superficial velocities influence the bubble length at different dominance levels. At the same ratio of $U_{Gs}/U_{Ls,}$ but in higher methanol flow rate, the bubble formed tends to be shorter. The methanol flow rate has a more decisive influence on flow patterns than air [7]. These observations were also performed on tubes of the same length but using the different methanol inlet tube diameter (ID = 1.5 mm) for confirming the effect of inlet tube diameter on bubble length. The observation results show that the various dimensions of the methanol inlet tube produced a similar bubble length.

These results are then considered for deciding the use of a 1 mm inside diameter tube to carry out further experiments.

3.4. Conclusion

In the preliminary study, the flow pattern observed in the tube with the range of dimensionless number: 2.47 < Re_G < 5.39; 36.45 < Re_L < 109.34; and 0.000706 < Ca <0.002117 was a slug flow or Taylor flow. This dimensionless number elucidated that in the air-methanol system observed, the inertia force and the surface tension force give a more dominant influence than the viscous force with the order of magnitude: surface tension > inertia force > viscous force. During the observation, it is found the stable flow and unstable flow inside the tube.

The utilization of a longer microtube in these observations brought up the more considerable pressure drop along the tube. The higher pressure drop triggered the bubble

length reduction throughout the tube, although sometimes the bubble coalescence phenomena are still occurring.

The air and methanol superficial velocities influenced the length of the bubble observed, with the strong influence was given by methanol velocity. At a constant air velocity and higher methanol velocity, the bubble dimension will decrease. Conversely, it will increase in line with the increase in gas velocity at a constant methanol velocity.

Literature

[1] K. A. Triplett, S. M. Ghiaasiaan, S. I. Abdel-Khalik, and D. L. Sadowski, "Gas-liquid two-phase flow in microchannels part I: Two-phase flow patterns," *Int. J. Multiph. Flow*, vol. 25, no. 3, pp. 377–394, 1999.

[2] S. Waelchli and P. Rudolf von Rohr, "Two-phase flow characteristics in gas-liquid microreactors," *Int. J. Multiph. Flow*, vol. 32, no. 7, pp. 791–806, 2006.

[3] K. A. Triplett, S. M. Ghiaasiaan, S. I. Abdel-Khalik, A. LeMouel, and B. N. McCord, "Gas–liquid two-phase flow in microchannels," *Int. J. Multiph. Flow*, vol. 25, no. 3, pp. 395–410, 1999.

[4] J. W. Coleman and S. Garimella, "Characterization of two-phase flow patterns in small diameter round and rectangular tubes," *Int. J. Heat Mass Transf.*, vol. 42, no. 15, pp. 2869–2881, 1999.

[5] G. Hetsroni, A. Mosyak, and Z. Segal, "Two-phase flow in microchannels," *Am. Soc. Mech. Eng. Heat Transf. Div. HTD*, vol. 369, no. 3, pp. 87–93, 2001.

[6] G. Puccetti, M. Tosi, B. Pulvirenti, and G. L. Morini, "Flow patterns of an air–water mixture at the exit of a micro T-junction," *Exp. Therm. Fluid Sci.*, vol. 67, pp. 62–69, 2015.

[7] P. S. Saljoshi and A. T. Autee, “Experimental investigation of two-phase flow patterns in minichannels at horizontal orientation,” *Heat Mass Transf. und Stoffuebertragung*, vol. 53, no. 9, pp. 2799–2811, 2017.

[8] P. Garstecki, M. J. Fuerstman, H. A. Stone, and G. M. Whitesides, "Formation of droplets and bubbles in a microfluidic T-junction - Scaling and mechanism of break-up," *Lab Chip*, vol. 6, no. 3, pp. 437–446, 2006.

[9] M. J. F. Warnier, M. H. J. M. De Croon, E. V. Rebrov, and J. C. Schouten, "Pressure drop of gas-liquid Taylor flow in round micro-capillaries for low to intermediate Reynolds numbers," *Microfluid. Nanofluidics*, vol. 8, no. 1, pp. 33–45, 2010.

[10] N. Völkel, "Design and characterization of gas-liquid microreactors," p. 135, 2009.

Chapter 4

Hydrodynamics of gas-liquid-liquid flow In microtube

Contents

4.1. Introduction

Gas-liquid-liquid three-phase flow develops in many industrial process applications such as the crystallization of protein [1], catalysis reaction [2], material production [3], and reaction-separation [4]. A chemical process is always attempted. It appears a large surface area between immiscible phases to obtain the necessary heat or mass transfer rate and controllable phase dispersion to ensure stable operation and production. Up to now, the studies on the gas-liquid-liquid flow system are being developed continuously for micro-fluidic reactor applications [2][5][6][7][8]. These studies are an essential step that provides much information to assess the performance of a gas-liquid-liquid micro-fluidic reactor, since knowledge about the rule of flow inside the tube, like hydrodynamic (characterization of various flow regimes, bubble/drop/slug formation mechanism), mixing, pressure drop, heat and mass transfer is required. Moreover, to controllably apply the gas-liquid-liquid systems, the micro-bubbles and microdroplets preparation control are quite important. Then, bubbles and droplets generations were individually controlled by several flows focusing on geometries [9], and the precise manipulation of bubbles, droplets, or immiscible fluid streams in microdevices is usually achieved by elaborate chip designs that well address fluid-fluid hydrodynamics under laminar flow conditions and fluid-solid interactions in engineered microchannels [6]. The generation of a stable and regular triphasic flow is more complicated than for a two-phase flow because the two different dispersed phases tend to interact with each other [7].

Here are some studies on three-phase flow in microdevices, including the application of a capillary microreactor for selective hydrogenation of α,β-unsaturated Aldehydes [1], generating gas/liquid/liquid three-phase micro-dispersed systems in double T-junction [2], and experimental characterization of gas-liquid-liquid flows in T-junction microchannels [3].

Yucel Onal et al. 2005 [1] applied two mixers connected in line to generate a regular and stable fluid dynamic behavior of GLL, as seen in figure 4.1.

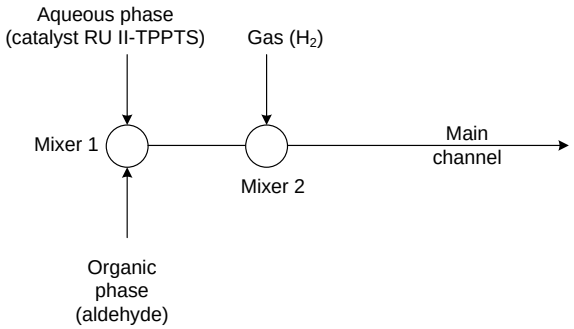

Figure 4.1. Schematic diagram of double mixer micro-fluidic

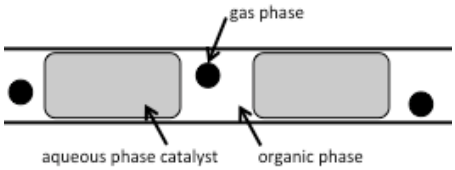

Figure 4.2. Schematic diagram of GLL flow in capillary reactor

Various inside diameter tubes were used (500, 750, 1000 µm) with a 3, 6, and 12 m long capillary tube. The organic phase was pumped with a constant volumetric flow rate of 250 µL/min, and the aqueous phase increased in the range of 0.19 to 0.51 ml/min, whereas the hydrogen flow rate was kept constant at 2800 µLn/min. The flow presented a plug flow of alternating fluid elements consisting of the aqueous and organic phase with the hydrogen gas located in the organic phase-only. The organic phase serves as the continuous phase, and it has a higher affinity to the PTFE than the aqueous phase [2].

V.M. Rajesh et al. 2012 [3] performed an experiment applied two mixers (figure 4.3), where an aqueous phase was introduced inside a tube in the last section. Capillary reactor was a square tube with dimensions 1000 µm width, 950 µm depth, and 210 mm long, of the main channel. The capillary tube was fabricated on a polymethyl methacrylate (PMMA) material.

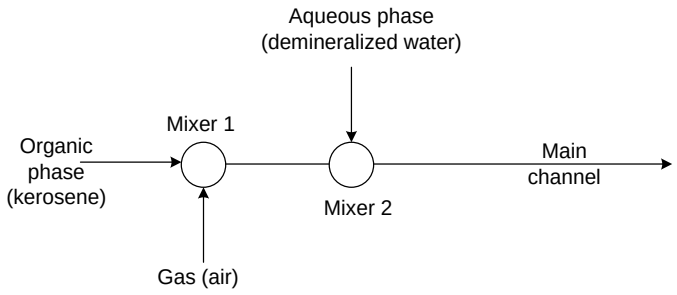

Figure 4.3. The schematic diagram of the double T-junction micro-fluidic

The regime GLL flow generated in a capillary reactor is presented in figure 4.4. In this figure, air bubbles/ slugs are seen in black color, form at the first T-junction (not visible), and then flow to the second T-junction (visible). Water drops/slugs formed at the second T-junction are seen in gray color [3].

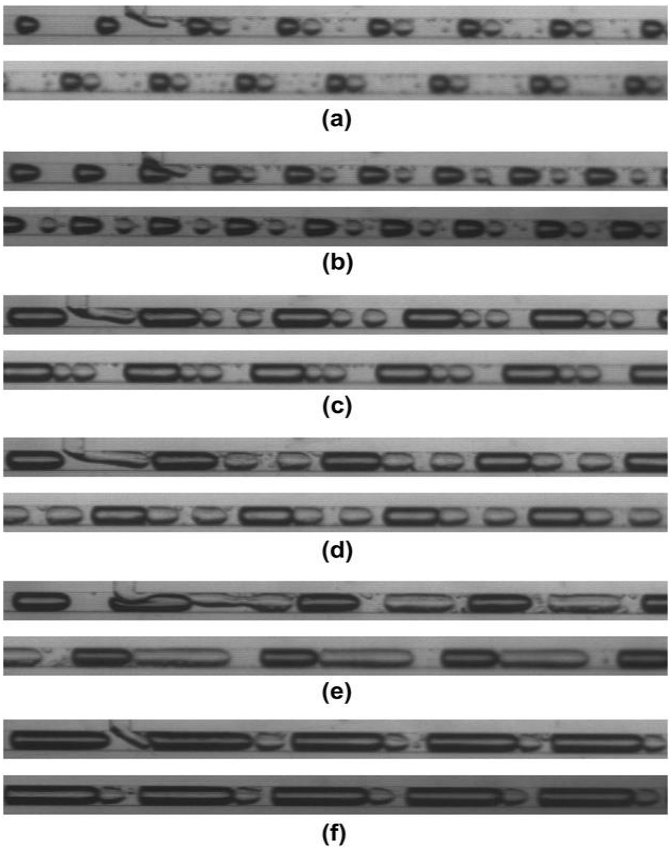

Figure 4.4. GLL flow regimes observed in microchannel: (a) bubble–drop (B–D) flow (Q_{oil} = 15 ml/min, Q_{water} = 2.76 ml/min, Q_{air} = 1.66 ml/min, Ca_{oil} = 0.0138, We_{air} = 4.60 $10^{-5}$$We_{water}$ = 0.0475); (b) slug–drop (S–D) flow (Q_{oil} = 15 ml/min, Q_{water} = 2.76 ml/min, Q_{air} = 7.746 ml/min, Ca_{oil} = 0.0138, We_{air} = 0.001, We_{water} = 0.0475); (c) slug–two slugs (S–2S) flow (Q_{oil} = 5 ml/min; Q_{water} = 2.283 ml/min; Q_{air} = 5.119 ml/min, Ca_{oil} = 0.00459, We_{air} = 4.37 10^{-4} ,We_{water} = 0.0325); (d) slug–two slugs (S–2S) (Q_{oil} = 5 ml/min; Q_{water} = 4.19 ml/min; Q_{air} = 5.12 ml/min, Ca_{oil} = 0.00459, We_{air} = 4.38 10^{-4}, We_{water} = 0.109); (e) slug– long slug (S–LS) flow (Q_{oil} = 5 ml/min, Q_{water} = 7.53 ml/min, Q_{air} = 5.12 ml/min, Ca_{oil} = 0.00459, We_{air} = 4.38 10^{-4}, We_{water} = 0.353); (f) long slug–slug (LS–S) flow (Q_{oil} = 5 ml/min, Q_{water} = 2.76 ml/min, Q_{air} = 13.93 ml/min, Ca_{oil} = 0.00459, We_{air} = 0.00324, We_{water} = 0.0475) [3].

Wang et al. 2010 [4] carried out GLL experiment by using two T-junction geometries. The perpendicular flow cutting method was adopted to generate bubbles at the first T-junction

since it is easy to produce a stabled segmented gas phase in the microchannel. The cross-flow cutting method was adopted for breaking-up the droplet at the second T-junction, and it was focused on how the oil droplet ruptures with the shearing of gas/liquid two-phase fluid. The capillary tube was fabricated from a polymethyl methacrylate (PMMA). The main channel's cross-section was an isosceles trapezoid, which had a 290 µm short edge, 450 µm long edge, and 340 µm depth. On the main channel, a wide measurement channel was placed before the outlet. It was used to observe the flow pattern and analyze the distribution of bubbles and droplets. The main channel and the measuring channel were designed as short as 25 and 15 mm, respectively [4].

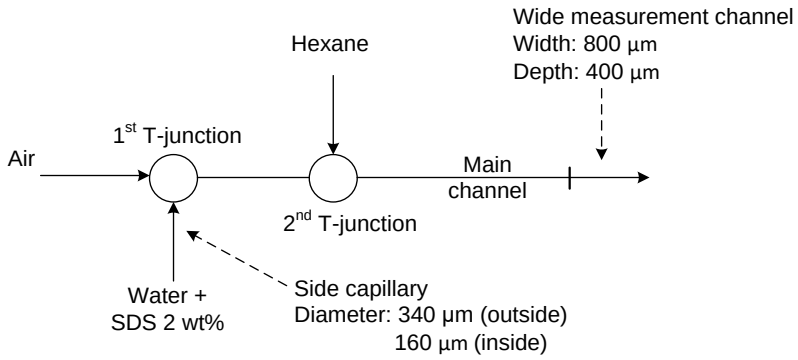

Figure 4.5. Schematic diagram of double T-junction microfluidic. Cross section of main channel is an isosceles trapezoid [4].

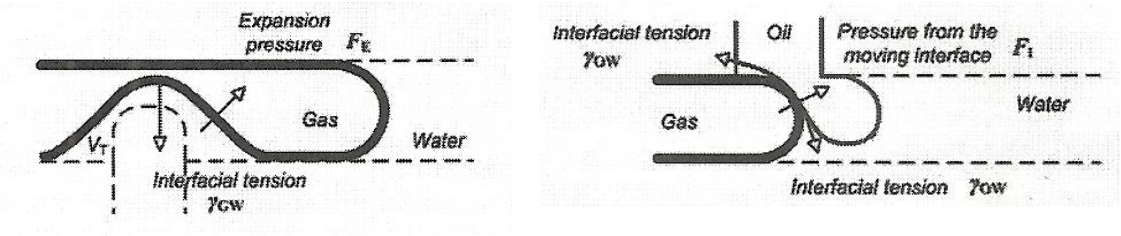

(a) (b)

Figure 4.6. (a) Schematic diagram of gas-phase rupturing moment. The main forces dominating the break-up of the bubbles are shown as the hollow arrows in the figure. (b) Schematic diagram of the oil phase rupturing moment with the cutting of the gas plug [4]

Figure 4.6 (a) (b) describes the bubbles and droplets break-up mechanism in the 1st and 2nd T-junction. Figure 4.6 (a) shows that the gas phase comes into the straight main channel and bypass the tip of the capillary first. Then it grows bigger and bigger. At the same time, water flows out of the capillary. Since the bubble almost blocks the main channel, the continuous phase accumulates in T-junction. Finally, the continuous phase takes up the main channel, and the bubble ruptures off. The break-up of the bubbles is mainly based on the competition of the two phases in T-junction. The volume occupied by the continuous phase increases with the bubble growing. The gas-liquid interface changes its shape to keep the force balance between the expansion pressure (FE) and the interfacial tension (γ_{GW}). When the interfacial tension cannot sustain the expansion pressure, the slot breaks' interface and the bubble ruptures off [9].

The break-up of oil droplets at the second T-junction geometry was investigated. It was found that the droplets were directly cut off by the incoming gas plugs in this situation, as shown in figure 4.6 (b). Since the gas/water-SDS system's interfacial tension was almost seven times higher than the oil/water-SDS system's interfacial tension, the gas plug works as a rigid piston in the channel [9].

The generated gas-liquid-liquid three-phase flows in the main channel are shown in figure 4.7.

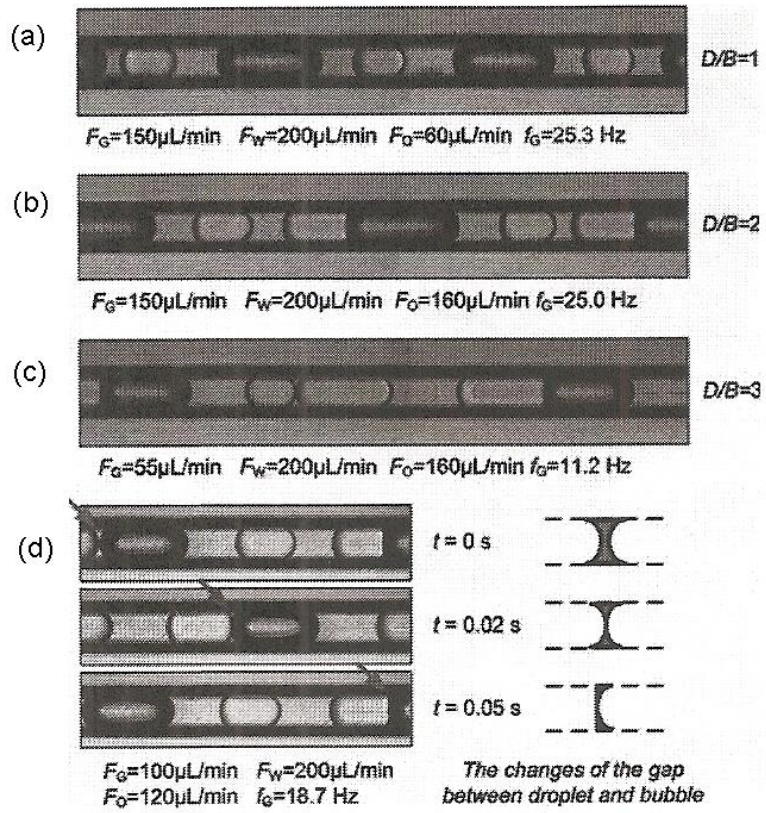

Figure 4.7 (a), (b), (c) Three-phase flow patterns in the main channel with different ratios of the droplet to bubble. (d) The changes of the gap between a droplet and a bubble. The left pictures record the process with the moving of dispersed fluids, and the right pictures are schematic views of the gap pointed by the arrows in the left pictures. It can be seen that the curved cap of the droplet become disappeared with the elapsing of time [4].

It can be seen that the bubbles and the droplets flow alternatively. An interesting phenomenon in the main channel is that the moving gas plug and its following droplet can strictly connect, as shown in figure 4.7 (a)(b). The channel's cross-section is nearly occupied entirely by the oil plug; there it gutters exist between the curved surfaces with the channel corners. The continuous phase in the gap between the droplet and bubble can slowly pass through the gutters with the bubbles moving, so the bubbles and the droplets can strictly connect. One curved cap of the droplets becomes disappeared with the extrusion proceeding [4].

4.2. Experimental set-up and method

4.2.1. Set-up description

4.2.1.1. Materials

The schematic diagram of the experimental apparatus is shown in figure 4.8. This scheme has a small modification from the previous one (in chapter 3) in the feeding of oil and methanol into the tube. Then, the observations used two types of immiscible liquid phases besides gas. For flowing immiscible-liquids into the reactor tube, it was used the high-pressure pumps NEMESYS.

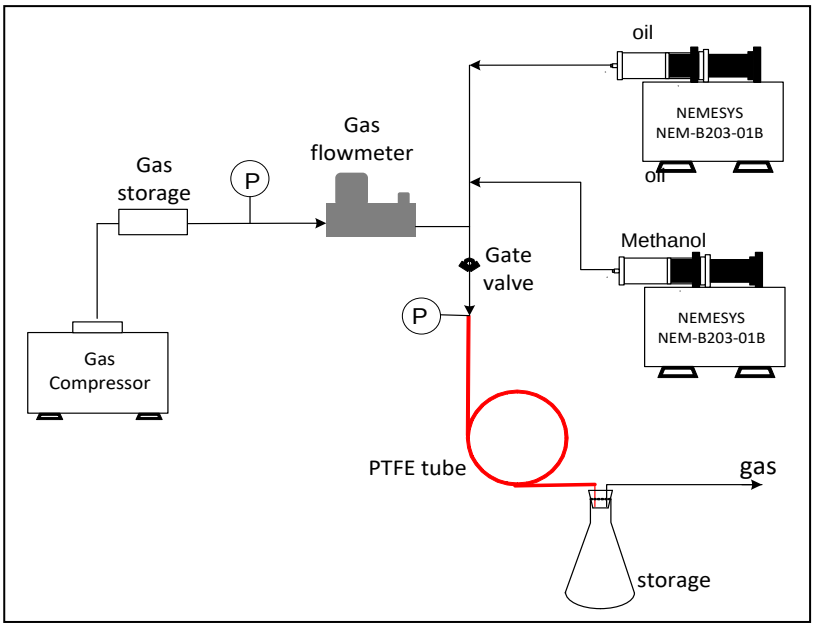

Figure 4.8. Experimental set-up for GLL observations (P = pressure indicator).

The gas-liquid-liquid three-phase was created through two T-junctions with similar types and dimensions, as seen in figure 4.9.

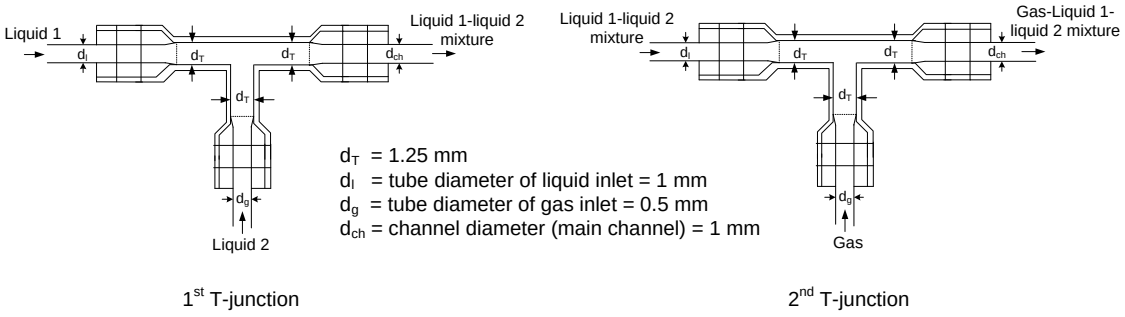

Figure 4.9. T-junction used in the experiment three-phase. The 1st T-junction was to mix liquid 1 and liquid 2; the 2nd T-junction was to mix gas and liquid 1 and liquid 2.

All T-junction was fabricated from a PTFE uniform inside diameter (d_T = 1.25 mm) in all branches. Then, figure 4.10 describes two types of feeding configurations for oil, methanol,

and air. The performance of them in producing a regular and stable flow at experimental conditions used would be compared.

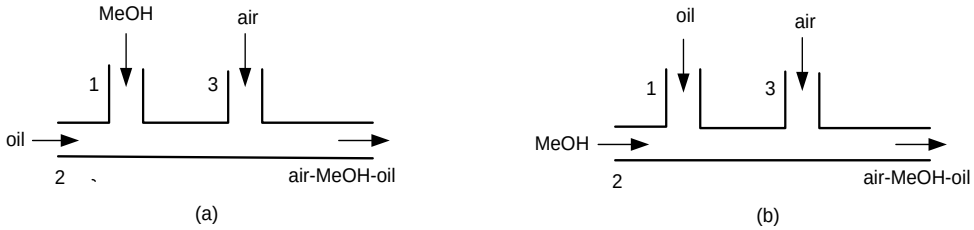

Figure 4.10. Inlet position of methanol/oil used in observation. (a) Configuration of methanol-oil-air, (b) Configuration of oil-methanol-air [5].

These configurations differ only in the placement of oil and methanol, while the air position is fixed. The inlet tube for oil and methanol has an inside diameter of 1 mm and 0.5 mm for gas.

4.2.1.2. Tube dimensions

The same inside diameter PTFE tubes of 1 mm in chapter 3 were used to observe the flow pattern formed inside the tube, with the various tube length including 1, 9, and 20m. Some tube lengths are used to study the flow phenomenon/stability of gas and two immiscible liquids, while gas and immiscible-liquids come into contact at specific flow rates. These observations did not use the smaller tubes than 1 mm inside diameter with the consideration that the utilization of smaller ones would have a huge potential for blockage, while the tube length was chosen by regarding residence time needed to carry out the synthesis reaction by setting of appropriate gas and liquid flow rate.

4.2.1.3. Observation technique

The observation field for GLL flow patterns within the tube was arranged, as shown in figure 4.11. All tubes here were connected, and they are on a lighted table for a good observation. The GLL flow pattern images were taken at different points on the tube, i.e., in figure 4.11 (a), the images were taken at around 50 cm from the beginning of the tube. Figure 4.11 (b) shows that the images were taken at two different positions, i.e., 50 cm and 8.5 m. Figure 4.11 (c) shows that the images were taken at four different positions, i.e., 50 cm, 6, 12.5, and 19.5 m from the beginning of the tube.

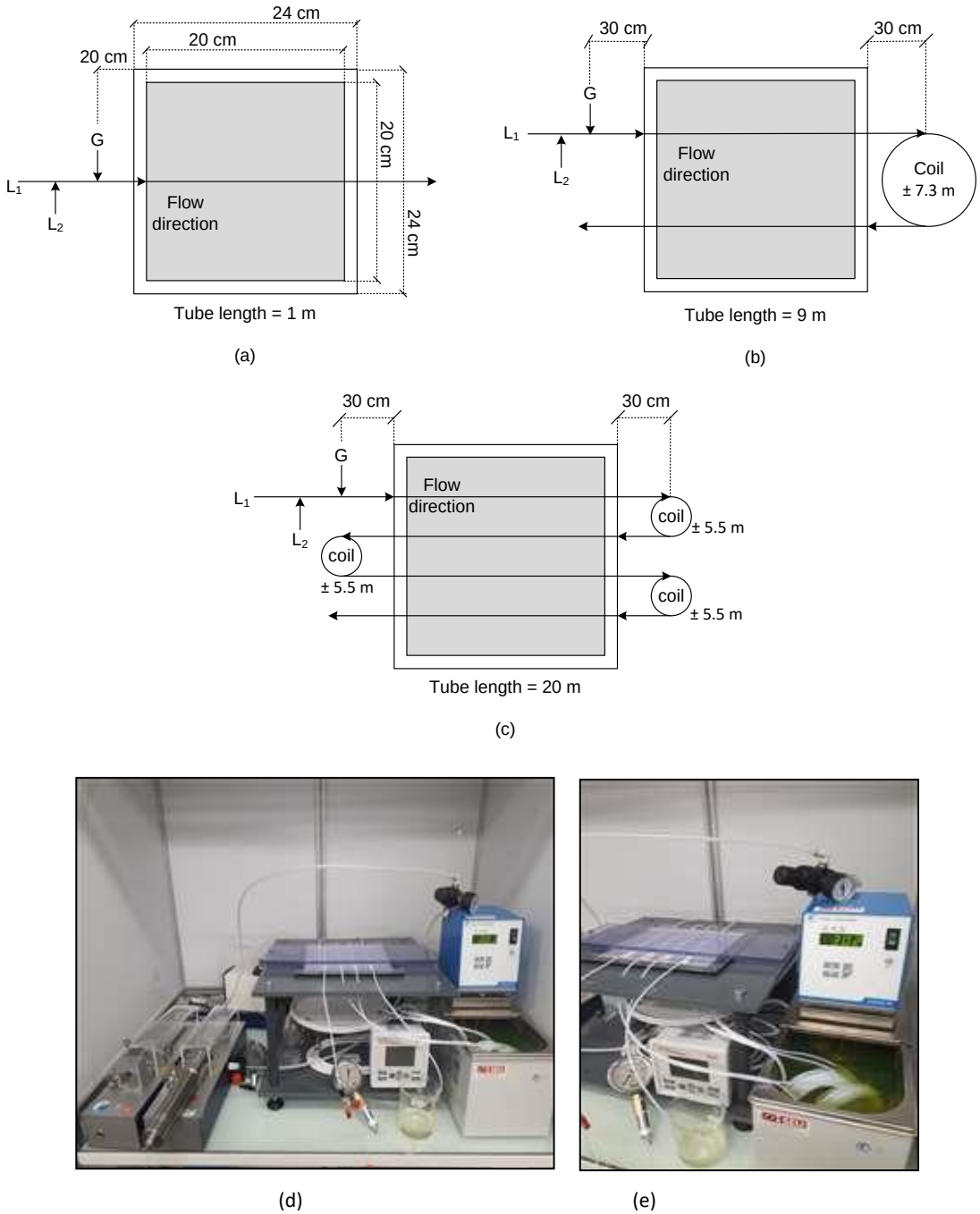

Figure 4.11. Field of flow pattern observation inside microtube, (a) tube length = 1 m, (b) tube length = 9 m, (c) tube length = 20 m, (d) experimental set-up, (e) tube rolls was dipped in water bath. Symbol G = gas, L_1 = liquid 1, L_2 = liquid 2.

4.2.2. Flow control

The scheme of the experimental set-up is given in figure 4.8. Air is supplied from a pressurized vessel and controlled employing SERV INSTRUMENTATION 0151B, which allows flow rates ranging from 0.00 to 20 Ncm^3/min gas with a maximum gas pressure 1.5 bars abs.

Then, to flow the liquid methanol and oil, the observation applied NEMESYS high-pressure syringe pump type NEM-B203-01 B. The pump has a specification that it can flow

liquid with minimum and maximum flow rate in the range of 171.0 nl/min–825 ml/min, maximum pumping pressure 12 bars for 100 ml syringe; and the liquid flow rate in the range of 42.7 nl/min-206 ml/min with maximum pumping pressure around 50 bars for 25 ml syringe.

All observation was performed at room temperature and atmospheric pressure. The gas inlet pressure was set and controlled before contact to ensure a constant gas flow rate in the tube.

4.2.3. Fluids properties

4.2.3.1. Effect of the temperature

These studies applied chemicals comprised of methanol, oil (sunflower oil), and air. The hydrodynamic of the gas-liquid-liquid phase inside a microtube depends on each component's physical properties like density and viscosity (see table 4.1) besides influenced by the operating parameters used like gas and liquid flow rate, inlet gas pressure, and temperature.

Table 4.1. Physical properties of methanol, oil, and air[6]

Temperature (°C)	Density (ρ), $kg.m^{-3}$			Viscosity (μ), $kg.m^{-1}.s^{-1}$		
	MeOH	Oil	Air	MeOH	Oil	Air
15	799	921.0	1.226	2.223	0.08849	1.802E-05
30	785	911.4	1.167	1.816	0.04417	1.866E-05

4.2.3.2. Effect of blue dye

The methylene blue is added to the aqueous phase to identify it in the channel well. In this way, it was important to be sure that the methylene blue does not modify the liquid's surface properties.

So, the surface tension, interfacial tensions, and contact angles were measured to determine how far the influence of the utilization of methylene bleu to the characteristic of three-phase flow-formed, and also to identify which liquids serve as a dispersed phase and a continuous phase, similar to section 4.3 but using different methods.

Table 4.2 summarizes the results obtained for measuring surface tension and interfacial tension of oil, methanol, and methanol with methylene blue by using Tensiometer Nouy described in Appendix A. Note that the error tolerance by applying these tools is around 1 mN/m.

Table 4.2. Surface tension and interfacial tension of the liquid mixture

Liquid	Surface tension-average (mN/m)	Liquid 1 – liquid 2	Interfacial tension-average (mN/m)
Oil	35.4	Oil – MeOH	2.8
MeOH	24.0	Oil – MeOH + bleu	1.3
MeOH + bleu	24.5		

A similar result of surface tension and interfacial tension for methanol pure and methanol plus methylene bleu (see table 4.2) proves that the presence of methylene blue does

not affect the surface tension of methanol. Still, it has little influence on the value of interface tension for the oil-methanol mixture.

Furthermore, the contact angle measurements have provided the contact angle of methanol, and the teflon surface is 143 °, and 130 ° for oil and teflon surface. Therefore, it could be concluded that the wetting level of methanol on the Teflon surface is better than oil.

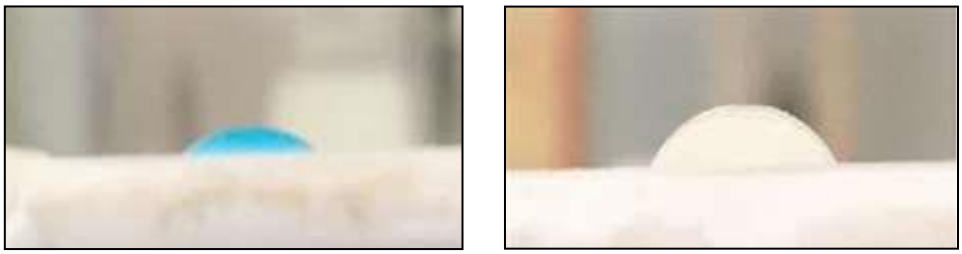

(a) (b)

Figure 4.12. (a) Methanol drop, (b) oil drop on Teflon surface

4.2.4. Experimental methodology

Principally, the experimental method is similar to section 3.2.4 (chapter 3). In the first step, liquid 1 and liquid 2 was mixed in the 1st T-junction to present liquid-liquid two-phase flow. Both liquids flow rates were adjusted in such a way to meet the oil to methanol molar ratio of 1:3, 1:5, 1:6, 1:7, 1:8, and 1:9 as the ratio that will be used in the next experiment. The second step, the mixture of liquid 1 and liquid 2, met the gas phase in the 2nd T-junction to form a gas-liquid-liquid three-phase flow. The appearance of gas and specific liquid behaves as a continuous phase, and another one as a dispersed phase indicated the formation of this flow. As additional information, the experiments here were performed without a catalyst; therefore, it could be assumed that no reaction was performed during the observation.

The next step, the flow patterns that appeared inside the tube, was visualized using a digital camera to measure the bubble/slug's length, either continuous or dispersed phase. The measurement method refers to section 3.2.4 (figure 3.6, chapter 3).

4.3. Identification of the nature of the continuous /dispersed phases

Gas-liquid-liquid flow formed a specified pattern in the small tube. This part would determine which component serves as a continuous phase and a dispersed phase. The determination was based on the geometric of liquid droplets in the small tube. The following pictures were taken at the observations performed using the molar ratio oil to methanol 1:3, 1:4, 1:5, 1:7, 1:8, 1:9, with total liquid flow rate (oil + methanol) and the gas flow rate was 1.5 respectively, and by using the inlet position of oil and methanol in T-junction followed the schematic diagram of figure 4.10 (a).

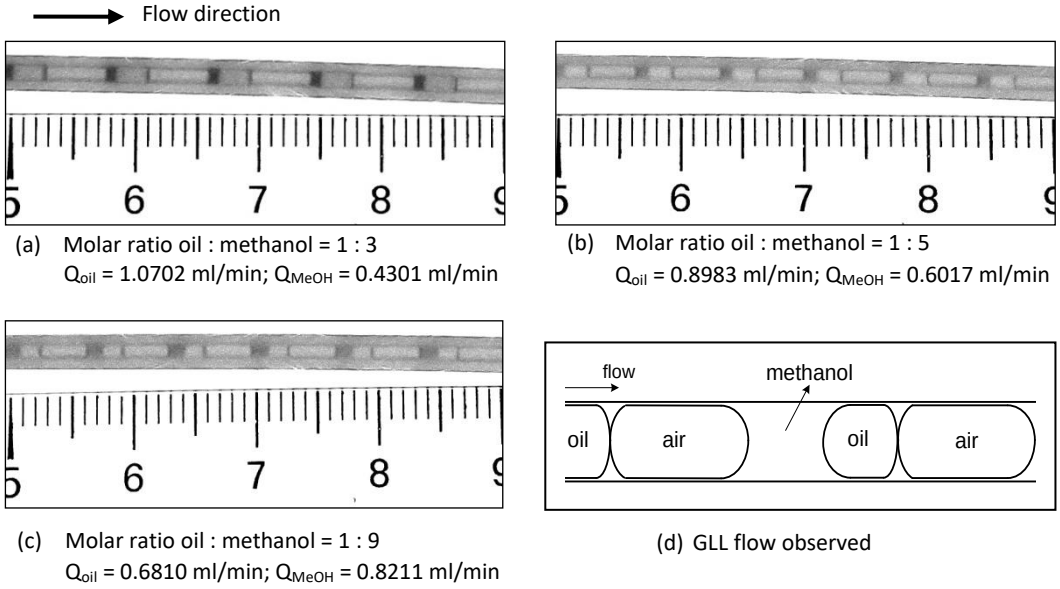

(a) Molar ratio oil : methanol = 1 : 3
Q_{oil} = 1.0702 ml/min; Q_{MeOH} = 0.4301 ml/min

(b) Molar ratio oil : methanol = 1 : 5
Q_{oil} = 0.8983 ml/min; Q_{MeOH} = 0.6017 ml/min

(c) Molar ratio oil : methanol = 1 : 9
Q_{oil} = 0.6810 ml/min; Q_{MeOH} = 0.8211 ml/min

(d) GLL flow observed

Figure 4.13. (a),(b),(c) three-phase flow pattern inside a microtube with variables on molar ratio oil to methanol. Dark color in figure (a),(b),(c) is methanol. (d) GLL flow observed.

Figure 4.13 (a), (b), (c) showed the flow patterns with a sequence of air-oil-methanol regularly throughout the microtube, as described clearly in figure 4.13 (d). The sequence of air-oil-methanol was found out for $Q_{oil} > Q_{MeOH}$ as well as $Q_{oil} < Q_{MeOH}$. Based on the form of oil droplets and methanol phase, it could be determined that methanol serves as a continuous phase; oil and air are the dispersed phases. These results are strengthened by the previous result in section 4.2.3.2, where the measurement of contact angles shows that methanol has a higher contact angle than oil drop on the teflon surface.

4.4. Influence of gas and liquids flow rates on a gas-liquid-liquid flow

4.4.1. Influence of air flow rate on GLL flow in 1 m long tube

The more significant liquid pressure than gas during the observations applying 30 m tube length has been considered to make observations applying a shorter tube of 1 m long with molar ratio oil to methanol 1:5 (table 4.3). The purpose of this observation is to investigate the influences of gas flow rate on the three-phase flow at constant liquids flow rate by using the inlet position configuration of methanol-oil-air (refers to figure 4.10 (a)).

Table 4.3. Oil, methanol, and air flow rate used in observations

Molar ratio	Oil flow rate (ml/min)	MeOH flow rate (ml/min)	Total liquid flow rate (ml/min)	Air flow rate (ml/min)
1 : 5	0.7567	0.5069	1.2636	0.50
1 : 5	0.7567	0.5069	1.2636	1.00
1 : 5	0.7567	0.5069	1.2636	1.50
1 : 5	0.7567	0.5069	1.2636	1.75

1 : 5	0.7567	0.5069	1.2636	2.00
1 : 5	0.7567	0.5069	1.2636	2.50
1 : 5	0.7567	0.5069	1.2636	3.50

All observable flows refer to table 4.3 showed a stable flow pattern. The stable flow was indicated by a constant gas-liquid-liquid flow rate inside the tube, and regularly, the flow was structured by the similar dimensions of bubbles and slugs during the observation times, as seen in figure 4.14.

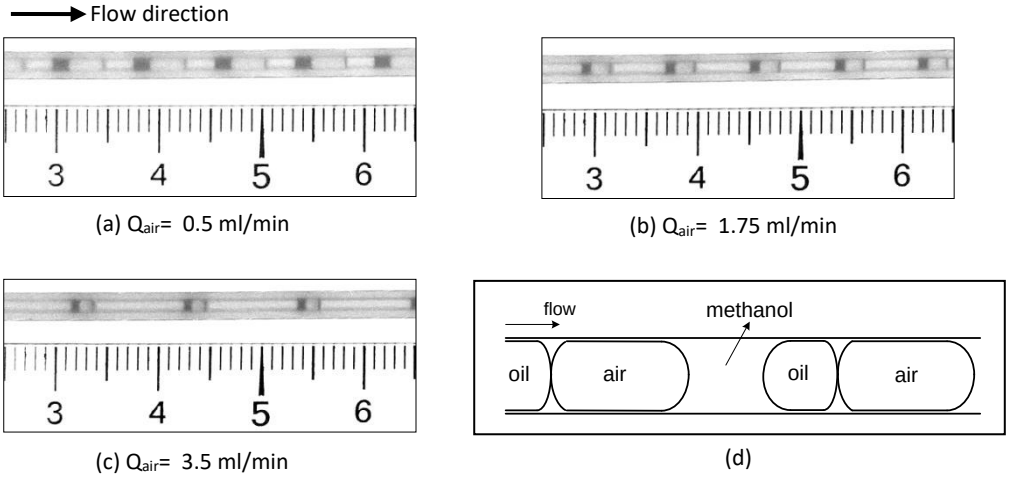

Figure 4.14. (a), (b), (c) Three-phase flow pattern inside microtube with the variable on air flow rate (Q_{air}). The dark color in figure (a), (b), (c) is the methanol phase. (d) GLL flow observed.

To make clear, figure 4.14 (d) shows the schematic diagram of the three-phase flow observed during the experiments. It shows the sequence of three-phase flow that comprises a gas bubble in the first part, followed by the oil phase and then the methanol phase.

By increasing gas velocity and keeping liquids velocity constant, the bubble's length increases linearly and sharply, while the length of the oil phase and the methanol phase decreases slightly. This section's liquid velocity refers to the total velocity of oil and methanol ($U_{L\text{-}oil}$ + $U_{L\text{-}MeOH}$) inside the tube. Further, figure 4.15 illustrates that the oil phase's length was more influenced by the increase in air flow rate than for methanol. The curve in figure 4.15 indicates that the oil phase's length reduced from 3.25 to 1.35 mm, whereas the length of the methanol phase reduced from 1.6 to 0.8 mm. This phenomenon could be explained by regarding oil as a dispersed phase and methanol as a continuous phase. Therefore, the increase in air-flow rate did not much influence on the dimension of the methanol phase. The unit cell ($L_{\text{-unit cell}}$) is the total length of bubbles, oil drops, and methanol phase.

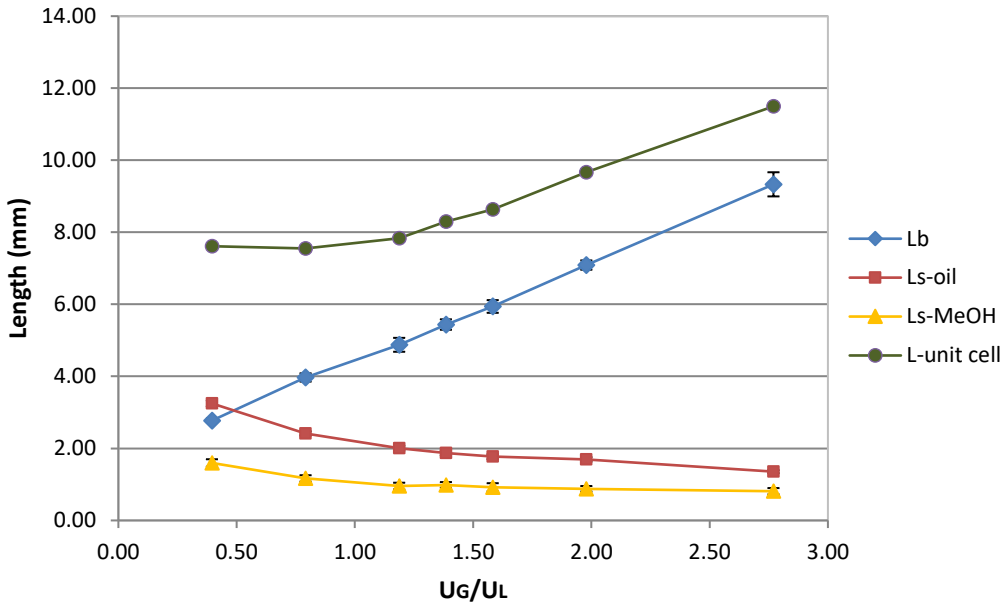

Figure4.15. Length of bubbles (L_b), length of the oil drops ($L_{s\text{-}oil}$), length of methanol phase ($L_{s\text{-}MeOH}$), and length of unit cells ($L_{\text{-unit cell}}$) at operating conditions refer to table 4.2.

4.4.2. Influence of oil/methanol flow rate on GLL flow in 1 m long tube

Further experiments were performed by varying the molar ratio of oil and methanol with a constant gas flow rate to understand the liquid flow rate's influence on GLL flow in 1 m long microtube. The gas and liquid flow rate used in the observation are presented in table 4.4.

Table 4.4. Oil, methanol, and air flow rate which was used for investigating the effect of oil/methanol flow rate on GLL flow

Molar ratio oil to MeOH	Oil flow rate (ml/min)	MeOH flow rate (ml/min)	Total liquid flow rate (ml/min)	Air-flow rate (ml/min)
1 : 9	0.6810	0.8211	1.502	1.50
1 : 8	0.7242	0.7762	1.500	1.50
1 : 7	0.7266	0.7782	1.505	1.50
1 : 5	0.8983	0.6017	1.500	1.50
1 : 4	0.9772	0.5237	1.500	1.50
1 : 3	1.0702	0.4301	1.500	1.50

The different molar ratio was stated by the different oil and methanol flow rate. The bubble length and the oil/methanol drop length is presented in figure 4.16 and figure 4.17. All of the GLL flow observed at these conditions showed stable flows.

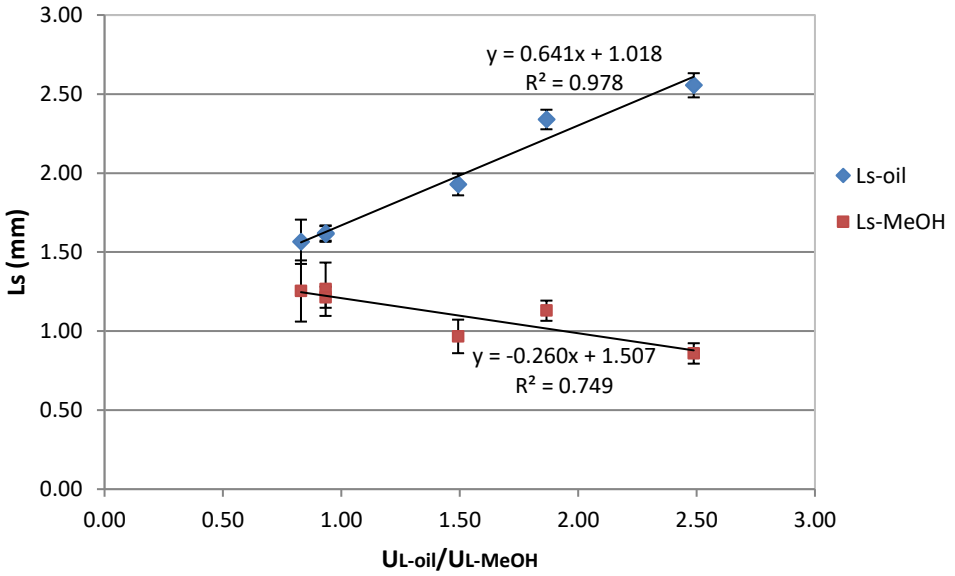

Figure 4.16. Length of oil drops ($L_{s\text{-}oil}$) and length of methanol phase ($L_{s\text{-}MeOH}$)at operating conditions refer to table 4.4

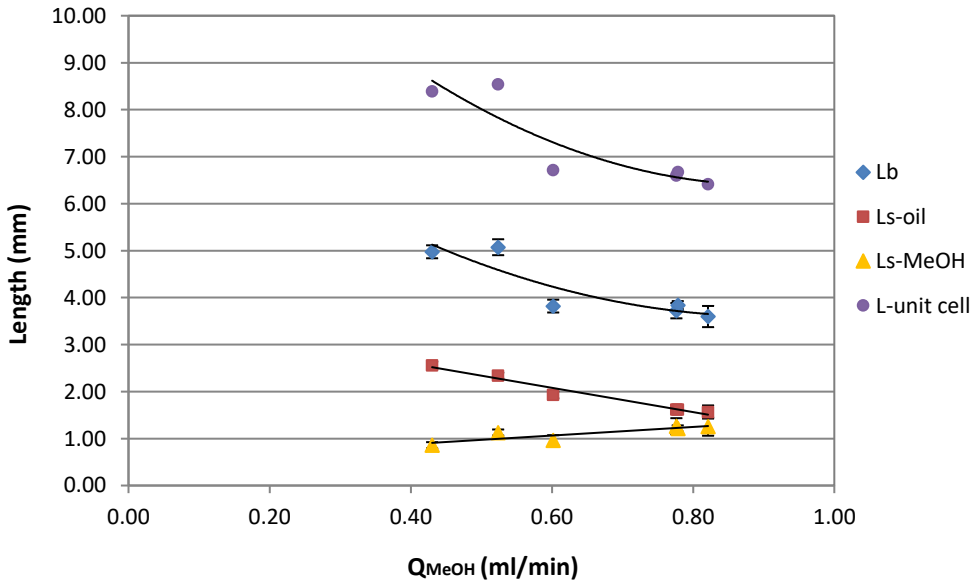

Figure 4.17. Effect of methanol flow rate on length of bubbles (L_b), length of oil ($L_{s\text{-}oil}$), length of methanol ($L_{s\text{-}MeOH}$), and length of unit cells ($L_{\text{-unit cell}}$) at operating conditions refer to table 4.4.

Figure 4.16 elucidates that the enhancing ratio of oil to methanol superficial velocity ($U_{L\text{-}oil}/U_{L\text{-}MeOH}$) would be followed by the increase in oil drop length ($L_{s\text{-}oil}$) and decrease in slug length of methanol phase ($L_{s\text{-}MeOH}$), which tends to be linear. This ratio has more influence on the oil drop length than the length of the methanol phase, indicated by the slope of $L_{s\text{-}oil}$ curve is greater than the slope of $L_{s\text{-}MeOH}$ curve. Otherwise, if the methanol flow rate was going up, the oil drop length will decrease, and the length of methanol between two consecutive bubbles will increase, as indicated in figure 4.17. Further, figure 4.17 explains the correlation

between the bubbles lengths and the methanol flow rate change. Both show inverse correlations, it is meant that the enhancement of methanol flow rate caused a reduction of bubbles lengths, and finally, it is also reducing the length of the unit cell.

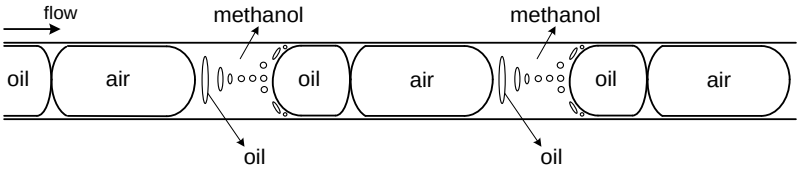

Figure 4.18. Flow phenomenon observed at molar ratio oil to methanol 1:4 and 1:3

Among the molar ratio used in table 4.4, the flow observed in figure 4.18 was only found at the molar ratio of oil to methanol 1:4 and 1:3. The phenomenon observed was, first, the oil drops phase appeared to transverse the methanol phase, moving straight toward the next oil drop in front of it, and the coalescence phenomena occurred. Next, the oil phase gets through the thin film of methanol around bubbles toward the next oil drop. The small oil drops that appeared in the methanol phase have the same dimensions, and overall the flow within the tube remains stable. This phenomenon took place in a certain part of the tube and in all the methanol phases throughout the microtube.

The appearance of this phenomenon within three-phase flow caused by the much greater oil flow rate than methanol flow rate at the molar ratio of oil to methanol 1:4 and 1:3, as seen in table 4.4, which at ratio 1:4, the oil flow rate is almost two times the methanol flow rate, even, for ratio 1:3, the oil flow rate is more than two times the methanol flow rate.

4.5. Influence of the tube length on gas-liquid-liquid flow

This observation aims to get information about the possibility of utilizing a longer tube to ensure enough residence time for reaction. The previous observations used 1 m tube length showed satisfying results in flow stability for all observation variables. However, the residence times found out in the 1 m microtube were less than 30 seconds, and it is too short and might be insufficient for carrying out the ozonolysis optimally. Moreover, the previous observations used 30 m tube length had also shown a slight possibility due to a so long tube that caused the increase in pressure drop throughout the tube for the gas flow rate applied. The same results were also shown with the shorter tube length of 29 m for all observation variables. Therefore, this section observed flow stability inside the microtube using the shorter tube of 20 and 9 m long. The flow characteristics were indicated in Table 4.5.

Table 4.5. The flow rate of oil, methanol, and air used for observations inside 9 m and 20 m length

Tube length (m)	Molar ratio oil to MeOH	Oil flow rate (ml/min)	MeOH flow rate (ml/min)	Total liquid flow rate (ml/min)	Air-flow rate (ml/min)	Flow Characteristic
9	1:5	0.92	0.6155	1.5355	3.50	Unstable
9	1:5	0.92	0.6155	1.5355	1.50	Unstable
9	1:5	0.46	0.3050	0.7650	0.75	Unstable
9	1:5	0.46	0.3050	0.7650	0.75	Unstable

9	1:5	0.46	0.3050	0.7650	0.75	Unstable
9	1:5	0.23	0.1525	0.3825	0.37	Unstable
20	1:5	0.23	0.1525	0.3825	0.37	Unstable

The unstable flow in table 4.5 was demonstrated by the regular flow initially, and sometimes irregular flow with the bubble dimension varied during observation. The irregular flow refers to the three-phase flow that flowed smoothly first, but in a certain period, the flow stopped for a moment and then flowed again. These phenomena took place in the same period.

If the flow rate of oil, methanol, and the air was added (3rd and 2nd columns from the right side), then, on the total flow rate of around 1.5 and 0.75 ml/min, the obtained residence time was 5 and 10 minutes respectively, for 9 m long microtube. Therefore, supposing the observation uses a 20 m long microtube at the same flow rate, the residence time would be around 10 and 20 minutes. This residence time is probably sufficient to attain a high yield and conversion of ozonolysis.

4.6. Influence of oil-methanol inlet position at T-junction by using 1 m long tube

There are two possibilities of oil and methanol inlet position in T-junction. Here, it has been performed the studies to investigate the influence of different inlet position on GLL flow formed. The schematic of the inlet position refers to figure 4.10 (a)(b).

The flow pattern formed in the microtube is presented in figures 4.19 and 4.20. Figure 4.19 showed the flow pattern by using methanol-oil-air configuration, and further, figure 4.20 showed the flow pattern by using an oil-methanol-air configuration.

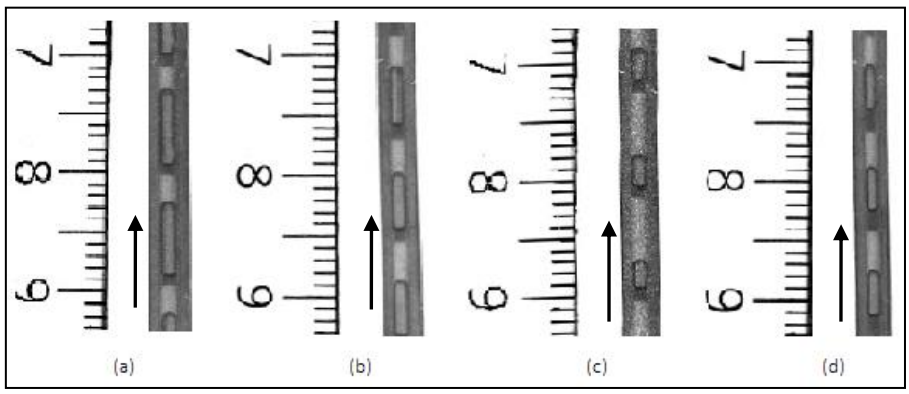

Figure 4.19. The GLL flow pattern used the configuration in figure 4.10(a). Figure 4.19(a) molar ratio oil to methanol 1:5, Q_{oil} = 1.081 ml/min, Q_{MeOH} = 0.7241 ml/min, Q_{air} = 3 ml/min; (b) molar ratio oil to methanol 1:9, Q_{oil} = 1.081 ml/min, Q_{MeOH} = 1.3034 ml/min, Q_{air} = 3 ml/min; (c) molar ratio oil to methanol 1:5, Q_{oil} = 1.8376 ml/min, Q_{MeOH} = 1.2310 ml/min, Q_{air} = 3 ml/min; (d) molar ratio oil to methanol 1:9, Q_{oil} = 1.4053 ml/min, Q_{MeOH} = 1.6944 ml/min, Q_{air} = 3 ml/min.

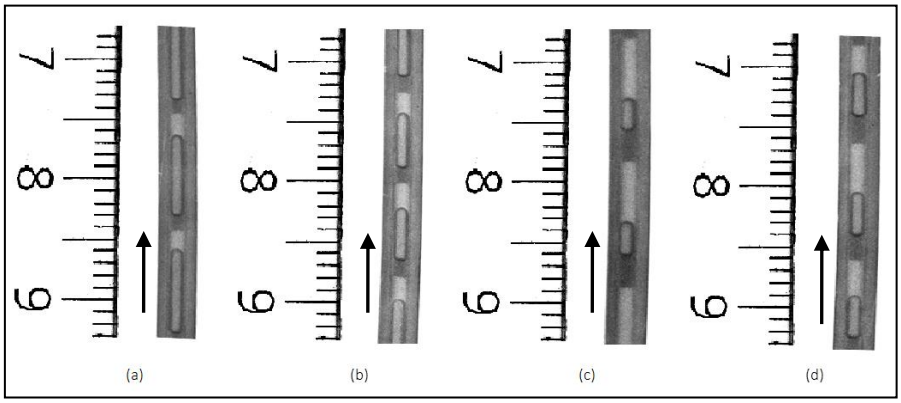

Figure 4.20. The GLL flow pattern used the configuration in figure 4.10.(b). Figure 4.20(a) molar ratio oil to methanol 1:5, Q_{oil} = 1.081 ml/min, Q_{MeOH} = 0.7241 ml/min, Q_{air} = 3 ml/min; (b) molar ratio oil to methanol 1:9, Q_{oil} = 1.081 ml/min, Q_{MeOH} = 1.3034 ml/min, Q_{air} = 3 ml/min; (c) molar ratio oil to methanol 1:5, Q_{oil} = 1.8376 ml/min, Q_{MeOH} = 1.2310 ml/min, Q_{air} = 3 ml/min; (d) molar ratio oil to methanol 1:9, Q_{oil} = 1.4053 ml/min, Q_{MeOH} = 1.6944 ml/min, Q_{air} = 3 ml/min.

The flow pattern in both configurations was different. As seen in figure 4.10 (a), the methanol-oil-air inlet system gave the stable flows, and otherwise, the oil-methanol-air system, as described in figure 4.10 (b), always gave unstable flows. The Methanol-oil-air system can produce a stable flow because methanol flow was strong enough to cut off oil flow (see figure 4.21 (a)).

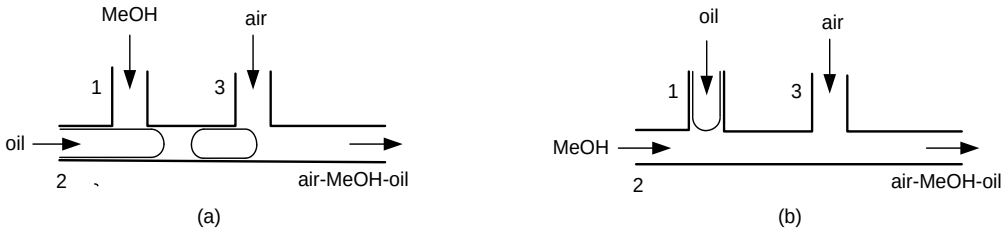

Figure 4.21 (a) Methanol was able to penetrate the narrow space between oil and channel wall, (b) oil was difficult to cut off methanol flow.

It was known that oil has a worse characteristic than methanol in terms of wetting wall channel (see figure 4.12); therefore, it always appeared the narrow space between oil and channel wall in the observation. The good wetting characteristic of methanol has made it easier to insert this narrow space, and cut oil flow formed a flow pattern composed of oil droplets followed by methanol phase [10]. However, a different phenomenon is shown in figure 4.21 (b). In this condition, it was difficult for the oil phase to fill out of the whole surface area channel to insert toward methanol flow and cut off it [9]. The last experimental condition might produce a stable flow by increasing the oil flow rate for making oil has a better power to cut methanol flow. However, if observed, both the inlet position's configuration above gives a different flow pattern with others. Here, the flow pattern is structured by a gas bubble (air), then methanol adheres to the tail of the bubble, and finally, oil is behind methanol. There is no specific information about it in the literature; therefore, more in-depth studies are critical to understanding the factors affecting the formation of 3 phase flow pattern.

4.7. Conclusion

The stable flow pattern was not found in the tube of 20, and 9 m long at all experimental conditions observed; however, it was found in the tube of 1 m long.

Pressure drop rises in line with an increase in the tube length used. The stable flow was challenging found out at a high-pressure drop inside the tube. On the ratio of gas to total liquid velocity was getting bigger, the bubbles' length sharply increased, whereas the methanol and oil phase tends to decrease slightly.

The Methanol-oil-air configuration for the inlet system produced stable flow patterns. In contrast, the oil-methanol-air system used in these studies could not produce stable flow patterns indicated by the variation of flow pattern every time during observation without repetition of a specific flow pattern in a certain period.

Literature

[1] Y. Önal, M. Lucas, and P. Claus, "Application of a capillary microreactor for selective hydrogenation of α,ß-unsaturated aldehydes in aqueous multiphase catalysis," *Chem. Eng. Technol.*, vol. 28, no. 9, pp. 972–978, 2005.

[2] K. Wang, Y. Lu, K. Qin, G. Luo, and T. Wang, "Generating Gas-Liquid-Liquid Three-Phase Microflows in a Cross-Junction Microchannel Device," *Chem. Eng. Technol.*, vol. 36, no. 6, pp. 1047–1060, 2013.

[3] V. M. Rajesh and V. V. Buwa, "Experimental characterization of gas-liquid-liquid flows in T-junction microchannels," *Chem. Eng. J.*, vol. 207–208, pp. 832–844, 2012.

[4] K. Wang, Y. C. Lu, J. Tan, B. D. Yang, and G. S. Luo, "Generating gas/liquid/liquid three-phase microdispersed systems in double T-junctions microfluidic device," *Microfluid. Nanofluidics*, vol. 8, no. 6, pp. 813–821, 2010.

[5] C. J. Gommes, S. Blacher, J. H. Dunsmuir, and A. H. Tsou, "Practical Methods for Measuring the Tortuosity of Porous Materials from Binary or Gray-Tone Tomographic Reconstructions," *AIChE J.*, vol. 55, no. 8, pp. 2000–2012, 2012.

[6] J. Mann, "Transport processes and unit operations," *The Chemical Engineering Journal*, vol. 20, no. 1. p. 82, 1980.

Chapter 5

Biodiesel synthesis by transesterification and ozonolysis reactions

Contents

5.1. Introduction

5.1.1. Biodiesel synthesis

The shortage of petroleum supply will cause the crisis of energy and give impact to the fluctuation of oil price. Current disposal of waste cooking oil (WCO) as animal feed source may no longer be accepted due to stringent prohibiting it to be used as animal feed source. Other ways of converting the WCO as soap precursor and other fatty acid-based products do not give high value add products. Alternative disposal methods to convert this WCO to high value add products needs to be developed. Environmental awareness to address global warming due to CO2 release is increasing. Hence, alternative energy that can ameliorate environmental degradation and global warming need to be promoted.

During this time, biodiesel is widely produced from foodstuffs such as soybean oil, rapeseed oil, and palm oil, therefore, the increase in production following the demands of the need will have an impact on the scarcity of food and the opening of new farming lands that are at risk of environmental damage.

Further, WCO has high potential as a biofuel source since WCO is still composed of high fatty acid content. The availability of an enormous volume of waste palm oil in Indonesia makes it suitable for feedstock of biodiesel synthesis.

Biodiesel is alternative diesel fuel and a renewable energy source that can reduce the utilization of fossil fuel. Generally, biodiesel synthesis is conducted through transesterification in a stirred tank reactor, which took place in batches /continuous processes. Biodiesel transesterification is sensitive to oxidation, and it has low stability due to the high concentration of unsaturated methyl esters. Further, stirred tank reactors in the synthesis process might only deliver low yield and conversion besides safety aspects that still become a serious issue in the chemical processes. In the last decade, some studies dedicated to enhance the biodiesel product stability have been performed using an ozonolysis reaction, which involves the cutting process of double bonds carbon chains of methyl ester compounds. The combination of transesterification and ozonolysis has a great potential in improving yield and conversion. Here, transesterification is intended to produce methyl ester product, whereas ozonolysis has the primary function to break the double bond carbon chains in unsaturated ester compounds to generate short-chain saturated esters. Reducing the total of double bonds improves the product quality, mainly in terms of higher stability aspect, flashpoint, and lower viscosity, which is suitable for use in motors in cold climates.

The availability of articles describing biodiesel synthesis using two reaction steps is very limited. The following are some previous works on biodiesel synthesis through transesterification and ozonolysis.

Baber et al. (2005) carried out the synthesis of biodiesel using two reaction-steps of transesterification using soybean oil as a feedstock at 60 °C, and ozonolysis of methyl soyate (biodiesel), which was conducted in the presence of methanol, dichloromethane (solvent), and triethyl amine (catalyst) at -75 °C during 2 hours. The molar ratio oil-methanol used was 1:28, and the synthesis was conducted in a tank reactor equipped with the fritted disk for dispersing O_3[1].

From transesterification, it was obtained long-chain methyl esters consists of methyl palmitate (C16:0, 11%), methyl stearate (C18:0, 5 wt%), methyl oleate (C18:1, 25 wt%), methyl

linoleate (C18:2, 51 wt%), and methyl linolenate (C18:3, 7 wt%). The second step, ozonolysis gives some short-chain methyl esters consisting of methyl myristate, methyl palmitate, methyl stearate and fragment products of unsaturated methyl esters as dimethyl malonate, methyl hexanoate, methyl nonanoate, and dimethyl azelate. The total amount of double bonds in the mixture was reduced by more than 90% in the ozonolysis product[1].

Riadi et.al. (2015), the experiment was carried out in two steps reactions, transesterification, first, on the oil-methanol molar ratio 1:5, waste palm oil as a feedstock, at 60 °C for 1 hour, and the second step, ozonolysis, was performed at various reaction temperatures 10, 20, and 30 °C during 2 hours in 2L of the stirred batch reactor. As the products, it was obtained long-chain methyl esters suck as methyl palmitate, methyl oleate, methyl stearate, methyl palmitoleate, methyl linoleate as transesterification products, and short-chain methyl esters consist of methyl nonanoate, methyl hexanoate, and methyl octanoate as ozonolysis products [2].

Combining transesterification and ozonolysis seems promising to improve biodiesel product, but this method still has some challenges related to the complexity of gas-liquid-liquid systems referred. For this, the results obtained in chapters 3 and 4 will give us some guidelines for the choice of the experimental conditions. The objective of this chapter is to carry out the biodiesel synthesis in microtube using sunflower oil as a model for waste cooking oil

5.1.1.1. Biodiesel product transesterification and ozonolysis: comparison

From previous studies, it can be made a comparison of the quality of biodiesel transesterification and ozonolysis (transesterification and ozonolysis simultaneously) as seen in table5.1.

Table 5.1. The comparison of biodiesel product transesterification and ozonolysis[3][4]

Remark	Biodiesel transesterification	Biodiesel ozonolysis
Heat value (kcal/kg)	9490	9730
Ash content (wt %)	< 0.01	< 0.01
Density (gr/cm3)	0.8841	0.8758
Flash point (°C)	130.1	51.3
Sulfur content (wt %)	0.01	0.01
Nitrogen content (wt %)	< 0.1	< 0.1
Stability	Low	High
Sediment	produce sediment in machine	doesn't produce sediment in the machine
Viscosity	High	Low

Further, biodiesel transesterification contains too much methanol producing the emissions of harmful organic compounds like formaldehyde, acrolein, benzene, and its derivative, whereas biodiesel ozonolysis is more environmentally friendly.

5.1.1.2. Transesterification and ozonolysis reactions

Ozonolysis can be defined as the reaction between ozone and ethylenic compounds to form an ozonolysis product. The ethylenic compounds can be double bonds in the vegetable

oils or free fatty acids and esters[5]. Some researchers pay more attention to the application of ozonolysis reaction for the synthesis of biodiesel since a high product selectivity can be achieved, low energy consumption, and environmentally friendly. The mechanism of transesterification and ozonolysis can be depicted below[6]:

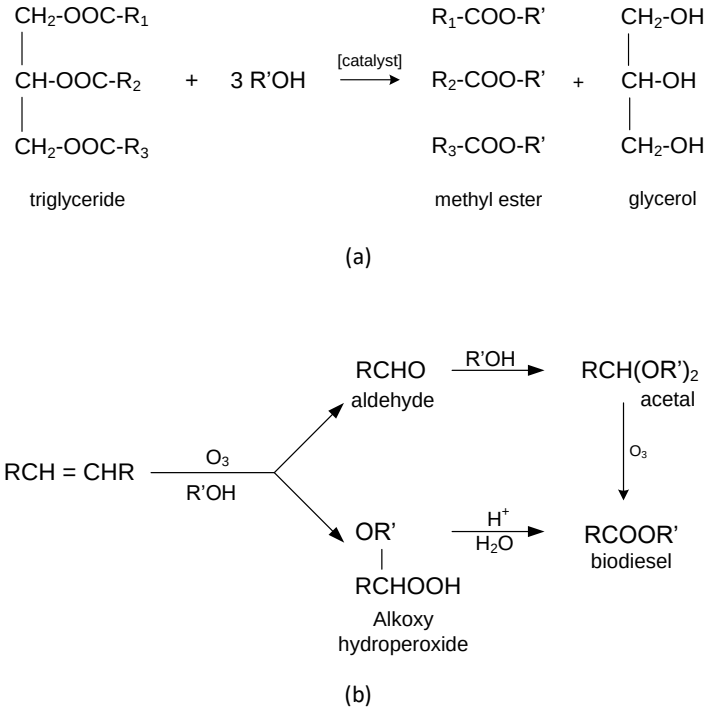

Figure 5.1. (a) Transesterification reaction, (b) transesterification and ozonolysis mechanism to produce biodiesel followsthe Criegee mechanism

Ozone is a strong oxidizing agent. Based on this fact, in these syntheses, there is some possibility where ozone could have attached several chemical compounds, and until now, this matter has not been explained clearly and is still presumptive. Some possibilities which will occur related to the use of ozone are:

a. Ozone attacks the double bonds of the carbon chain (C = C) which is found in vegetable oils/free fatty acid (FFA) and ester compounds.
   If the double bond of vegetable oils/FFA is broken, the ozonolysis reaction produces short-chain methyl ester due to the "C" bond broken will react following the Criegee mechanism to form alkyl ester product. The same product in the form of a short-chain of alkyl ester will be found when the ester compound's double bond formed by transesterification is broken. In the previous work, Baber et al. (2005) managed to inventory short-chain methyl ester due to the breaking double bonds carbon chain of esters compound (see Figure 5.2).

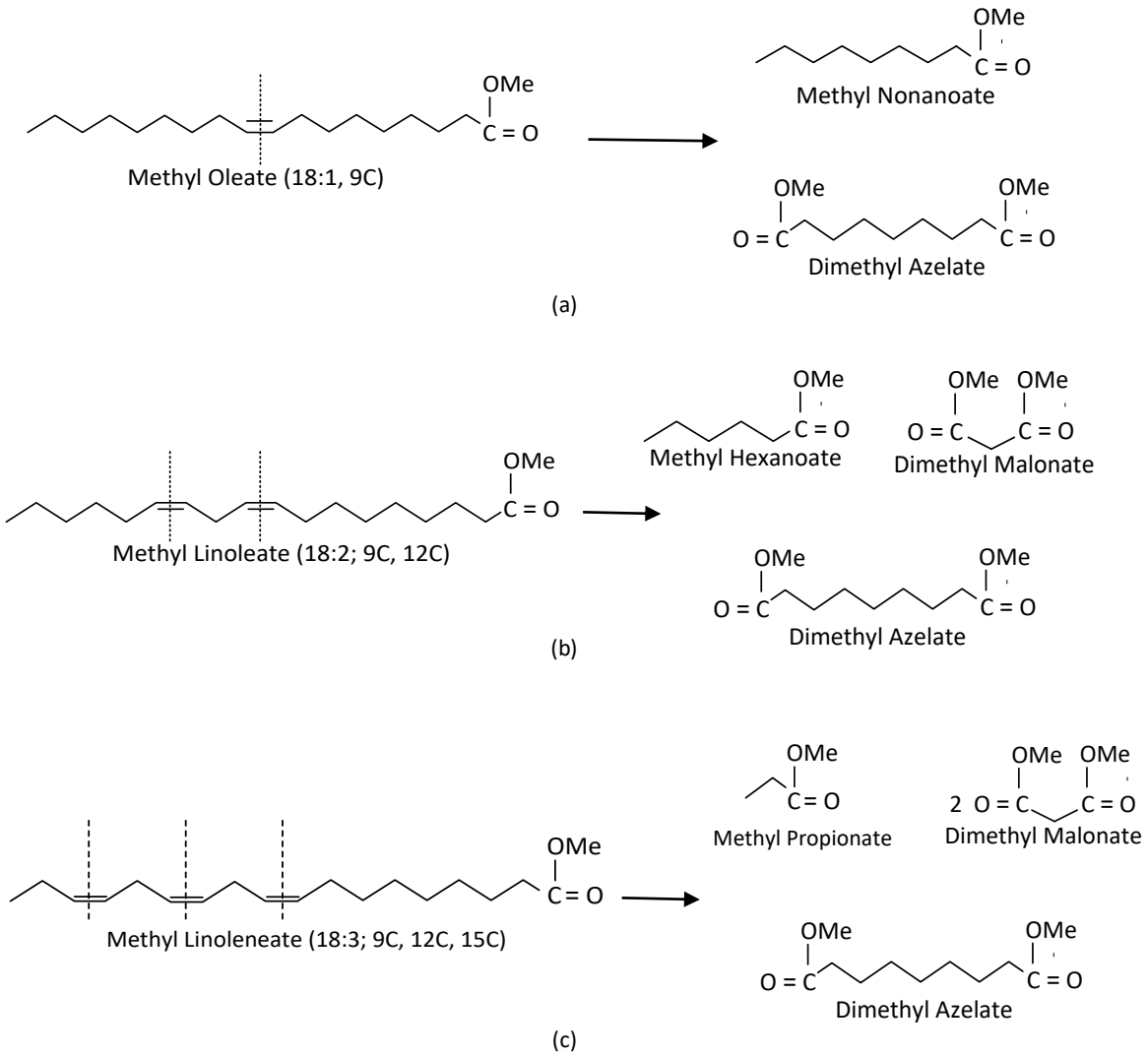

Figure 5.2. (a)(b)(c) The fragment products of unsaturated methyl ester compounds.

b. Ozone tends not to react with saturated methyl esters. The ozonolysis rate is much higher in fatty ester-containing multiple double bonds than a single bond or no double bond [5].
c. Ozone will react with methanol and other oxygen-containing compounds. The reaction between ozone and methanol may proceed through the formation of the transition state below: (i) Ozone attacks C-H bond, (ii) ozone attacks O-H bond and (iii) ozone attacks atom oxygen.

Since the methylated terminal end between methanol and methyl ester compound have a similar structure, then ozone could have possibly reacted with this functional group and with the double bonds simultaneously. Furthermore, the expected esters formed could have been further attacked by ozone and methanol at these methylated sites[1].

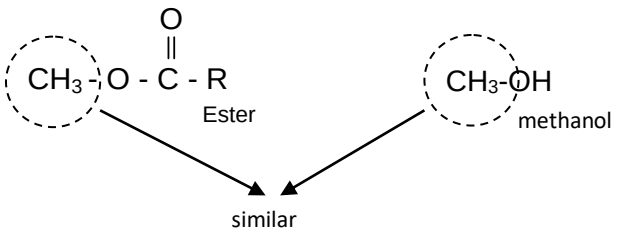

Figure 5.3. Ozone could attack the methylated terminal end of ester and methanol.

5.1.2. Microdevices application for synthesis of biodiesel

Microreactor is a novel concept in reactor technology that enables introducing new reaction procedures in chemistry, the pharmaceutical industry, and molecular biology. Miniaturized reaction systems offer many exceptional technical advantages for a large number of applications. The high surface-to-volume ratio was allowing a significant enhancement of process control and heat management. Moreover, the unique possibilities of microchemical systems pave the way to a distributed point-of-use and on-demand production of extremely harmful and toxic substances.

Microreactors offer many advantages for the performance of heat and mass transfer-limited reactions. Large gradients in concentration and temperature are achieved by shrinking the characteristic dimensions of a microreactor down to the micro-scale. It is especially advantageous in the case of highly exothermal reaction as well as in the case of mass-transport-limited processes. Based on these technical advantages, new and unusual process regimes become technically feasible. These advantages make it a great opportunity for various GLL applications, especially for hazardous reactions limited by mass and heat transfer such as ozonolysis. The miniaturized reactors have great potential and suitable for biodiesel synthesis, which involves two immiscible liquids and dangerous gas.

5.2. Experimental apparatus and method

This chapter shows the synthesis of methyl ester by using two types of reaction, i.e., transesterification and ozonolysis, that takes place simultaneously and sequentially, involving three-phase reactants comprising of oil, methanol (CH_3OH),and ozone (O_3). The schemeof the detailed experimental tool is shown in figure 5.4.

5.2.1. Microtube design

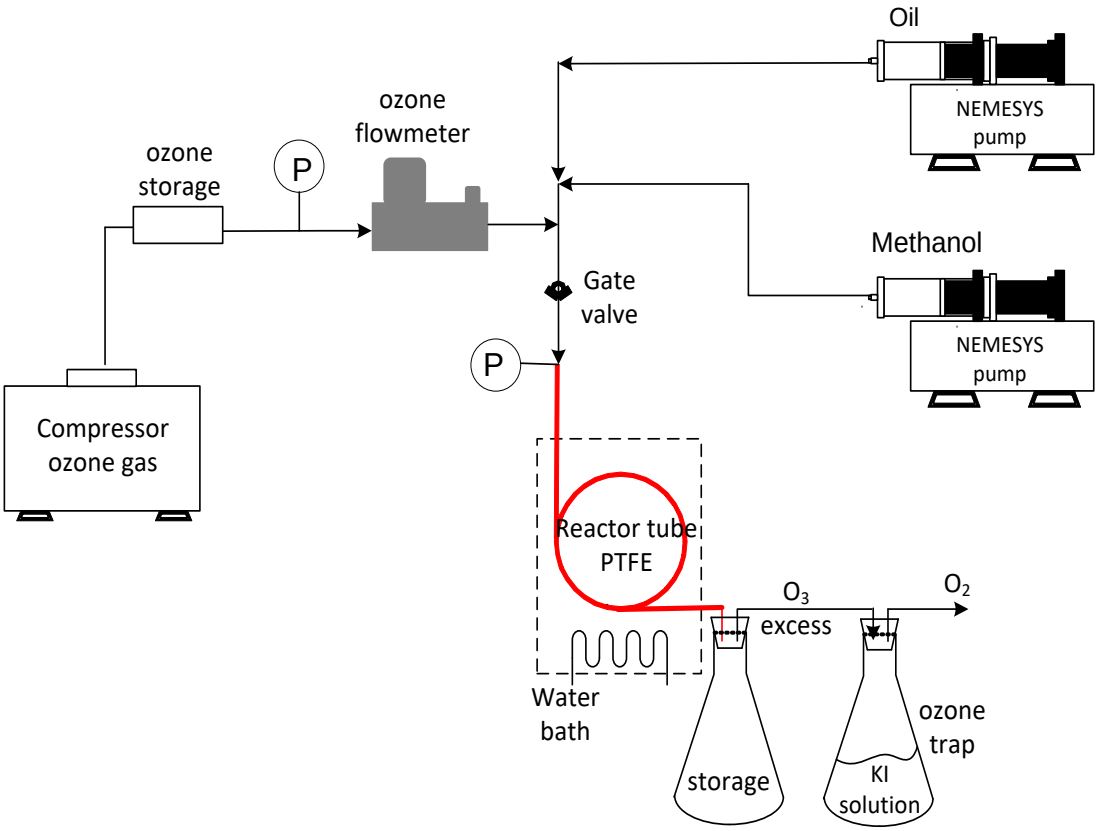

Figure5.4. Experimental design of simultaneous process

The tube used to study the hydrodynamics of gas-liquid flow is a circular micro-tube in Poly-tetra-fluoro-ethylene (PTFE). PTFE present the advantage of being transparent intended to visualize flow patterns. In order to set and maintain the reaction temperature during the experiment, the PTFE coil tube (red color in figure 5.4) was dipped in a water bath.

5.2.2. Flow control

Ozone was supplied from a pressurized vessel and controlled employing SERV INSTRUMENTATION 0151B, which allows flow rates ranging from 0.00 to 20 Ncm^3/min O_3 with a maximum gas pressure is 1.5 bar abs.

For liquids, the flow control equipment used was two high-pressure syringes pump (NEMESYS),which served to flow oil and methanol, respectively. These pumps have a good performance because they can generate a stable liquid flow with the minimum and maximum flow rate in the range of 0.0001 µl/hr (for 0.5 µl syringe) to 220.82 ml/min (for 140 ml syringe).

All experiments were performed at ambient pressure in the outlet section of the tube. The gas pressure was set and controlled to present a constant gas flow rate inside the tube during the reaction.

5.2.3. Fluid properties and raw material

The synthesis of biodiesel required the reactants of methanol, oil, and ozone. Their properties significantly contributed to the bubble/slug formation within a micro-tube, which influenced the formation of surface area for mass and heat transfer. Table 5.2 presents ozone, oil, and methanol properties used for conducting the synthesis of methyl ester.

Table 5.2. Ozone, oil and methanol properties

Fluid	ρ (kg/m^3)	μ (kg/m.s)	σ (N/m)
Ozone	1.2041	1.82E-05	-
Methanol	792	5.90E-04	2.27E-02
Oil	925	4.914E-2	3.35E-02 [7]

ρ = density, μ = viscosity, σ = surface tension. The physical properties of ozone (table 5.2) are measured at 20 °C, 1 atm.

Sunflower oil has been prepared as a raw material in this work. It is composed of saturated and unsaturated fatty acids, as shown in table 5.3.

Table 5.3. The composition of sunflower oil[8]

Fatty Acid	wt%	Characteristic
Palmitic acid	7	Saturated
Stearic acid	5	Saturated
Oleic acid	19	Unsaturated
Linoleic acid	68	Unsaturated
Linolenic acid	1	Unsaturated
Total	100	

Oleic and linoleic acid as unsaturated fatty acid is two major components which composing sunflower oil. Therefore, it is excellent potential to make it a raw material for presenting a model for the synthesis of biodiesel.

5.2.4. Experimental method

The synthesis of methyl ester was carried out using two methods, i.e., first, simultaneously reaction between transesterification and ozonolysis, and second, series reaction transesterification followed by ozonolysis and vice versa. The catalysts of 1 wt% NaOH and 1.5 wt% H_2SO_4 was prepared for reaction performing. For simultaneous reaction, the synthesis of alkyl esters was conducted by flowing oil and methanol through a microtube of 1 mm inside diameter and applying two similar T-junction designs to present gas and liquid-liquid reaction. The first T-junction is to bring a contact of oil and methanol; then, the second T-junction serves to introduce ozone gas to the oil-methanol mixture. At the end of the tube, the product was stored in small storage and at once intended to separate gas from the liquid product. During a reaction, sometimes, a small volume of warm water was added into the product storage to prevent the continuous reaction take place. For getting the pure methyl ester, these products should be purified follow the steps:

1. Deactivation of the base catalyst (NaOH) using warm water and at once to separate methyl ester product from glycerol, water, and the remaining methanol by utilizing a separatory funnel. The addition of warm water into the solution is also intended to release inert components from biodiesel (washing). The washing step will be stopped when the pH wash water reaches 7 (neutral).
   Methyl ester forms a separated phase, usually occupies the top layer, and does not dissolve into other liquid-phase.
2. Reducing the water content in the product by adding magnesium sulfate anhydrous ($MgSO_4$).
3. Separation of methyl ester and magnesium sulfate by using filter paper.

A different method was applied for a series reaction. In this method, oil and methanol were reacted first (transesterification); then, the product was purified using the same steps as above. Second, ozonolysis of transesterification product used methanol and ozone at the same experimental conditions. Finally, to obtain the pure product, the product must be purified to follow the same procedure as mentioned above.

Another type of series reaction is to carry out ozonolysis first and then followed by the transesterification. In the implementation, the similar methods used previously are reversed.

5.2.5. Characterization methods

The experiment used two types of chemical analysis; there are the iodine value test and gas chromatography analysis. Iodine value test is used to know the amount of unsaturation in fatty acid/ester by detecting the total double bond carbon chain in the solution. Iodine value is the mass of iodine in grams that is consumed by 100 grams of a chemical substance. Further,gas chromatography was used to measure the alkyl ester concentration in the ozonolysis product. These analyzes are explained as follow:

1. Iodine value test

Iodine value test applied a method proposed by Wijs. The detailed analysis procedure is as follow:

- Prepare 0.1 – 0.5 gr blank solution and sample in two different erlenmeyer.
- Into each erlenmeyer, add 10 ml chloroform and 25 ml wijs iodine solution.
- Put these erlenmeyers in a dark place at room temperature for 30 minutes.
- At the end of 30 minutes, in each erlenmeyer, add 10 ml 15% KI solution and 50 ml water.
- Titration sample using 0.1 N $Na_2S_2O_3$ until yellow color almost disappeared
- Then, add a few drops of starch indicator, and continue the titration until the blue color completely disappeared.
- The total required volume of $Na_2S_2O_3$ for titration is known.

Here, chemicals were added with their respective functions. Chloroform was applied to enhance the oil solubility in the solution due to its solubility in the organic solvent (chloroform). Oil and chloroform have the same polarity (non-polar). Wijs iodine solution (I-Cl) served to drive an addition-reaction of double bond carbon chain in oil. I-Cl will be bound by oil in its double bonds. Then, a blank solution was applied for calibration purposes; KI solution

was used to bind the rest of the un-reacted I-Cl compound, and the starch indicator served as a binding agent to the iode compounds, which were contained in the sample.

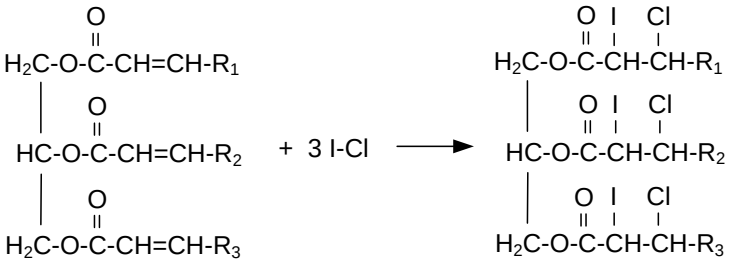

$$I\text{-}Cl + KI \xrightarrow{\text{excess}} KCl + I_2$$

$$I_2 + 2Na_2S_2O_3 \longrightarrow 2NaI + Na_2S_4O_6$$

Figure5.5. Chemical reactionsteps during iodine value test.

Iodine value is calculated by using the equation (1).

$$\text{Iodine value} = \frac{(B-S).N.(12.69)}{C} \qquad \ldots\ldots(1)$$

Where S = volume of $Na_2S_2O_3$ solution required for titration of samples (ml)
B = volume of $Na_2S_2O_3$ solution required for titration of blank solution (ml)
C = weight of sample (gr)
N = normality of $Na_2S_2O_3$ solution

For simultaneous reaction, an iodine value test was conducted on oil and methyl ester product. Further, for series reaction (transesterification-ozonolysis), iodine value test was carried out to transesterification product (after purification) and ozonolysis product. A similar method was performed if the reaction scheme comes first with ozonolysis then transesterification.

2. Characterization Methyl Ester composition of Biodiesel Product by using Gas Chromatography

Analysis of all standards (FAME mix $C_4 – C_{24}$ and $C_8 – C_{24}$) and oil samples will be carried out using Hewlett- Packard (Palo Alto, CA) model HP-5890 Series II equipped with an Alltech Associates (Deerfield, IL) Heliflex AT-1 capillary non-polar column (15-m length, 0.53-mm ID, 1.5-µm thickness) and a flame-ionization detector. Helium is carrier gas, whereas nitrogen is auxiliary make up gas with total flow rate for both gases is 25 mL/min. The programming condition in the column temperature is as follows: temperature is initially set at 40°C for 2 min; rate 1 is 10°/min from 40 to 180°C, conducted isothermally for 8 min; rate 2 is 5°C/min from 180 to 240°C, conducted isothermally for 5 min; rate 3 is 30°c/min from 240 to a final

temperature of 300°C, conducted isothermally for 5 min. The flow rate of hydrogen is 35 mL/min, and the flow rate of air is 400 mL/min. The temperatures of the injector and detector were 280 and 320°C, respectively. The injection volume is used for a sample size of 1.0µL.

Samples were prepared in vial bottles with the composition of 20 µL sample solution, 10 µL ethyl acetate, and 970 µL n-hexane. Ethyl acetate served as an internal standard and n-hexane as a solvent.

5.3. Synthesis of methyl esters

The methyl ester was synthesized in two different ways, including simultaneous and sequential reactions, which involves transesterification and ozonolysis. Each process system has different challenges. Conducting transesterification and ozonolysis simultaneously faces some obstacles, i.e., the reaction mechanism is not known clearly; to get optimum yield, transesterification requires high reaction temperature while ozonolysis requires low reaction temperature. Further, transesterification needs a base catalyst like NaOH/KOH, while ozonolysis needs an acid catalyst (H_2SO_4/HCl). On the other hand, conducting transesterification and ozonolysis in a consecutive way faces some difficulties, i.e., the overall process also takes extra time to decrease the reaction temperature from 60 °C (for transesterification) to room temperature (for ozonolysis) and the conditioning of the use of a catalyst from base to acid catalyst.

The detailed result of the synthesis process using simultaneous and series reactions was explained in the following section.

5.3.1. Transesterification and ozonolysis in one pot

In this section, biodiesel was synthesized by using simultaneous reactions. Table 5.4 and 5.5 below show the experimental conditions used and the experimental results, respectively. Molar ratio oil : methanol of 1 : 5 and 1 : 3 were chosen considering that these ratios can generate stable gas-liquid-liquid flow inside the microtube used in the experiments. These ratios represent the oil and methanol flow rates where the number “1” refers to oil and the number “5” and “3” relates to methanol, respectively. Temperature and catalyst were chosen based on the previous works on biodiesel synthesis[2][9]. The experiment used the tube length of 1 and 5 m, considering the residence time needed and flow stability.

Table 5.4.Experimental conditions in simultaneous reactions

Experimental conditions	Experiments				
	2B	3C	4A	4B	5B
Molar ratio oil :MeOH	1 : 5	1 : 5	1 : 5	1 : 3	1 : 3
Q_{oil} (ml/min)	0.1621	0.1621	0.1621	0.1621	0.1621
Q_{MeOH} (ml/min)	0.1086	0.1086	0.1086	0.0652	0.0652
Q_{ozone}(ml/min)	0.6	0.6	0.6	0.6	0.2
Temperature (°C)	30	30	30	30	30
O_3 concentration (gr/Nm3)	40 - 44	40 - 44	50 - 54	40 - 44	60 -64
L_{tube} (m)	1	5	5	5	5
Catalyst (NaOH)	1 wt%	1 wt%	1 wt%	1 wt%	1 wt%

Table 5.5. Methyl ester concentration (ppm) from GC analysis

Component	2B	3C	4A	4B	5B
methyl arachidate	-	-	0.2	0.6	-
methyl myristate	-	0.63	1.3	1.3	1.70
methyl octanoate	2.73	6.69	12.1	14.4	15.97
methyl palmitate	22.38	70.94	83.0	112.8	161.82
methyl stearate	9.68	26.14	24.9	38.0	52.79
methyl linoleate	180.27	591.21	698.2	958.7	1351.54
methyl linoleneate	-	-	0.1	0.4	-
methyl oleate	64.57	228.95	243.0	352.6	515.54
methyl palmitoleate	0.31	3.54	4.1	2.4	2.01
Total concentration	279.93	928.10	1066.9	1481.3	2101.37

Note: methyl linoleate, methyl linoleneate, and methyl oleate are unsaturated methyl esters

Table 5.4 and 5.5 provide information on the effect of the experimental conditions used in these studies. Molar ratio oil to methanol represents the ratio of oil flow rate to methanol flow rate. Related to the molar ratio, by comparing the result of experiment 3C with 4B, it was obtained that molar ratio 1:3 gives a better result than ratio 1:5. It is indicated by the total concentration of experiment 4B nearly two-fold of 3C. This result is different from the previous one on the synthesis of biodiesel in a batch stirred tank reactor [9] [11][14][15]. Baber et al. 2005 [11] used the molar ratio of methyl soyate-methanol 1:28 at -75 °C, 2 hours reaction time for reducing 90% total double bonds, Lieke et al. 2012 [14] found the best molar ratio oil-methanol 1:5 at 30 °C, 3 hours, and 5.8% ozone concentration.

By referring to the reaction stoichiometry of biodiesel synthesis [12], an ideal molar ratio needed to reach maximum oil conversion to methyl ester compound is 1:3; one for oil and three for methanol. However, in many previous works on biodiesel synthesis, yield and conversion reached were relatively low at applying this ratio. The different result is found in this work. The utilizing of molar ratio 1:3 within a small tube produced a higher concentration of methyl ester, as shown in experiments 4B and 5B. It happened since the molar ratio 1:3 was able to generate a smaller methanol slug length ($X_3 - X_4$), which lies between the oil phase and gas bubble, as shown in figure 5.6 (c). The intensive flow circulation and mass transfer between phases take place in this location. The smaller methanol slug dimension is able to create a smaller diffusion route for mass transfer.

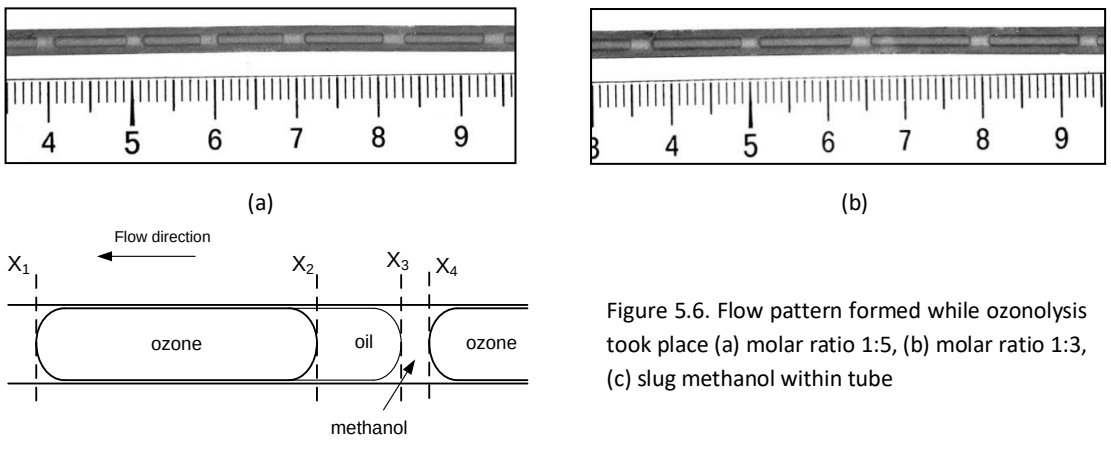

Figure 5.6. Flow pattern formed while ozonolysis took place (a) molar ratio 1:5, (b) molar ratio 1:3, (c) slug methanol within tube

The methyl ester concentration is continuously increased by applying higher ozone concentration, as seen in table 5.4 for experiment 5B.

Another quantitative analysis used besides gas chromatography is the iodine value test. Table 5.6 shows the result of the iodine value test for all experiments simultaneously. The iodine values obtained is also representing the conversion of ozonolysis. The lowest iodine value indicates the highest ozonolysis conversion due to the greater total double bond carbon chain cut by ozone. The lowest conversion was reached by experiment 2B, and the highest value was obtained the experiment 5B. Several things caused the lowest conversion in experiment 2B, i.e., utilizing a shorter tube (1 m) and the improper placement of NaOH catalyst. In experiment 2B, NaOH was placed in the oil phase. Even though NaOH is not soluble in the oil phase. Whereas for other experiments 3C - 5B, NaOH was put in the methanol phase, which was proven able to raise the ozonolysis conversion. Figure 5.6 at once can explain the highest iodine value was in experiment 5B. At experiment 5B, utilizing a lower ozone flow rate at molar ratio 1:3 can produce a similar flow pattern with figure 5.6 (b) with a smaller bubble dimension since the ozone flow rate is only 0.2 ml/min.

Table 5.6. Iodine value (I.V.) and percent cutting of double bond carbon chain for simultaneous reactions

Remarks	Experiments					
	Blanco	2B	3C	4A	4B	5B
I.V. average	125.4	122.9	105.4	98.05	83.15	75.4
% conversionozonolysis	-	2.00%	15.93%	21.83%	33.71%	39.88%

5.3.2. Sequential reactions (transesterification and ozonolysis)

Sequential processes were performed in this section to obtain information on possible routes of reaction in optimizing biodiesel synthesis. The purpose of the sequential process application here is to convert the remaining fatty acid, which has not reacted yet. Some alternative ways of the sequential process have been done: (1) transesterification and ozonolysis (2) ozonolysis and transesterification. Both of them applied a similar base catalyst NaOH. The next sequential process is (3) transesterification and ozonolysis (4) ozonolysis and transesterification. In the two last points, transesterification was performed using 1 wt% NaOH catalyst, and ozonolysis using acid catalysts of 1.5 wt% H_2SO_4. All series reactions above were performed under the best experimental condition obtained from previous works in the simultaneous process involved of a molar ratio of oil-methanol 1:3; oil and methanol flow rate 0.1621 ml/min and 0.0652, respectively; ozone flow rate 0.2 ml/min; temperature 30 °C; ozone concentration 60-64 gr/Nm3; and tube length 5 m. The catalyst used, NaOH/H_2SO_4, was put in the methanol phase, and the transesterification was carried out without involving ozone gas. The residence time for this operating condition is around 17 minutes.

5.3.2.1. Transesterification (NaOH catalyst), ozonolysis (NaOH catalyst)

The composition of methyl ester obtained is shown in table 5.7. The schematic processes applied in table 5.7 are the sequential process of:

(1) ozonolysis – transesterification

(2) transesterification – ozonolysis

The methods applied under the same NaOH catalyst for both reactions, as a whole, indicate that series reactions did not increase in the concentration of methyl ester, but conversely, utilizing these methods has decreased each methyl ester concentration in the final product. The reverse reaction of transesterification might cause a decrease in methyl ester concentration, because transesterification is a reversible reaction. This result has already been observed in previous work [2]. The use of the series process meant the use of double residence time. Therefore, these sequential processes' configurations are not suitable to enhance the total concentration of methyl ester product, either saturated or unsaturated methyl ester.

Table 5.7. Methyl ester concentration produced by sequential reaction (ppm)

Component	Oz-1	Trans-1	Trans-2	Oz-2
methyl arachidate	23.8	6.5	33.8	8.5
methyl hexanoate	-	-	-	0.6
methyl laurate	0.3	0.1	0.4	0.3
methyl myristate	9.7	4.1	12.4	4.7
methyl octanoate	5.6	4.5	-	4.3
methyl palmitate	785.7	309.3	1015.9	368.7
methyl stearate	391.4	147.0	525.2	181.1
methyl linoleate	6622.3	2633.5	8561.9	3106.5
methyl linoleneate	8.4	3.8	-	4.7
methyl oleate	2909.2	552.4	3813.7	1322.5
methyl palmitoleate	15.8	6.8	21.4	8.0
Total concentration	10772.2	3668.0	13991.0	5009.8

For transesterification–ozonolysis (Trans-2-Oz-2), in first reaction (transesterification), it was not found the components of methyl hexanoate, methyl octanoate, and methyl nonanoate in the product (see column Trans-2). Nevertheless, methyl hexanoate and methyl octanoate are found in the product of the second step (ozonolysis) (see column OZ-2). This result indicates that ozonolysis in these syntheses has produced the components of methyl hexanoate and methyl octanoate. Methyl hexanoate and methyl octanoate are fragments produced from unsaturated methyl ester cracking by ozone [16].

If table 5.7 on the sequential reaction is compared to table 5.5 on the simultaneous reaction, it is known that methyl hexanoate as one of the fragment products of unsaturated ester was not delivered transesterification-ozonolysis in one pot. Nevertheless, methyl octanoate, which is supposed to be another fragment product of unsaturated ester, appeared in both simultaneous and series reactions. Even in the simultaneous reaction under the smallest molar ratio of oil-methanol (1:5), and low ozone concentration around 40-44 gr/N.m3 and more, using a 1 m long tube only with a residence time 3.39 min, methyl octanoate has been produced. All reactions compared herein use the same catalyst (NaOH).

Further, the sequential reaction took place in two-step reactions; the sequential reaction has a longer residence time two times than that in simultaneous reaction. However, it seems that the longer residence time has not increased the amount of methyl ester produced.

The methyl ester concentrations in sequential reactions show significantly different values than simultaneous reactions, although the experiments have already been repeated two times under the same experimental conditions. This result has not been explained yet.

5.3.2.2. Transesterification (NaOH catalyst), ozonolysis (H_2SO_4 catalyst)

This part implemented the sequential process consist of transesterification and ozonolysis used NaOH and H_2SO_4 catalyst, respectively. Table 5.8 presents the methyl ester products of this synthesis. The reaction configurations used involve transesterification (Trans 1Q) followed by ozonolysis (Oz 1QQ) and vice versa, ozonolysis (Oz 2QQ) followed by transesterification (Trans 2Q).

Table 5.8. Methyl ester concentration produced by sequential reaction (ppm)

Component	Trans 1Q	Oz 1QQ	Oz 2QQ	Trans 2Q
methyl hexanoate	-	0.69	-	-
methyl myristate	0.94	0.66	1.09	1.71
methyl octanoate	-	2.59	1.69	1.75
methyl palmitate	78.07	53.66	69.04	113.22
methyl stearate	33.68	23.37	31.21	46.90
methyl linoleate	654.89	469.67	576.58	986.03
methyl linoleneate	4.39	3.09	1.08	1.86
methyl oleate	259.40	176.65	239.39	366.36
methyl palmitoleate	2.22	-	1.86	3.46
Total concentration	1033.60	730.37	921.95	1521.30

Transesterification (Trans 1Q)–ozonolysis (Oz 1QQ) configuration shows that all of the resulting methyl ester concentrations decrease in the end product. Transesterification did not produce methyl hexanoate and methyl octanoate, but these methyl esters have been found in the ozonolysis product. In this sequence, transesterification produced methyl myristate, methyl palmitate, methyl stearate, methyl linoleate, methyl linolenate, methyl oleate, and methyl palmitoleate only. Some other methyl ester compounds, such as methyl palmitoleate and methyl myristate, almost always appear in transesterification and ozonolysis products. The origin of these compounds is difficult to explain. They are usually derived from palmitoleic acid and myristic acid, respectively. But refers to the feedstock, sunflower oil does not contain palmitoleic acid and myristic acid. It indicated that other reactions had taken place.

Further, the different result is indicated by the ozonolysis configuration (Oz 2QQ) followed by transesterification (Trans 2Q). Here, the series process can improve the concentration of all methyl ester products. An acid catalyst such as sulphuric acid and hydrochloric acid is a suitable catalyst for ozonolysis since the acid compound can increase in ozonolysis rate, while transesterification is most suitably carried out with an acid/base catalyst. However, the utilizing of acid catalysts will produce methyl ester compounds in a long time of transesterification. Therefore, the ozonolysis product's transesterification has generated a higher methyl ester concentration from the remaining methyl ester, which has not yet reacted.

As a whole, the result obtained in this work shows a good inclination and according to the fatty acid concentration in the sunflower oil. As mentioned in table 5.3, sunflower oil contains linoleic acid as the primary component, followed by oleic acid in the second position, palmitic acid, stearic acid, and linolenic acid fewest component. However, in numbers, the concentration of all methyl ester products is relatively small. The small methyl ester concentration was caused by the short residence time due to a short tube (only 5 m). The use of small ozone concentration since the maximum capacity of generator ozone is around 3.4%. The challenge in applying a longer tube than 5 m is the high-pressure drop appeared throughout the tube. Pressure drop increase with an increase in tube length. Therefore, to flow ozone and viscous liquid (oil), a higher compressor capacity/pressure and a high-pressure liquid pump will be needed. Further, the observation results indicate that the stable flow pattern was not found during observation using a longer tube than 5 m. The bubble length along the tube changed due to more pressure drop, and sometimes occurring the bubbles coalescence phenomena.

The chromatogram Gas Chromatography shows some methyl esters compound peaks according to the raw material. These chromatograms prove that transesterification and ozonolysis have happened. The change in iodine value of oil at the beginning and after ozonolysis, reinforce that the cutting process of double bonds C=C had been going on.

In series reaction transesterification-ozonolysis, total methyl ester transesterification produced was ± 24 ml from 30 ml virgin oil. Further, in ozonolysis, the total methyl ester produced was ±12 ml from 20 ml product transesterification (after washing and purifying).
In the simultaneous reactions, the total methyl ester produced was ± 24 ml from 30 ml virgin oil.

5.3.3. Reaction kinetics

In order to know the reaction kinetics of simultaneous reaction for synthesis biodiesel, the simultaneous reactions were performed in a different residence time with the trend of some methyl ester concentration presented in the following figures. In this part, transesterification and ozonolysis simultaneously took place at molar ratio 1:3, temperature 30 °C, ozone flow rate 0.2 ml/min with ozone concentration around 60 – 64 gr/Nm3, and tube of 5 m long.

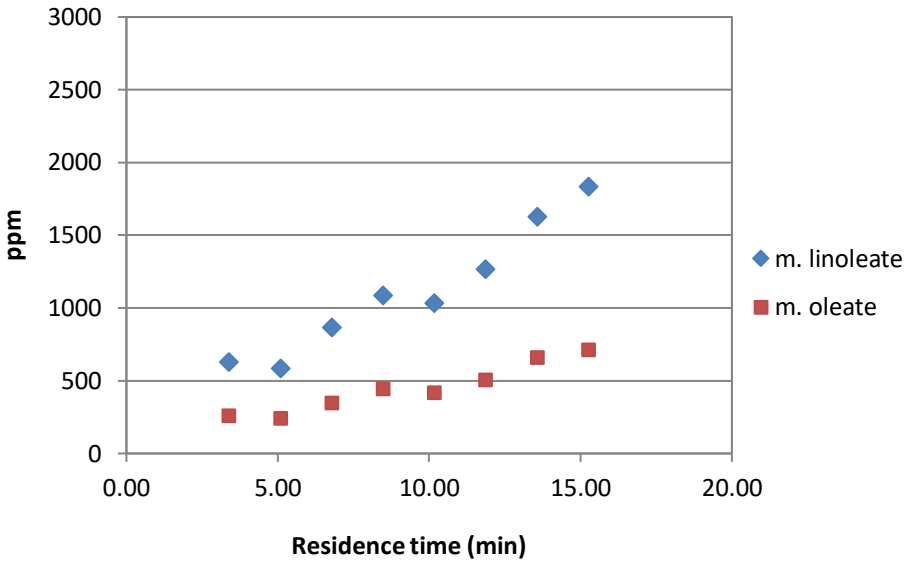

Figure 5.7. The concentration of methyl linoleate and methyl oleate products

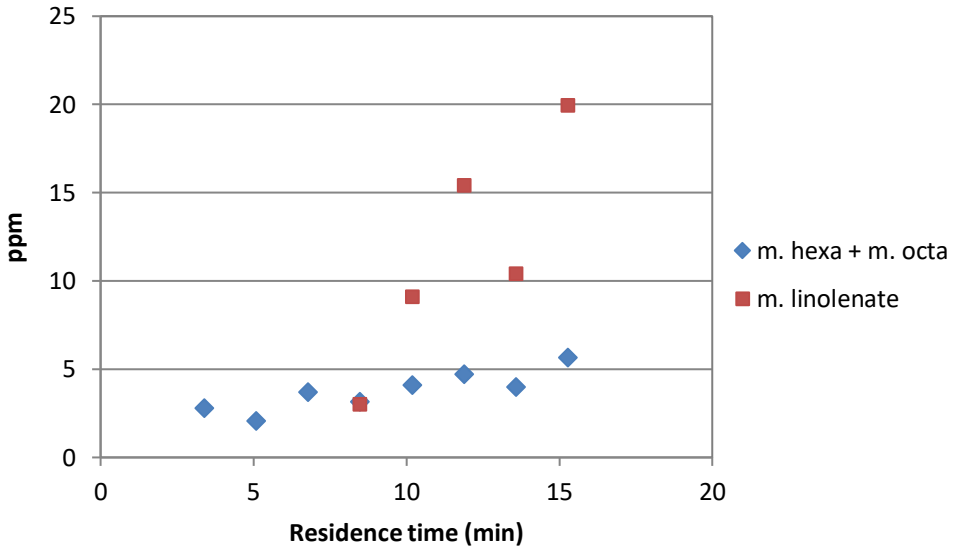

Figure 5.8. The concentration of methyl linolenate and total methyl hexanoate+methyl octanoate products

Methyl linoleate, methyl oleate, and methyl linolenate are unsaturated methyl ester products. The concentration of methyl linoleate and methyl oleate increased nearly linear at the beginning of ozonolysis but risen sharply in the last step, whereas methyl linolenate appeared in a low product concentration. The concentration remains low 10-20 ppm. The fluctuation might be caused by the reaction competition between transesterification and ozonolysis. Transesterification is to enhance a concentration, but ozonolysis caused a decrease in the concentration, because of the cutting process.

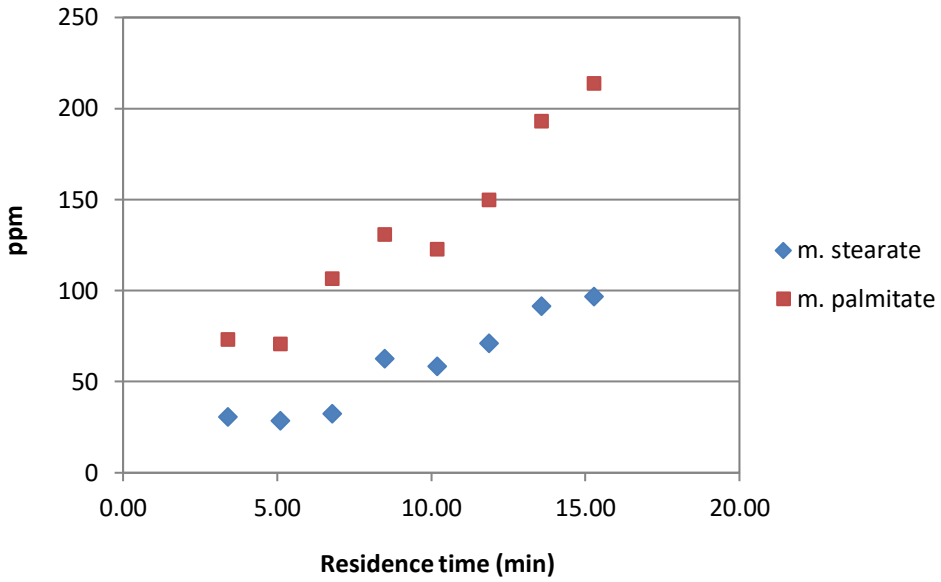

Figure 5.9. The concentration of methyl stearate and methyl palmitate products

Figure 5.9 shows a similar trend in figure 5.7. Figure 5.8 indicates the slow increase of short-chain methyl esters concentration (max 6 ppm), i.e., methyl hexanoate and methyl octanoate. As a small concentration and there was a reaction competition, so the concentration of these components fluctuated.

From the result, it can be estimated some important phenomenon for predicting mechanism and reaction kinetics, as followed:

1. Transesterification and ozonolysis took place spontaneously and simultaneously. It is indicated in figure 5.7 - 5.9, at residence time 3.39 min has been produced saturated methyl ester consisted of methyl arachidate, methyl laurate, methyl myristate, methyl palmitate, and methyl stearate; and unsaturated methyl ester consisted of methyl linoleate, methyl oleate, methyl linolenate, and methyl palmitoleate) as the transesterification products, and short-chain methyl ester with total C < 10 (methyl hexanoate and methyl octanoate) as the ozonolysis fragment products.
2. At once, identification mentioned in point 1 proves that transesterification went well at temperature 30 °C. In general, transesterification needs a temperature of 60 °C.
3. Figure 5.8 shows that ozonolysis is still going on until the residence time at 16.96 min. The total concentration of methyl hexanoate and methyl octanoate tends to increase.
4. Ozonolysis performance can utilize acid and base catalyst. In a base catalyst, ozone will not oxidize the organic compound directly but first, ozone will form OH^- radical follows the reaction mechanism:

$$O_3 + OH^- \longrightarrow O_2^* + HO_2^*$$
$$O_3 + HO_2^* \longrightarrow 2O_2 + OH^*$$
$$HO_2^{**} \longrightarrow O_2 + H_2O$$
$$H_2O_2 + O_2^* \longrightarrow OH^- + OH^* + O_2$$

In an acid catalyst, ozone will react directly to attack the organic compounds follow the reaction [10]:

$$O_3 + R \longrightarrow ROX$$

5. Degradation of organic compounds by ozone follows a 2nd order reaction mechanism, first order for organic compound and ozone concentration, respectively [11].

5.4. Conclusion

Transesterification and ozonolysis can deliver methyl ester compounds at low reaction temperature 30 °C and high molar ratio oil to methanol 1:3 by using sunflower oil as a feedstock. The reactions under moderate conditions, of course, have reduced energy consumption, which has been a challenge for biodiesel synthesis in the last decade.

In this work, transesterification is able to produce saturated methyl ester consisted of methyl palmitate, methyl stearate, methyl laurate, methyl myristate, methyl arachidate, and unsaturated methyl ester consisted of methyl linoleate, methyl linolenate, methyl oleate, and methyl palmitoleate, while ozonolysis succeeded in breaking the double bonds carbon chain unsaturated methyl esters and produced short-chain methyl ester as the fragment products, i.e., methyl hexanoate ($C_7H_{14}O_2$) and methyl octanoate ($C_9H_{18}O_2$). Some other methyl ester compounds always appear in the products; however, their origin is difficult to explain.

Two biodiesel synthesis methods were performed in this work involve transesterification-ozonolysis in one pot and sequential reactions transesterification-ozonolysis. Transesterification-ozonolysis carried out in one pot, can deliver methyl ester products in a short time residence time around 16.96 min at low reaction temperature 30 °C. Therefore, the use of two different reactions in one pot certainly can shorten the time of synthesis and simplifies the process cycle. Whereas, the sequential reactions show that the reaction carried out by using a base catalyst in both transesterification and ozonolysis cannot improve the methyl ester products. Further, it tends to drive the loss of methyl ester, which perhaps is caused by the reverse reaction of transesterification. Nevertheless, specific for the sequential reaction of ozonolysis-transesterification by utilizing H_2SO_4 catalyst for ozonolysis and NaOH catalyst for transesterification, this system succeeds in improving methyl ester concentration in the final product. This reaction system can be applied for increasing the yield of methyl ester product, but the reaction time needed is longer with a more complex synthesis cycle.

A reaction kinetics approach has been undertaken to provide a clear picture of the continuity of possible chemical reactions in biodiesel synthesis. From the experiment data, transesterification and ozonolysis took place spontaneously and simultaneously with a high mass transfer rate.

Literature

[1] T. M. Baber, D. Graiver, C. T. Lira, and R. Narayan, “Application of catalytic ozone chemistry for improving biodiesel product performance,” *Biomacromolecules*, vol. 6, no. 3, pp. 1334–1344, 2005.

[2] L. Riadi, A. Y. Widianto, E. Purwanto, A. Pono, and R. Theresia, “Synthesis of biodiesel from waste cooking oil by two steps process transesterification and ozonation,” *J. Chem. Pharm. Res.*, vol. 7, no. 9, pp. 17–21, 2015.
[3] J. Fu, S. Q. Turn, B. M. Takushi, and C. L. Kawamata, “Storage and oxidation stabilities of biodiesel derived from waste cooking oil,” *FUEL*, vol. 167, pp. 89–97, 2016.
[4] Z. Yaakob, B. N. Narayanan, S. Padikkaparambil, S. Unni K., and M. Akbar P., “A review on the oxidation stability of biodiesel,” *Renew. Sustain. Energy Rev.*, vol. 35, pp. 136–153, 2014.
[5] D. Milan and D. Peal, “(12) Patent Application Publication (10) Pub . No .: US 2002/0187020 A1,” 2013.
[6] M. F. Díaz, F. Hernández, O. Ledea, J. A. Gavín Sazatornil, and J. Moleiro, “1H NMR study of methyl linoleate ozonation,” *Ozone Sci. Eng.*, vol. 25, no. 2, pp. 121–126, 2003.
[7] E. A. Melo-Espinosa *et al.*, “Surface tension prediction of vegetable oils using artificial neural networks and multiple linear regression,” *Energy Procedia*, vol. 57, pp. 886–895, 2014.
[8] J. Orsavova, L. Misurcova, J. Vavra Ambrozova, R. Vicha, and J. Mlcek, “Fatty acids composition of vegetable oils and its contribution to dietary energy intake and dependence of cardiovascular mortality on dietary intake of fatty acids,” *Int. J. Mol. Sci.*, vol. 16, no. 6, pp. 12871–12890, 2015.
[9] L. Riadi, E. Purwanto, and Y. Chandra, “Ash Base-Catalysed in Promoting Ozonolysis of Used Cooking Oil,” *Int. J. Eng. &Technology*, vol. 12, no. 06, pp. 87–90, 2012.
[10] J. Hoigné and H. Bader, “The role of hydroxyl radical reactions in ozonation processes in aqueous solutions,” *Water Res.*, vol. 10, no. 5, pp. 377–386, 1976.
[11] Y. Li, X. Wang, H. Yang, X. Wang, and Y. Xie, “Oxidation of isoprothiolane by ozone and chlorine: Reaction kinetics and mechanism,” *Chemosphere*, vol. 232, pp. 516–525, 2019.

Chapter 6

Conclusion and Future Work

6.1. Conclusion

In order to improve the yield and quality of biodiesel products in terms of stability and to optimize the synthesis processes of biodiesel, this work has focused on utilizing simultaneous reaction transesterification-ozonation inside the microtube reactor at involving low energy consumption and safety in the process.

The first part of this work aims to create a framework to identify different scenarios that can be used to choose or implement a specific GLL contacting mechanism. Three simple-contacting models were proposed regarding that every three-phase chemical reactions always involve the partial dissolution or diffusion of a species from one phase to another. If not, the different species are not brought into contact, and chemical reaction is not possible. Some of the gas-liquid-liquid applications were reviewed, and each gas-liquid-liquid reaction system was classified in one of the proposed models for getting a description of contacting and mass transfer mechanism so that a chemical reaction can take place. All at once, these models give information on where the reactions occur and which one is the controlling parameter for reaction performance. It could be in the liquid-liquid interface with the liquid-liquid mass transfer as a controlling parameter; gas-liquid interface with the surface contact between gas and liquid is a controlling parameter, and in the continuous liquid phase with residence time is a controlling parameter. By understanding the model of a specific reaction, the appropriate strategy for optimizing reaction performance can be determined. Further, it is useful for predicting of contacting mechanism in the synthesis of biodiesel that will be explained in the last chapter [1][2].

The second part elucidated the developed reactor technologies in the previous works for the gas-liquid-liquid system, including a tubular reactor with static mixers, microreactor-minichannel reactor, jet loop reactor, and rotor-stator reactor (RSR) + stirred tank reactor (STR) tandem process. The main objective of this section is to understand gas-liquid-liquid reactors' performance, strength, and weaknesses of each reactor and the selecting steps of appropriate reactor type for a specific GLL reaction. Therefore, some aspects were considered in selecting a gas-liquid contactor, which covers of contacting pattern, the mass transfer coefficient of gas and liquid, gas and liquid flow rate, the solubility of gas in a liquid, and the mass transfer resistance in the gas phase and or liquid film [3]. The use of a specific reactor type must be adapted to the reactant's physical properties involved in realizing an optimum reaction yield. Further, a better process will generate a small volume of waste, lower pollution impact on the environment, and finally, reduce operational cost.

The first implementation of this study is the observation of gas-liquid (air-methanol) two-phase flow in the microtube of 1 mm inside diameter. The studies have focused on the generation of bubbles/slugs in the various tube lengths, the stability and regularity of flow pattern inside a small tube, the influence of gas-liquid pressure drop throughout the tube on

the generation of bubbles/slugs, and more, the effects of superficial gas and liquid velocity to bubble length. In this preliminary study, the flow pattern observed in the tube at the range of dimensionless number: 2.47 < *ReG* < 5.39; 36.45 < *ReL* < 109.34; and 0.000706 < *Ca* <0.002117 was a slug flow or Taylor flow. In this value, the inertia force and the surface tension force have the dominant influence than the viscous force on the order of magnitude is surface tension > inertia force > viscous force. Further, the higher pressure drop triggered the bubble length reduction throughout the tube, although sometimes the bubble coalescence phenomena were still occurring. Moreover, the air and methanol superficial velocities influenced the observed bubble's length, with the dominant influence is the methanol velocity.

The second implementation of this study is the observation of gas-liquid-liquid three-phase flow (air-oil-methanol) in the microtube of 1 mm inside diameter. As in the previous section, this part focused on the generation of bubbles/slugs in the various tube lengths of 1, 9, and 20 m, the stability and regularity of flow pattern inside the small tube, the influence of air and oil/methanol flow rate on gas-liquid-liquid flow, the influence of oil-methanol inlet position in T-junction, the determination of continuous/dispersed phase, as well as the measurement of surface tension, interfacial tension, and contact angle of oil/methanol, with the main purpose is to find a stable and regular flow pattern which is able to produce a large surface area for better mass transfer. The observation result showed that the stable flow nearly was not found in the tube of 20 and 9 m long at all experimental conditions observed. However, it was found in a tube of 1 m long. The pressure drop rises in line with an increase in the tube length used, and the bubbles' length sharply increased on the bigger gas to liquid velocity ratio. Further, the methanol-oil-air configuration in the T-junction was able to produce stable flow patterns. The studies in this section did not involve a chemical reaction because the observations did not use catalysts. The study's results on the two-phase and three-phase flow have become an important consideration to determine microtube design and operating parameters to synthesize biodiesel through the three-phase reaction ozonolysis.

Then, in the last section, methyl ester was synthesized in two ways reactions, i.e., first, transesterification and ozonolysis in one pot, and second, in the sequential reactions. This part aims to get a biodiesel synthesis model using sunflower oil as a feedstock in the microtube. The assumption used in this work is that the distribution of concentration is uniform in each point inside the micro-tube. As the final product, it was found saturated methyl ester consisted of methyl hexanoate, methyl octanoate, methyl laurate, methyl palmitate, methyl stearate, methyl myristate, methyl arachidate, and unsaturated methyl ester consisted of methyl linoleate, methyl oleate, methyl linolenate, and methyl palmitoleate. Some methyl ester compounds such as methyl palmitoleate and methyl myristate almost always appear in the product. The origin of these compounds is difficult to explain by refers to the composition of fatty acid in the feedstock. It is an indication that other reactions have occurred during the synthesis took place. Methyl hexanoate and methyl octanoate are found in the products. These components are supposed as the fragmented product of unsaturated methyl ester by ozonolysis.

The best-operating conditions for the biodiesel synthesis in current studies are the molar ratio of oil-methanol 1:3 (oil flow rate 0.1621 ml/min and methanol flow rate 0,0652 ml/min), ozone flow rate 0.2 ml/min, reaction temperature 30 °C, ozone concentration 60-64 gr/Nm3,

using 5 m long tube of 1 mm ID, and 1 wt% NaOH catalyst for the reactions in one pot, and 1 wt% NaOH and 1.5 wt% H2SO4 catalyst for transesterification and ozonolysis respectively in the sequential process. Methanol is continuous-phase, and oil and ozone is a dispersed phase. Gas-liquid-liquid contacting models can explain the simultaneous reaction mechanism, but these models should be modified to describe the sequential reaction mechanism.

6.2. Future Work

The direct outlooks of this work concerning the biodiesel synthesis are, first, to find the stable and regular bubbles/slugs flow inside the small tube. The caused factors of the instability/irregularity of gas-liquid flow inside a small tube could be understood initially since the bubbles/slugs generation step in the T-junction, and then, the flow pattern appeared across the entire length of the tube. By understanding the cause of instability/irregularity flow could be cultivated a solution to minimize this irregularity. Therefore, it is essential to use a transparent PTFE as the tube's raw material and T-junction in this study. The regularity of flow patterns is principal information required since the reaction carried out in the regular and stable flow will produce a constant product concentration.

Second, ozone concentration is a critical factor in the study, which involved an ozonolysis reaction. The current work used a relatively small ozone concentration around 60-62 gr/Nm3 or 3.4 %v/v as the ozone generator's maximum capacity. The utilizing of higher ozone concentration is required in the studies at purposing to understand the influence of ozone on the cutting of double-bound carbon chain (C=C) more clearly, and further, it becomes easier to create the model of synthesis biodiesel. Utilizing small ozone concentration was not clearly indicated the change that occurred.

Third, related to the catalyst application. The simultaneous reaction of transesterification-ozonolysis in the previous work took place using a base catalyst (NaOH/KOH), as has been done in this experiment. For future work, to improve the yield product, it is necessary to enhance/reduce the percentage of the catalyst of 1 wt% in these studies by 0.5, 1.5, or 2 wt% refers to the weight of methanol because it is not possible to mix catalyst and oil. Sodium hydroxide is not dissolved in the oil phase.

Fourth, the experiment's result on ozonolysis in biodiesel synthesis using sunflower oil is to get a model. In the next steps, it is essential to implement this model for synthesis biodiesel by using the other oil type as raw material, mainly using the waste palm oil/cooking oil, which is very abundant in Indonesia. Another interesting point of the kinetic model is the model could be used to determine the optimum tube length in attaining the highest yield and the residence time needed, and further, the length of tube optimum could be known.

Literature

[1] A. Y. Widianto, J. Aubin, C. Xuereb, and M. Poux, "Gas-liquid-liquid reactions: Contacting mechanisms and effective process technologies," *Catal. Today*, no. November 2018, 2019.

[2] S. Lu, L. Wang, Y. Wang, and Z. Mi, "Kinetic Model of Gas-Liquid-Liquid Reactive Extraction for Production of Hydrogen Peroxide," *Chem. Eng. Technol.*, vol. 34, no. 5, pp. 823–830, 2011.

[3] J. Wiley and K. Hepburn, *Chemical Reaction Engineering - Boston.* 1982.
[4] C. J. Gommes, S. Blacher, J. H. Dunsmuir, and A. H. Tsou, "Practical Methods for Measuring the Tortuosity of Porous Materials from Binary or Gray-Tone Tomographic Reconstructions," *AIChE J.*, vol. 55, no. 8, pp. 2000–2012, 2012.
[5] V. M. Rajesh and V. V. Buwa, "Experimental characterization of gas-liquid-liquid flows in T-junction microchannels," *Chem. Eng. J.*, vol. 207–208, pp. 832–844, 2012.
[6] K. Wang, Y. C. Lu, J. Tan, B. D. Yang, and G. S. Luo, "Generating gas/liquid/liquid three-phase microdispersed systems in double T-junctions microfluidic device," *Microfluid. Nanofluidics*, vol. 8, no. 6, pp. 813–821, 2010.

Appendix A

I. Calculation

1. The calculation of oil and methanol volume

$\rho_{methanol\ (gr/ml)}$ = 0.7915

$\rho_{WCO\ (gr/ml)}$ = 0.9251

Composition of sunflower oil :

Free Fatty Acid (FFA)	wt%	Mr (gr/gmol)
Palmitic acid	7	256.424
Stearic acid	5	284.477
Oleic acid	19	282.461
Linoleic acid	68	280.446
Linolenic acid	1	278.440
Total	100	

WCO mass base = 0.15 gram

$\frac{1}{Mr\ WCO} = \sum \frac{Xi}{Mr}$ = (7%/256.424) + (5%/284.477) + (19%/282.461) + (68%/280.446) + (1%/278.44)

= 0.00358203

Molecular weight of WCO = Mr WCO = 279.1714 gr/gmole

Mole WCO = $\frac{mass\ of\ WCO}{Mr\ WCO}$ = 0.15/279.1714 = 0.000537 mole

For mole ratio WCO : methanol = 1: 5,

Volume WCO (ml) = $\frac{mass\ of\ WCO}{\rho_{WCO}}$ = 0.162145 ml

Mole methanol = 5 x 0.0005373 = 0.002687 mole

Volume methanol = $\frac{mass\ of\ methanol}{\rho_{methanol}} = \frac{(n \times Mr)_{methanol}}{\rho_{methanol}}$ = 0.108615 ml

The calculation result of WCO-oil molar ratio is shown in table below:

Molar Ratio		Volume (ml)		Volume
WCO	methanol	WCO	methanol	Total (ml)
1	3	0.1621	0.0652	0.2273
1	6	0.1621	0.1303	0.2925
1	7	0.1621	0.1521	0.3142
1	8	0.1621	0.1738	0.3359
1	9	0.1621	0.1955	0.3577

2. The calculation of KI powder (gr) that is used for KI solution (ozone trap)

Reaction between ozone and KI:

$2e + O_3 + H_2O$ ---------> $O_2 + 2OH^-$ (reduction)

$2I^-$ ---------> $I_2 + 2e$ (oxidation)

$O_3 + 2I^- + H_2O$ ---------> $O_2 + 2OH^- + I_2$

The reaction product will be analyzed by titration $Na_2S_2O_3$ to measure the concentration of KI solution:

$I_2 + S_2O_3$ --------> ……

$2e + I_2$ --------> $2I^-$

$2S_2O_3^{2-}$ --------> $S_4O_6^{2-} + 2e$

$I_2 + 2S_2O_3^{2-}$ --------> $2I^- + S_4O_6^{2-}$

Mass molecule relative: Mr KI = 166 gr/gmole, Mr O_3 = 48 gr/gmole

The concentration of ozone output ozone generator is 35 gr/m^3

Ozone concentration is the ratio between ozone outputs to oxygen flow, therefore it can be stated that: ozone output = 35 gr/time

Oxygen flow = 1 m^3/time

Ozone output = 35 gr/time = 35/48 mole/time = 0.7282 mole/time

Assuming that oxygen is an ideal gas, therefore the calculation can be used the formula P.V = n.R.T

P = 1 atm V = 1 m^3/time

R = 8.21 . 10^{-05} m^3.atm/mole.K T = 298 K

n = oxygen flow = P.V/(R.T) = 40.9 . 10^{-1} mole/time

$$\% \text{ ozone} = \frac{\text{ozone output}}{\text{oxygen flow}} = 1.78\ \%$$

The concentration of KI needed in KI solution (ozone trap) is based on the reaction in the right side:

Mole KI = 2 x mole O_3 = 0.0357 mole

Mass KI = mole KI x the molecular relative of KI = 5.919694 gr

II. Method to measure contact angle, surface tension and interfacial tension

a. Contact angle

In general, the method used to measure the contact angle between liquid and teflon as a raw material of the tube consists of first, makes a drop of liquid on the teflon surface using a pipette. Second, the contact angle formed between liquid and teflon surface was recorded by a camera, and next, analyzing the photos of contact angle manually using a protractor.

b. Surface tension and interfacial tension

Nouy tensiometer is a tool for measuring surface tension and interfacial tension. Surface tension was measured by inserting a platinum ring into a solution and then bringing it to the surface by lowering the liquid buffer as well as keeping the beam remains horizontal so that the ring could come out of the surface. The same procedure applied to measure interfacial tension. The ring was immersed in the first solution, then a second solution was added gently on topside, and the force was adjusted until the ring released from the two liquid phase interface. The measurements with methanol were made with pure methanol and concentrated methanol plus methylene blue. Each measurement was done three times, and the average value was calculated.

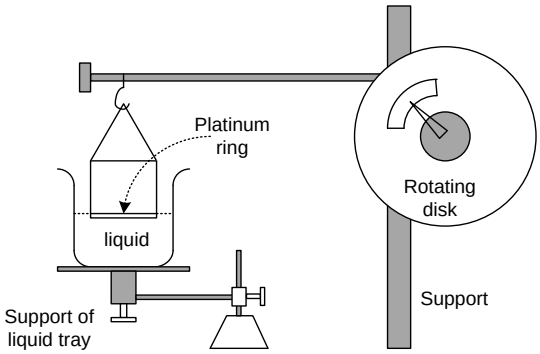

Figure 1. Sketch of Tensiometer Nouy

Appendix B

1. Observation two phases flow pattern (gas-liquid).
   a. Tube (ID 1 mm), cross sectional area tube = 0.785 mm^2, tube = 30 meters long.

QL (ml/min	QG (ml/min)	UL (m/s)	UG (m/s)	Lb in (mm)	Lb out (mm)	Ls in (mm)	Ls out (mm)	UG/UL	Lb/Win	Lb out / Lb in
1.50	0.75	0.0318	0.0159	irregular bubble/ slug length		-	-	0.50	-	-
1.00	0.75	0.0212	0.0159	irregular bubble/ slug length		-	-	0.75	-	-
1.00	1.50	0.0212	0.0318	irregular bubble/ slug length		-	-	1.50	-	-
0.40	2.00	0.0085	0.0425	20	40	37.5	22	5.00	40.00	2.00
0.40	2.25	0.0085	0.0478	23	43	37	32	5.63	46.00	1.87
0.40	2.45	0.0085	0.0520	23	45	32	35	6.13	46.00	1.96
0.40	2.70	0.0085	0.0573	26	48	36	36	6.75	52.00	1.85
0.20	2.70	0.0042	0.0573	28	43	20	25	13.50	56.00	1.54
0.20	2.25	0.0042	0.0478	28	40	20	10	11.25	56.00	1.43
0.10	2.75	0.0021	0.0584	35	45	6	37	27.50	70.00	1.286
0.10	2.25	0.0021	0.0478	30	38	7	35	22.50	60.00	1.267
0.10	2.00	0.0021	0.0425	28	35	7.5	36	20.00	56.00	1.250
0.10	1.50	0.0021	0.0318	28	35	8	20	15.00	56.00	1.250
2.00	2.75	0.0425	0.0584	irregular bubble/ slug length				1.38	-	-
2.00	2.25	0.0425	0.0478	irregular bubble/ slug length				1.13	-	-

b. Tube (ID 0.53 mm), cross sectional area tube = 0.22051 mm^2, tube = 1 meter long.

QL (ml/min)	QG (ml/min)	UL (m/s)	UG (m/s)	Lb in (mm)	UG/UL	Lb/Win
0.05	0.10	0.0038	0.0076	unstable bubble velocity	2.000	-
0.05	0.20	0.0038	0.0151	unstable bubble velocity	4.000	-
0.10	0.20	0.0076	0.0151	unstable bubble velocity	2.000	-
0.10	0.15	0.0076	0.0113	unstable bubble velocity	1.500	-
0.07	0.10	0.0049	0.0076	-	1.538	-
0.07	0.13	0.0049	0.0098	-	2.000	-
0.07	0.15	0.0049	0.0113	unstable bubble velocity	2.308	-
0.07	0.20	0.0049	0.0151	unstable bubble velocity	3.077	-
0.07	0.23	0.0049	0.0174	unstable bubble velocity	3.538	-
1.50	0.75	0.1134	0.0567	unstable bubble velocity	0.500	-
1.00	0.75	0.0756	0.0567	unstable bubble velocity	0.750	-
1.00	1.50	0.0756	0.1134	unstable bubble velocity	1.500	-
0.10	1.00	0.0076	0.0756	49.25	10.000	98.50
0.09	1.00	0.0068	0.0756	55.83	11.111	111.67
0.08	1.00	0.0060	0.0756	65.25	12.500	130.50
0.07	1.00	0.0049	0.0756	94.00	15.385	188.00
0.07	0.80	0.0049	0.0605	93.00	12.308	186.00
0.06	0.80	0.0042	0.0605	121.50	14.545	243.00
0.90	0.80	0.0680	0.0605	20.50	0.889	41.00
0.75	0.80	0.0567	0.0605	18.75	1.067	37.50
0.65	0.80	0.0491	0.0605	20.50	1.231	41.00
0.45	0.80	0.0340	0.0605	24.00	1.778	48.00
0.25	0.80	0.0189	0.0605	34.80	3.200	69.60
0.10	0.80	0.0076	0.0605	77.83	8.000	155.67
0.50	1.15	0.0378	0.0869	25.90	2.300	51.80
0.50	1.35	0.0378	0.1020	24.07	2.700	48.14
0.50	1.55	0.0378	0.1172	26.56	3.100	53.13
0.40	2.25	0.0302	0.1701	54.00	5.625	108.00
0.40	2.45	0.0302	0.1852	55.00	6.125	110.00
0.40	2.70	0.0302	0.2041	60.00	6.750	120.00
0.20	2.70	0.0151	0.2041	71.50	13.500	143.00

c. Tube (ID 1.5 mm), cross sectional area tube = 1.766 mm^2, tube = 6 meter long.

QL (ml/min)	QG (ml/min)	UL (m/s)	UG (m/s)	Lb in (mm)	Lb out (mm)	Ls in (mm)	Ls out (mm)	UG/UL	Lb/Win	Lb out/ Lb in
1.5	0.75	0.0142	0.0071	1.5	2.5	17	18	0.500	3.00	1.667
1.0	0.75	0.0094	0.0071	3.0	2.5	16	17	-	6.00	-
0.4	2.00	0.0038	0.0189	2.0	3.0	3.5	3.5	5.000	4.00	1.500
0.4	2.25	0.0038	0.0212	2.5	3.5	3.5	3.5	5.625	5.00	1.400
0.4	2.70	0.0038	0.0255	2.5	4.0	3.5	3.5	6.750	5.00	1.600

0.4	3.25	0.0038	0.0307	3.0	4.0	3.0	3.0	8.125	6.00	1.333
0.2	2.70	0.0019	0.0255	1.35	1.9	1.1	1.1	13.500	2.70	1.407
0.1	2.25	0.0009	0.0212	4.5	5.5	1.5	1.5	22.500	9.00	1.222
0.1	1.50	0.0009	0.0142	4.5	6.0	1.5	1.5	15.000	9.00	1.333
0.175	1.50	0.0017	0.0142	4.0	5.0	2.0	2.0	8.571	8.00	1.250
2.0	2.75	0.0189	0.0259	-	-	-	-	1.375	-	-
2.0	2.25	0.0189	0.0212	-	-	-	-	1.125	-	-
0.3	1.50	0.0028	0.0142	-	-	-	-	5.000	-	-

d. Tube (ID 1.5 mm), cross sectional area tube = 1.766 mm^2, tube = 6 meter long.

QL (ml/min)	QG (ml/min)	UL (m/s)	UG (m/s)	Lb in (cm)	Lb in (mm)	UG/UL	Lb/Win
0.10	1.00	0.0236	0.2359	1.27	12.67	10.00	25.33
0.09	1.00	0.0212	0.2359	1.14	11.44	11.11	22.88
0.75	0.80	0.1769	0.1887	0.70	7.03	1.07	14.07
0.90	0.80	0.2123	0.1887	0.80	8.00	0.89	16.00
0.08	1.00	0.0189	0.2359	unstable	-	12.50	-
0.06	0.80	0.0142	0.1887	unstable	-	13.33	-
0.75	1.00	0.1769	0.2359	unstable	-	1.33	-
0.65	0.90	0.1533	0.2123	unstable	-	1.38	-
0.45	0.90	0.1062	0.2123	unstable	-	2.00	-
0.25	0.95	0.0590	0.2241	unstable	-	3.80	-
0.25	0.75	0.0590	0.1769	unstable	-	3.00	-
0.15	0.75	0.0354	0.1769	unstable	-	5.00	-
0.06	1.25	0.0142	0.2949	unstable	-	20.83	-

2. The data observation of the influence of the pressure drop air-methanol to the bubble length between the entrance and the end section of channel.

   a. Tube dI = 1 mm, d_{ch} = 1 mm, 30 meters long

QL (ml/min)	QG (ml/min)	UL (m/s)	UG (m/s)	$\Delta P_{TP,in}$ (bar)	$P_1 = P_2 + \Delta P$ (bar)	Vb in (mm^3)	Vb out (mm^3)	Lb out (mm)	
								theo	exp
0.40	2.00	0.00849	0.04246	0.13199	1.14524	4.86161	5.49489	6.99	8.56
0.40	2.25	0.00849	0.04777	0.13050	1.14375	5.74554	6.48554	8.25	9.93
0.40	2.45	0.00849	0.05202	0.13519	1.14844	6.11735	6.93351	8.82	11.64
0.40	2.70	0.00849	0.05732	0.14269	1.15594	6.33482	7.22695	9.20	11.57
0.20	2.70	0.00425	0.05732	0.10257	1.11582	8.25000	9.08514	11.56	16.00
0.20	2.25	0.00425	0.04777	0.09153	1.10478	7.96939	8.68932	11.06	14.79
0.10	2.75	0.00212	0.05839	0.09334	1.10659	8.39732	9.17086	11.67	18.28
0.10	2.25	0.00212	0.04777	0.07762	1.09087	8.29911	8.93489	11.37	17.11
0.10	2.00	0.00212	0.04246	0.07233	1.08558	8.25000	8.83890	11.25	17.07
0.10	1.50	0.00212	0.03185	0.05725	1.07050	8.08163	8.53828	10.87	16.29

b. Tube dI = 1.5 mm, d_{ch} = 1 mm, 30 meters long

QL (ml/min)	QG (ml/min)	UL (m/s)	UG (m/s)	ΔPTP,in (bar)	$P_1 = P_2 + \Delta P$ (bar)	Vb in (mm^3)	Vb out (mm^3)	Lb out (mm)	
								theo	exp
1.00	3.03	0.02123	0.06433	0.18808	1.20133	6.5040	7.7112	9.8143	13.2500
1.00	2.80	0.02123	0.05945	0.17863	1.19188	6.5040	7.6506	9.7371	12.3889
1.00	2.60	0.02123	0.05520	0.17536	1.18861	6.1548	7.2199	9.1890	11.4375
1.00	2.40	0.02123	0.05096	0.17321	1.18646	5.7455	6.7277	8.5626	11.2500
1.00	2.20	0.02123	0.04671	0.16246	1.17571	5.7357	6.6553	8.4704	10.9000
1.00	2.00	0.02123	0.04246	0.16096	1.17421	5.3036	6.1461	7.8222	10.7143
1.75	2.00	0.03715	0.04246	0.20837	1.22162	5.1071	6.1574	7.8367	9.3333

c. Tube dI = 1 mm, d_{ch} = 1 mm, 20 meters long

QL (ml/min)	QG (ml/min)	UL (m/s)	UG (m/s)	ΔPTP,in (bar)	$P_1 = P_2 + \Delta P$ (bar)	Vb in (mm^3)	Vb out (mm^3)	Lb out (mm)	
								theo	exp
2.00	3.00	0.04246	0.06369	0.1498	1.1630	6.50397	7.46530	9.501	11.188
3.00	3.00	0.06369	0.06369	0.2475	1.2607	3.89286	4.84364	6.165	7.875
4.00	6.00	0.08493	0.12739	0.3465	1.3597	4.22321	5.66731	7.213	9.438
5.75	6.00	0.12208	0.12739	0.4976	1.5109	2.43080	3.62458	4.613	5.308
6.00	2.75	0.12739	0.05839	0.5627	1.5760	1.10000	1.71093	-	-
1.50	3.00	0.03185	0.06369	0.0981	1.1113	9.11842	10.00109	12.729	19.000

d. Tube dI = 1 mm, d_{ch} = 1.5 mm, 6 meters long

QL (ml/min)	QG (ml/min)	UL (m/s)	UG (m/s)	ΔPTP,in (bar)	P1 = P2 + ΔP (bar)	Vb in (mm^3)	Vb out (mm^3)	Lb out (mm)	
								theo	exp
0.175	1.500	0.0017	0.0142	0.00161	1.01486	11.73214	11.75077	6.647	6.800
0.100	1.500	0.0009	0.0142	0.00148	1.01473	11.75625	11.77345	6.660	6.875
0.100	2.250	0.0009	0.0212	0.00180	1.01505	14.36384	14.38937	8.139	8.500
0.200	2.700	0.0019	0.0255	0.00276	1.01601	11.49107	11.52232	6.518	6.625
0.400	3.250	0.0038	0.0307	0.00360	1.01685	11.38058	11.42103	6.460	6.813
0.400	2.700	0.0038	0.0255	0.00306	1.01631	11.78571	11.82133	6.687	6.750
0.400	2.250	0.0038	0.0212	0.00281	1.01606	10.98597	11.01644	6.232	6.714
0.400	2.000	0.0038	0.0189	0.00255	1.01580	10.98597	11.01356	6.230	6.714

3. The data observation of the influence of gas-liquid superficial velocity to bubble length

a. Tube d_{ch} = 1 mm, 20 meters long

QL (ml/min)	QG (ml/min)	UL (m/s)	UG (m/s)	UTP (m/s)	UG/UL	Bubble length				Std dev
						L0	Lt	Lt-L0	average (cm)	
2	3	0.0424	0.0636	0.1061	1.500	1.95	2.75	0.80	0.805556	0.039087
						3.50	4.25	0.75		
						4.70	5.50	0.80		
						5.95	6.70	0.75		

						7.20	8.00	0.80		
						8.75	9.60	0.85		
						10.05	10.85	0.80		
						11.15	12.00	0.85		
						12.50	13.35	0.85		
3	3	0.0636	0.0636	0.1273	1.000	2.45	2.90	0.45	0.495455	0.041560
						3.40	3.85	0.45		
						4.45	4.95	0.50		
						5.45	5.95	0.50		
						6.50	7.00	0.50		
						7.55	8.00	0.45		
						8.45	9.00	0.55		
						9.45	10.00	0.55		
						10.45	10.95	0.50		
						11.45	11.90	0.45		
						12.60	13.15	0.55		
4	6	0.0848	0.1273	0.2121	1.500	2.25	2.75	0.50	0.537500	0.043301
						3.15	3.70	0.55		
						4.10	4.65	0.55		
						5.05	5.60	0.55		
						6.15	6.70	0.55		
						7.10	7.65	0.55		
						8.05	8.65	0.60		
						9.00	9.50	0.50		
						9.85	10.45	0.60		
						10.85	11.35	0.50		
						11.75	12.20	0.45		
						12.65	13.20	0.55		
5.75	6	0.1220	0.1273	0.2492	1.043	2.75	3.10	0.35	0.309375	0.032755
						3.35	3.65	0.30		
						4.00	4.30	0.30		
						4.70	5.00	0.30		
						5.30	5.60	0.30		
						5.95	6.25	0.30		
						6.65	6.95	0.30		
						7.30	7.55	0.25		
						7.90	8.25	0.35		
						8.60	8.85	0.25		
						9.20	9.50	0.30		
						9.85	10.15	0.30		
						10.55	10.85	0.30		
						11.20	11.55	0.35		
						11.85	12.20	0.35		
						13.15	13.50	0.35		
6	2.75	0.1273	0.0583	0.1856	0.458	3.50	3.65	0.15	0.140000	0.020702
						4.00	4.15	0.15		

						4.65	4.80	0.15		
						5.45	5.60	0.15		
						6.30	6.40	0.10		
						7.00	7.15	0.15		
						7.55	7.70	0.15		
						8.15	8.30	0.15		
						8.85	9.00	0.15		
						9.70	9.80	0.10		
						10.30	10.40	0.10		
						11.25	11.40	0.15		
						11.90	12.05	0.15		
						12.50	12.65	0.15		
						13.40	13.55	0.15		
1.5	3	0.0318	0.0636	0.0955	2.000	2.70	3.75	1.05	1.046429	0.036502
						4.20	5.25	1.05		
						5.95	7.00	1.05		
						7.40	8.45	1.05		
						9.10	10.10	1.00		
						10.60	11.60	1.00		
						12.10	13.10	1.00		
						3.20	4.25	1.05		
						4.60	5.65	1.05		
						5.90	7.00	1.10		
						7.50	8.60	1.10		
						10.20	11.25	1.05		
						11.40	12.40	1.00		
						13.10	14.20	1.10		

b. Tube d_{ch} = 1 mm, 30 meters long

QL (ml/min)	QG (ml/min)	UL (m/s)	UG (m/s)	UTP (m/s)	UG/UL	Bubble length				Std Dev
						L0	Lt	Lt-L0	average (cm)	
2	3	0.0424	0.0636	0.1061	1.500	2.55	3.18	0.63	0.627500	0.008660
						3.51	4.13	0.62		
						4.50	5.11	0.61		
						5.48	6.11	0.63		
						6.48	7.12	0.64		
						7.49	8.12	0.63		
						8.47	9.10	0.63		
						9.42	10.04	0.62		
						10.38	11.00	0.62		
						11.34	11.97	0.63		
						12.30	12.93	0.63		
						13.25	13.89	0.64		
3	3	0.0636	0.0636	0.1273	1.000	3.05	3.45	0.40	0.411429	0.009493

						3.88	4.30	0.42		
						4.70	5.12	0.42		
						5.53	5.95	0.42		
						6.37	6.78	0.41		
						7.19	7.61	0.42		
						8.01	8.41	0.40		
						8.82	9.23	0.41		
						9.64	10.04	0.40		
						10.44	10.84	0.40		
						11.23	11.65	0.42		
						12.05	12.47	0.42		
						12.85	13.27	0.42		
						13.69	14.09	0.40		
4	6	0.0848	0.1273	0.2121	1.500	4.60	5.05	0.45	0.450667	0.011629
						5.40	5.86	0.46		
						6.21	6.68	0.47		
						7.02	7.49	0.47		
						7.86	8.31	0.45		
						8.66	9.12	0.46		
						9.47	9.91	0.44		
						10.26	10.70	0.44		
						11.05	11.50	0.45		
						11.83	12.27	0.44		
						12.60	13.05	0.45		
						13.39	13.84	0.45		
						14.18	14.61	0.43		
						14.96	15.40	0.44		
						15.72	16.18	0.46		
5.75	6	0.1220	0.1273	0.2492	1.043	2.69	2.98	0.29	0.298824	0.006966
						3.40	3.70	0.30		
						4.12	4.41	0.29		
						4.89	5.20	0.31		
						5.60	5.90	0.30		
						6.32	6.63	0.31		
						7.08	7.37	0.29		
						7.80	8.10	0.30		
						8.53	8.82	0.29		
						9.29	9.59	0.30		
						10.00	10.30	0.30		
						10.70	11.00	0.30		
						11.44	11.75	0.31		
						12.19	12.48	0.29		
						12.90	13.20	0.30		
						13.65	13.95	0.30		
						14.40	14.70	0.30		
6	2.75	0.1273	0.0583	0.1856	0.458	4.60	4.80	0.20	0.195714	0.006462

5.45	5.65	0.20
6.30	6.49	0.19
7.15	7.35	0.20
8.00	8.20	0.20
8.83	9.03	0.20
9.69	9.89	0.20
10.50	10.70	0.20
11.32	11.51	0.19
12.15	12.33	0.18
12.95	13.14	0.19
13.80	13.99	0.19
14.60	14.80	0.20
15.43	15.63	0.20

c. Tube d_{ch} = 1.6 mm, 6 meters long

QL (ml/min)	QG (ml/min)	UL (m/s)	UG (m/s)	UTP	Lb in (mm)	Lb in (cm)	Std Dev	Ls in (mm)	Std Dev	UG/UL
0.175	1.500	0.0017	0.0142	0.0158	6.636	0.664	0.0452	1.682	0.0252	8.571
0.100	1.500	0.0009	0.0142	0.0151	6.800	0.680	0.0412	1.611	0.0220	15.000
0.100	2.250	0.0009	0.0212	0.0222	8.250	0.825	0.0443	1.563	0.0320	22.500
0.200	2.700	0.0019	0.0255	0.0274	6.563	0.656	0.0378	1.625	0.0354	13.500
0.400	3.250	0.0038	0.0307	0.0344	6.438	0.644	0.0417	1.688	0.0530	8.125
0.400	2.700	0.0038	0.0255	0.0293	6.778	0.678	0.0354	1.750	0.0378	6.750
0.400	2.250	0.0038	0.0212	0.0250	6.214	0.621	0.0393	1.786	0.0699	5.625
0.400	2.000	0.0038	0.0189	0.0226	6.214	0.621	0.0267	1.786	0.0636	5.000

4. The influence of air and oil/methanol flow rate to GLL flow by using tube length of 1 m.

a. The influence of air flow rate to GLL flow

Ratio Oil : MeOH	Q_{oil} (ml/min)	Q_{MeOH} (ml/min)	Q_{air} (ml/min)	$Q_{tot-liq}$ (ml/min)	UL_{oil} (m/s)	UL_{MeOH} (m/s)	UL (m/s)	UG (m/s)	Lb (mm)	Std Dev	Ls_{oil} (mm)	Std Dev	Ls_{MeOH} (mm)
1 : 5	0.757	0.507	0.50	1.264	0.016	0.0108	0.0268	0.0106	2.77	0.0634	3.25	0.0771	1.596
1 : 5	0.757	0.507	1.00	1.264	0.016	0.0108	0.0268	0.0212	3.97	0.1144	2.42	0.0557	1.166
1 : 5	0.757	0.507	1.50	1.264	0.016	0.0108	0.0268	0.0318	4.88	0.1930	2.00	0.0691	0.954
1 : 5	0.757	0.507	1.75	1.264	0.016	0.0108	0.0268	0.0372	5.44	0.1447	1.87	0.0593	0.986
1 : 5	0.757	0.507	2.00	1.264	0.016	0.0108	0.0268	0.0425	5.94	0.1764	1.77	0.0679	0.922
1 : 5	0.757	0.507	2.50	1.264	0.016	0.0108	0.0268	0.0531	7.09	0.1290	1.70	0.0628	0.878
1 : 5	0.757	0.507	3.50	1.264	0.016	0.0108	0.0268	0.0743	9.33	0.3351	1.35	0.0404	0.811

Std Dev	L-unit	UG/UL	UG/UL_{oil}	UG/UL_{MeOH}	UL_{oil}/UL_{MeOH}
0.1028	7.6166	0.40	0.661	0.9864	1.4928
0.0890	7.5509	0.79	1.322	1.9728	1.4928
0.0929	7.8322	1.19	1.982	2.9592	1.4928
0.0785	8.2964	1.38	2.313	3.4524	1.4928
0.1118	8.6347	1.58	2.643	3.9456	1.4928
0.0773	9.6628	1.98	3.304	4.9319	1.4928
0.0878	11.4966	2.77	4.625	6.9047	1.4928

b. The influence of oil/methanol flow rate to GLL flow

Ratio oil : MeOH	Q_{oil} (ml/min)	Q_{MeOH} (ml/min)	Q_{air} (ml/min)	$Q_{tot-liq}$ (ml/min)	UL_{oil} (m/s)	UL_{MeOH} (m/s)	UL (m/s)	UG (m/s)	Lb (mm)	Std Dev	Ls (oil) (mm)	Std Dev
1 : 10	0.6411	0.8589	1.50	1.5000	0.013611	0.01823567	0.031847	0.031847	5.480	0.1319	1.818	0.0887
1 : 9	0.6810	0.8211	1.50	1.5021	0.014459	0.01743312	0.031892	0.031847	3.597	0.2251	1.565	0.1401
1 : 8	0.7242	0.7762	1.50	1.5004	0.015376	0.01647983	0.031856	0.031847	3.722	0.1633	1.615	0.0499

1 : 7	0.7266	0.7782	1.50	1.5048	0.015427	0.01652229	0.031949	0.031847	3.840	0.0852	1.620	0.0484
1 : 5	0.8983	0.6017	1.50	1.5000	0.019072	0.01277495	0.031847	0.031847	3.820	0.1365	1.928	0.0688
1 : 4	0.9772	0.5237	1.50	1.5009	0.020747	0.0111189	0.031866	0.031847	5.073	0.1695	2.339	0.0619
1 : 3	1.0702	0.4301	1.50	1.5003	0.022722	0.00913163	0.031854	0.031847	4.975	0.1381	2.555	0.0764

Ls_{MeOH}	Std Dev	L-unit	UG/UL	UG/UL_{oil}	UG/UL_{MeOH}	UL_{oil}/UL_{MeOH}
2.0225	0.0658	9.3201	1.00	2.340	1.74642	0.74642
1.2537	0.1936	6.4160	1.00	2.203	1.82682	0.82938
1.2649	0.1688	6.6014	1.00	2.071	1.93249	0.93301
1.2141	0.0667	6.6750	1.00	2.064	1.92753	0.93369
0.9664	0.1061	6.7140	1.00	1.670	2.49294	1.49294
1.1291	0.0640	8.5407	1.00	1.535	2.86424	1.86595
0.8588	0.0646	8.3895	1.00	1.402	3.48756	2.48826